North Atlantic Ocean decadal variability over the past millennium from climate model simulations and proxy based reconstructions

Dissertation zur Erlangung des Doktorgrades
an der Fakultät für Mathematik, Informatik und Naturwissenschaften
Fachbereich Geowissenschaften
der Universität Hamburg

vorgelegt von
Maria Pyrina

Hamburg, Juni 2017

North Atlantic Ocean decadal variability over the past millennium from climate model simulations and proxy based reconstructions

Dissertation zur Erlangung des Doktorgrades
an der Fakultät für Mathematik, Informatik und Naturwissenschaften
Fachbereich Geowissenschaften
der Universität Hamburg

vorgelegt von
Maria Pyrina

Hamburg, Juni 2017

Gutachter:
Dr. Eduardo Zorita
Prof. Dr. Johanna Baehr

Hamburg, Juni 16, 2017

Abstract

The present work is focused on the study of North Atlantic (NA) past ocean variability during the last millennium and the potential influence of natural external forcing. The analysis is conducted by using both molluscan-based proxy records and output of state-of-the-art comprehensive Earth System Models. The marine proxy records that are used are the growth increments of the bivalve shell Arctica islandica. The model simulations used participate in the fifth phase of the Climate Model Intercomparison Project (CMIP5).

In particular, with this work I seek to answer the following questions:

i) Does Arctica islandica have the potential to be used in Climate Field Reconstructions (CFRs) of the sea-surface-temperatures (SSTs) in the NA Ocean?

ii) If there is a NA basin signal registered in Arctica islandica locations, which CMIP5 models can reproduce that signal?

iii) Which climate reconstruction techniques are the most suited to reconstruct SSTs based on Arctica islandica?

iv) Is the climate model or the statistical reconstruction method more important to evaluate the skill of the reconstruction?

v) Do changes in solar forcing affect upper ocean circulation during summer?

Initially, I investigated the spatial covariance of the SSTs over two Arctica islandica collection sites with the North Atlantic wide SST field, using COBE2 reanalysis data and CMIP5 model output, during the second half of the 20th century. The SSTs co-located with the Arctica islandica collection sites are found to co-vary with the north-east Atlantic basin. Therefore, Arctica islandica has the potential to provide a skillful spatial reconstruction of the SSTs over this area. These results are shown by both COBE2 data and CMIP5 models. Additionally, eleven CMIP5 models were evaluated regarding the possibility to be used as test beds for the assessment of CFR methods that can be applied to reconstruct basin wide SSTs from the collection of proxy records of Arctica islandica. The best performing CMIP5 models in this regard are: CanESM2, CCSM4 and MPI-ESM.

Two statistical methods to reconstruct the past SSTs (pre-industrial and industrial era) of the NA Ocean based on the marine proxy records of Arctica islandica were tested in a pseudo-proxy experiment (PPE) set-up using the models CCSM4 and MPI-ESM-P, and reanalysis data from the COBE2 SST data set. The CFR techniques are Canonical Correlation Analysis and Principal Component Regression. The latter method was found to be more appropriate to be used for CFRs based on the Arctica islandica network. The choice of the climate model used as the surrogate reality in the PPE has a more significant effect on the reconstruction skill than the statistical reconstruction method itself, most likely due to the different internal co-variance structure of the models investigated.

A general conclusion is that the network of Arctica islandica is found to be a valuable proxy archive for the study of NA marine climate, as it records the climate signal of the NA basin. Performing a NA climate field reconstruction based on Arctica's network and appropriate CFR techniques is important for the further investigation of the effect of solar forcing to NA Ocean circulation.

Regarding the investigation of the effect of solar forcing on ocean circulation, we focused on the response of the pre-industrial NA climate (850—1849 AD), as simulated by an only solar forced experiment of the MPI-ESM-P model, to Total Solar Irradiance (TSI) changes. In this analysis three methods were used. For the first method we use techniques that measure the linear dependence between variables. These techniques (Pearson Correlation and Linear regression) were found to be inadequate to detect robust changes in the climatic variables studied. The second method is based on the comparison of two climatically different periods during the last millennium, namely the Medieval Climate Anomaly (MCA) and the Little Ice Age (LIA). The third method used was Composite Analysis, with which we focused on the separate effect of the most prominent TSI maxima and minima during the 1000 year period. Signals of solar forcing were detected on the simulated climate of the NA basin with the two latter methods, but the spatial response of the NA climate is found to be different depending on the method. The magnitude of the simulated climate response cannot be solely explained by TSI changes.

Zusammenfassung

Die vorliegende Arbeit befasst sich mit der Untersuchung der vergangenen Klimaschwankungen des Nordatlantischen (NA) Ozeans während der letzten 1000 Jahre und dem möglichen Einfluss äußerer Klimafaktoren. Die Analysen werden unter Verwendung von proxy-basierten Archiven von Muscheln und den Ausgabefeldern der jüngsten Generation von komplexen Erdsystemmodellen durchgeführt. Die verwendeten Proxy Archive beziehen sich auf Wachstumsringe der zweischaligen Muschel Arctica Islandica. Die verwendeten Modellsimulationen nehmen in der fünften Phase der Internationalen Klimamodellvergleichsstudie CMIP5 teil.

Im Detail möchte ich die folgenden Fragen beantworten:

i) Besitzt Arctica Islandica das Potential um für räumliche Klimarekonstruktionen (CFRs) für Meeresoberflächentemperaturen (SSTs) im NA Ozean verwendet zu werden?

ii) Falls ein Signal im NA Ozean in den Verbreitungsgebieten von Arctica Islandica aufgezeichnet wird, welche CMIP5 Modelle können dieses Signal wiedergeben?

iii) Welche Klimarekonstruktionsmethoden sind am besten geeignet um die SSTs basierend auf Arctica Islandica zu rekonstruieren?

iv) Ist das Klimamodell oder die statistische Rekonstruktionsmethode bedeutsamer für die Güte der Rekonstruktion?

v) Beeinflussen Veränderungen der Solaraktivität die Zirkulation des oberflächennahen Ozeans während der Sommermonate?

Zu Beginn der Arbeit untersuche ich die räumliche Kovarianz der SSTs für zwei Verbreitungsregionen von Arctica Islandica für das gesamte nordatlantische SST Feld. Hierzu verwende ich den COBE2 Reanalyse Datensatz und die CMIP5 Ausgabefelder während der zweiten Hälfte des 20. Jahrhunderts. Es zeigt sich, dass die ausgewählten Verbreitungsregionen von Arctica Islandica mit den SSTs im nordostatlantischen Becken zusammenhängen. Demzufolge besitzt Arctica Islandica grundsätzlich das Potential um für eine adäquate Rekonstruktion von SSTs in diesen Regionen benutzt zu werden. Diese Resultate zeigen sich sowohl für COBE2 Daten als auch die CMIP5 Modelle. Zusätzlich wurden elf CMIP5 Modelle dahin gehend evaluiert als Test Bett für die Abschätzung der Güte verschieden räumlich aufgelöster SST-Klimarekonstruktionen für den Nordatlantik, basierend auf den Verbreitungsregionen von Arctica Islandica benutzt zu werden. Die am besten geeignetsten Modelle in diesem Zusammenhang sind CanESM2, CCSM4 und MPI-ESM.

Zwei statistische Methoden wurden angewandt um vergangene SSTs (vorindustriell und industrielle Periode) des NA Ozeans basierend auf den marinen Proxy von Arctica Islandica in einem Pseudo-Proxy Ansatz zu testen. Hierzu wurden die Modelle CCSM4 und MPI-ESM-P sowie die COBE2 SST Reanalysen verwendet. Die CFR Methoden beziehen sich auf die

Kanonische Korrelationsanalyse und die Hauptkomponenten-Regressionsanalyse. Letztere hatte sich als geeigneter erwiesen um für räumlich aufgelöste Rekonstruktionen basierend auf dem Netzwerk von Arctica Islandica verwendet zu werden. Die Wahl des Klimamodells, welches die virtuelle Wahrheit innerhalb des Pseudo Proxy Ansatzes darstellt, besitzt dabei einen stärkeren Einfluss auf die Rekonstruktionsgüte als die eigentliche Rekonstruktionsmethode. Dies liegt höchst wahrscheinlich in den unterschiedlichen internen räumlichen Kovarianz Strukturen innerhalb der untersuchten Modelle begründet.

Eine übergeordnete Schlussfolgerung ist, dass das Netzwerk von Arctica Islandica ein geeigneter Proxy für die Untersuchung des Nordatlantisch ozeanischen Klimas darstellt, da es Klimasignale im Nordatlantischen Becken aufzeichnet. Die Erzeugung einer räumlich aufgelösten Klimarekonstruktion für den Nordatlantik basierend auf dem Netzwerk von Arctica Islandica und geeigneter CFR-Methoden ist zudem bedeutsam für weitere Untersuchungen hinsichtlich der Auswirkungen der Solaraktivität auf die Ozeanzirkulation innerhalb des Nordatlantischen Beckens.

Bezüglich der Untersuchungen der Auswirkungen der Solaraktivität auf Änderungen der Ozeanzirkulation konzentriere ich mich auf den Einfluss auf das vor-industrielle Klima des NA (850-1849 AD). Hierzu wurde eine Simulation mit dem MPI-ESM-P Modell verwendet, welche nur durch den Antrieb von Änderungen der Solaraktivität durchgeführt wurde. In diesem Kontext wurden drei Analysemethoden angewendet: Die erste Methode beschreibt ein Maß für die Bestimmung des linearen Zusammenhangs zwischen Variablen. Diese Methode (Lineare Korrelation nach Pearson/lineare Regression) wurden als inadäquat eingestuft, um robuste Zusammenhänge zwischen Änderungen der Solaraktivität und den untersuchten Klimavariablen herauszustellen. Die zweite Methode bezieht sich auf den Vergleich zwischen zwei klimatisch unterschiedlichen Perioden während des letzten Jahrtausends hinsichtlich der mittelalterlichen Klimaanomalie und der kleinen Eiszeit. Die dritte Methode bezieht sich auf die Komposit-Methode, welche auf den jeweiligen Einfluss solarer Maxima und Minima Phasen während der 1000jährigen Periode abhebt. Der Einfluss der Solaraktivität wurde im simulierten Klima des Nordatlantischen Beckens mittels der beiden zuletzt genannten Methoden erfasst. Allerdings variieren die Amplitude und das räumliche Muster in Abhängigkeit der gewählten Methode. In diesem Zusammenhang kann die Größe der simulierten Klimaänderungen nicht allein mit Hilfe der Änderungen der Solaraktivität erklärt werden.

1. Introduction

1.1 Thesis Motivation

Climate variability operates in different time scales ranging from annual variations (high frequency variability), to variations on longer time scales of decades to millennia (low frequency variability). Persistence on longer time scales is an indication of potential predictive skill in the stochastic processes that are internal to the climate and may arise from atmospheric processes, oceanic processes or their coupled interactions. Therefore, understanding the physical processes involved in producing low-frequency variability is crucial for the prediction of climate change and for allowing the separation of anthropogenic and natural variability (IPCC, 2013). To distinguish between the anthropogenic effects on climate and natural climate variability it is important to first assess the changes that are expected to result from external influences that are not anthropogenically induced. These changes arise from natural external forcing (i.e. solar, volcanic).

The instrumental record is affected by both anthropogenic and natural external forcings and is usually too short for the investigation of climate variability on multi-decadal and longer time scales. Past periods offer the potential to provide information, not available from the instrumental record, for the assessment of the role of the coupled atmosphere-ocean mechanisms on multi-decadal to centennial climate variability. Currently, the understanding of past climate fluctuations is mostly derived from numerical climate models and proxy archives. Evidence derived from marine proxy records has indicated that there were broad scale changes in the North Atlantic dynamics over the last millennium, but low temporal resolution and dating uncertainties on the proxy archives hinder so far the identification of causal relationships between ocean dynamics and atmospheric variability (Reynolds et al., 2016). Therefore, there is a need to develop precisely-dated and robustly calibrated proxy archives that can be used for quantitative reconstructions of past climate changes (Reynolds et al., 2017). An important reason for the development and improvement of climate reconstructions is that they can help to both evaluate climate model responses and sharpen our understanding of important mechanisms and feedbacks (Jones et al., 2009). Furthermore, reconstructing spatiotemporal patterns of past climate variability helps us to understand and quantify the influence of externally forced and internal dynamics of the global climate system (Ahmed et al., 2013; Snyder, 2010).

As outlined above, current climate models are an essential source and a tool for investigating climate variability on different time scales. However, to obtain robust conclusions derived from those models a thorough evaluation must be carried out first to test their ability to realistically simulate present-day climate variability, in our case over the North Atlantic Ocean and its neighboring continental areas. In turn, the empirical evidence used for paleoclimatic reconstructions and the proxy network used for climate field reconstructions also need to be evaluated for their suitability and quality.

For instance, the dendrochronological community has developed annually resolved spatial networks of tree ring chronologies which have the decisive advantage of being absolutely-dated. They have been profusely used for the reconstruction of terrestrial climate variability over the past centuries (Ahmed et al., 2013; Moberg et al., 2005; Wilson et al., 2016). On the other hand, spatial networks of marine archives have so far been of more limited use for the reconstruction of recent climate variability, because of the lack of absolutely-dated marine proxies. For example, networks of marine sedimentary proxy archives are of typically low temporal resolution (multi-decadal to centennial) and major uncertainty remains in terms of dating due to the ocean's variable seasonal stratification that makes it difficult to ascribe one particular proxy datum to a precise and correct date. Recently, a new type of marine proxy has been put forward that is annually resolved and can be, as in the case of tree-rings, absolutely dated. This proxy is the width of the growth increments of shells of long-lived marine bivalve mollusks (i.e. Arctica islandica, Glycymeris glycymeris) that enables the generation of absolutely dated sclerochronological records (Butler et al., 2013; Reynolds et al., 2016) and an opportunity for development of annually resolved marine spatial networks directly analogously to the dendrochronological records (Reynolds et al., 2017).

In the following, a couple of examples will introduce the importance of the North Atlantic Ocean for different controlling factors. This will serve as a basis for the subsequent chapters where modelling and empirical evidence are used to assess uncertainties in the context of North Atlantic climate variability over the last millennium.

1.2 Atlantic Ocean Circulation

The second largest of the world's oceans, the Atlantic Ocean, covers approximately 20 percent of the Earth's surface. The Atlantic Ocean is on average the saltiest major ocean, with the surface water salinity ranging from 33 to 37 parts per thousand by mass, but with latitudinal and seasonal dependence. Maximum salinity values occur at about 25° north and south, in subtropical regions with low rainfall and high evaporation, while the lowest salinity values are north of the equator (due to heavy tropical rainfall), in the high latitudes and along coasts where large rivers enter (Talley 2002). Water temperature is also an important physical property of the marine environment, as it exerts an influence on many physical, chemical, geochemical and biological events. Surface water temperatures in the Atlantic Ocean vary with latitude, season and current systems, reflecting the latitudinal distribution of solar energy. Maximum temperatures occur north of the equator, and minimum values are found in the Polar Regions. Temperature and salinity variations combine to determine the density of sea water which influences water movements (Lalli and Parsons 1997).

Water mass is a body of ocean water with identifiable properties (i.e. temperature, salinity, density, chemical tracers) resulting from its unique formation process (IPCC, 2013: Annex III). The Atlantic Ocean consists of four major upper water masses with distinct temperature and salinity; the Atlantic Subarctic Upper Water (ASUW), the Western North Atlantic Central Water (WNACW), the Eastern North Atlantic Central Water (ENACW) and the South Atlantic Central Water (SACW) (see Figure 1 in Emery and Meincke 1986). There are five intermediate waters identified in the Atlantic; four low-salinity waters formed at subpolar regions (Western and Eastern Atlantic Subarctic Intermediate Water, Antarctic and Arctic Intermediate Water) and one high-salinity formed through evaporation in a marginal sea (Mediterranean Water) (see Figure 2 in Emery and Meincke 1986). The North Atlantic Deep Water (NADW) is a complex of four water masses. Changes in the formation of NADW have been linked to global climate changes in the past (Clark, Marshall et al. 2001).

Paleoceanographic records suggest that the largest changes in the North Atlantic (NA) climate were associated with transitions among three possible modes of the NADW formation (Alley and Clark 1999). The modern mode is characterized by deep water formation in the Nordic Seas and its subsequent flow over the Greenland-Scotland ridge (Dickson and Brown 1994). The newly formed NADW flows into the Labrador Sea where it entrains recirculating relatively cold and fresh Labrador Sea intermediate waters. During the glacial mode, NADW forms through open ocean convection in the subpolar NA (Labeyrie, Duplessy et al. 1992), while during the Heinrich mode, waters from the Antarctic filled the NA basin to depths as shallow as 1000 m (Sarnthein, Winn et al. 1994).

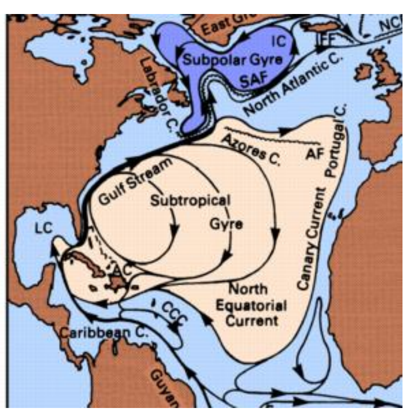

Figure 1-1 The Subtropical and Subpolar gyres (Source: http://peswiki.com/directory:ocean-trash-vortexes-gyres-)

The redistribution of water masses in the North Atlantic is related to the transport of heat, and more specifically to the meridional polar transport of heat. It is, therefore, important to quantify and understand the mechanisms that give rise to variations in the ocean circulation in the past and in the future. In particular, the last few centuries display climate conditions that are roughly similar of those today, but that also include distinct multi-decadal episodes with clear temperature deviations from the long-term mean that were likely caused by anomalous external climate forcing, as indicated from many climate reconstructions based on proxy data. This period offers the opportunity to evaluate climate models in their simulation of past variability of North Atlantic circulation. This thesis has investigated to what extent it is possible to reconstruct variations of the North Atlantic circulation from the evidence provided by proxy data, and to assess current climate models in their capability to simulate this circulation variability.

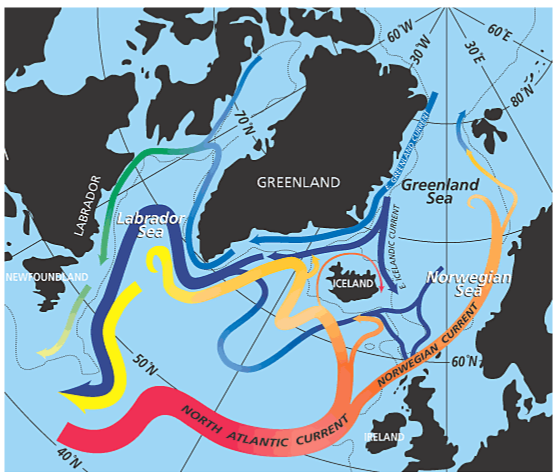

Figure 1-2 Circulation patterns in the North Atlantic Ocean. Cold, dense water is shown in blue flowing south, while warm less dense water flows north (Source: Jack Cook for Ocean and Climate Change Institute, Woods Hole Oceanographic Institution)

The surface circulation in the NA Ocean consists by three inter-connected currents; the Gulf Stream which flows north-east from the North American coast at Cape Hatteras, the North Atlantic Current (NAC) a branch of the Gulf Stream which flows northward from the Grand Banks and the Subpolar Front which is the northern and eastern extension of the NAC (Marchal, Waelbroeck, and Colin de Verdière 2016). The Subpolar Front is a relatively wide region that separates the subtropical gyre from the subpolar gyre (Figure 1-1). This system of currents (Figure 1-2) transports warm water into the North Atlantic, without which temperatures in the North Atlantic and Europe would drop dramatically (Rossby 1996). However, an alternative hypothesis supports that that the principal cause for the moderate NA and European winter temperatures is advection by the mean winds and not the movement of heat by the ocean (Seager et al. 2002). The global thermohaline circulation (Figure 1-3) is caused by the joint effect of thermohaline forcing, that is forcing due to heat and salinity, and turbulent mixing (Rahmstorf 2003). A very efficient vertical transfer process, deep convective mixing, is an essential ingredient of the THC. One of the major sites of known open ocean deep convection is the Labrador Sea. The subpolar gyre forms an important part of the global thermohaline circulation (Figure 1-3) and plays a key role in climate variability (Tréguier et al. 2005; Moreno-Chamarro et al. 2016) as there is a link between the gyre strength and the cessation of deep convection in the Labrador Sea, indicating a possible importance of the dynamical variability in the subpolar gyre for the evolution of the thermohaline circulation in the Atlantic (Böning et al. 2006).

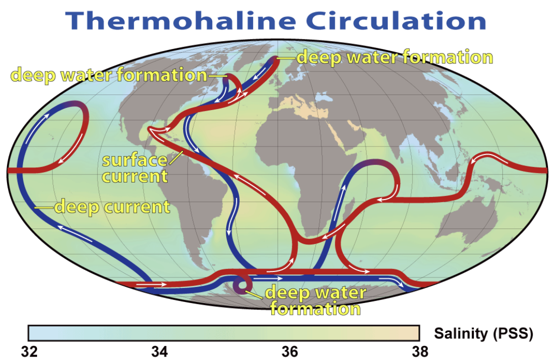

Figure 1-3 Thermohaline Circulation (Source: NASA Earth Observatory. Map by Robert Simmon, based on data provided by Alley 2004)

1.3 Reconstructing Past Ocean Variability

The ocean affects the climate system not only by being a part of the planetary energy cycle, but also by participating in the biogeochemical cycles and exchanging gases with the atmosphere (Rahmstorf 2002). The instrumental record is not long enough to provide a complete picture of climatic variability. The role of ocean circulation changes in major climate changes during the last millennium can be registered in proxy archives. Proxies can be natural (physical and biological) and documentary archives (i.e. tree rings, sediment cores, corals, mollusks). Several attempts have been made to extend the instrumental record across the North Hemisphere (NH) to cover the last 1000 years (Crowley and Lowery 2000; Jones et al. 1998). The common approach to reconstruct climate from natural proxies, is to use statistical regression to establish a connection between climatic observations and climate variability over an overlapping period (Jones, Osborn, and Briffa 2001).

Reconstructions of past ocean climate can be derived from various types of proxy data, but of different temporal resolution (sub-annual to centennial). There is a wide range of paleoclimate archives that can provide with high resolution reconstructions. The most important feature of the high resolution proxies is that the process involves as near to absolute dating as possible, which means assigning exact calendar years to the proxy records. Tree-ring derived proxy records and corals provide high time resolution (annual), but in the case of corals this is rarely the case, because most of the corals come from sites with little seasonality (Jones, Briffa et al. 2009). In both the cross section of trees and the skeleton of reef-building corals we can see that annual bands are formed as growth occurs (Figure 1-4). In areas of strong seasonality this banding is very clear, allowing the development of robust annual chronologies, but in regions with little or no seasonality the annual banding may be muted and therefore the chronology must rely on the detection of seasonality in geochemical and/or isotopic time series (Druffel 1997).

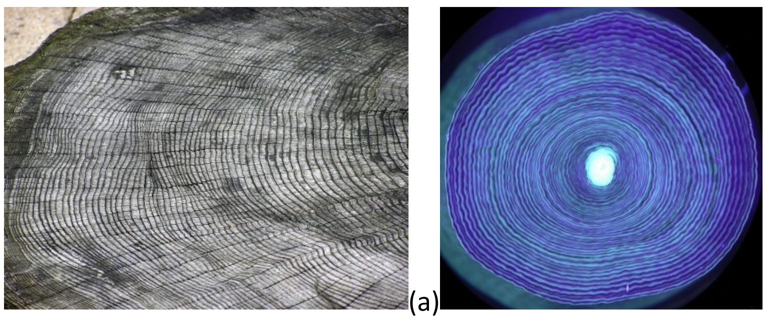

(a) (b)

Figure 1-4 a) The growth rings of an unknown tree species, at Bristol Zoo, Bristol, England (Source: https://en.wikipedia.org/wiki/File:Tree.ring.arp.jpg). b) Growth rings (illuminated with ultra violet light) in a cross-section of a 44-year-old deep-sea coral (Source: http://ocean.si.edu/ocean-photos/coral-growth-rings; Credit: Owen Sherwood).

Ice core records are the main source of information on past external climate forcing, such as concentrations of all the major long-lived greenhouse gases (MacFarling Meure, Etheridge et al. 2006), past solar variations and volcanic activity. They also provide information about climate variables themselves, such as air temperature, global ice volume, and even atmospheric circulation. Ice cores preserve annual layers (Figure 1-5a), but the layers become harder to see while moving deeper in the ice core. The ability to resolve annual variations from ice cores depends on variables such as the amount of snow deposited, the removal, re-deposition and mixing of near-surface snow by the wind, the modification of the seasonal signal by processes such as vapor diffusion and the disturbance by meltwater percolation. Varved sediment records from terrestrial (eg, lake and wetland) and marine environment also have layered structures (Figure 1-5b), but with distinct sequences of laminae through time. However, they are rarely of use for reconstructing high resolution paleoclimatology because in most cases their chronology and climate sensitivity is not well understood.

As tree rings, bivalve mollusks are biological chart recorders with their shells containing a record of environmental conditions in the form of geochemical variations (Goodwin, Schöne et al. 2003). Absolute dating techniques can be applied to the annual growth increments of the hard parts (Figure 1-6C) and derive proxy records of annual resolution (Helama, Schöne et al. 2006). Growth series from live-collected animals are dated by assigning the outermost complete increment to the year before collection and counting back increments. Bivalve mollusks live in populations where synchronous growth occurs amongst individuals and therefore missing or false increments can be identified by comparing many increment series from the same population (Butler et al. 2009).

Figure 1-5 a) GISP2 ice core at 1837 meters depth with clearly visible annual layers (Source: https://en.wikipedia.org/wiki/Ice_core). b) Lake Malawi sediment record (Image courtesy of the Lake Malawi Drilling Project, Source: https://thenaturalhistorian.com/2013/06/14/the-lake-malawi-sediment-chronometer-and-thetoba-super-eruption/).

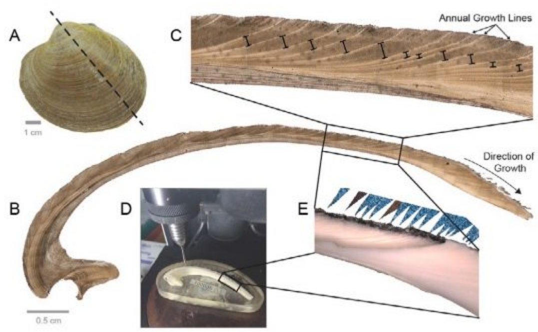

Figure 1-6 A) Dashed line shows the shell's maximum growth. B) Cross-section of a shell cut along its maximum growth axis. C) The annual growth lines. D) Embedded shell in an epoxy block, ready to be drilled. E) Partially drilled for isotope samples. (Source: https://blog.mares.com/clam-shells-used-to-compile-1000-record-of-ocean-climate-3009.html)

After dating the proxy archives, a statistical link between the proxy record and the local climate can be established over an overlapping period with climatic observations. The statistical relationship that links proxy records and local climatic variables allows the reconstruction of climate back in time where no observations exist. Additionally to local climate reconstructions, spatially resolved climate reconstructions (CFRs - Climate Field Reconstructions) can be achieved with the usage of spatial networks of proxy records. However, the performance of CFRs is difficult to establish due to the limited temporal extent of the observational record. The skill of algorithms used to combine proxy records into a climate field reconstruction (see e.g. in Moberg et al. 2005, for a reconstruction of the Northern Hemisphere temperature) may be tested using a technique known as pseudoproxy experiments (PPEs). With this technique, output from a climate model is sampled at locations corresponding to the known proxy network, and the climate reconstruction produced is compared to the climate of the model (Mann and Rutherford 2002; von Storch, Zorita, and González-Rouco 2009).

1.4 Climate Models

Numerical models of the climate system are essential in the formation and exploration of quantitative hypotheses about the dynamics of climate changes, as the system is too complex to be understood only by analytical calculations (Rahmstorf 2002). There are many types of models and the type we choose to use for the exploration of a specific hypothesis depends on the hypothesis itself. For example, despite their limited capability, analog models such as bowls or globes filled with viscous fluids can be used to demonstrate fundamental principles of fluid motion (Edwards 2011). Large-scale weather dynamics can be computed since the early 20th century using only primitive equations of motion and state (Bjerknes 1906, 1910). As the complexity of the research question that is set increases, the climate model's complexity needs to be increased as well.

To simulate past oceanic changes there is need for Earth System Models (ESMs), which are the current state-of-the-art models. ESMs expand on Atmosphere Ocean General Circulation Models (AOGCMs) to include the representation of various biogeochemical cycles such as those involved in the carbon cycle, the sulphur cycle, or ozone (Flato 2011). These models are the most comprehensive tools available for simulating past and future response of the climate system to external forcing, in which biogeochemical feedbacks play an important role (Flato et al. 2013). Figure 1-7 depicts the evolution of the complexity of climate models in the way they represent climate since 1970. The FAR, SAR and TAR labels refer to the models used in the first, second and third IPCC (Intergovernmental Panel on Climate Change) assessment reports.

A set of coordinated climate model experiments that involves ESMs comprises the fifth phase of the Coupled Model Inter-comparison project (CMIP5). CMIP5 models are used in the 5th IPCC Assessment Report, AR5. The CMIP5 project builds on the successes of earlier phases of CMIP (see Meehl et al. 2000, 2005) and provides a multimodel context for assessing the mechanisms responsible for model differences in poorly understood feedbacks associated with the carbon cycle and with clouds, examining climate "predictability" and, more generally, determining why similarly forced models produce a range of responses (Taylor, Stouffer, and Meehl 2012).

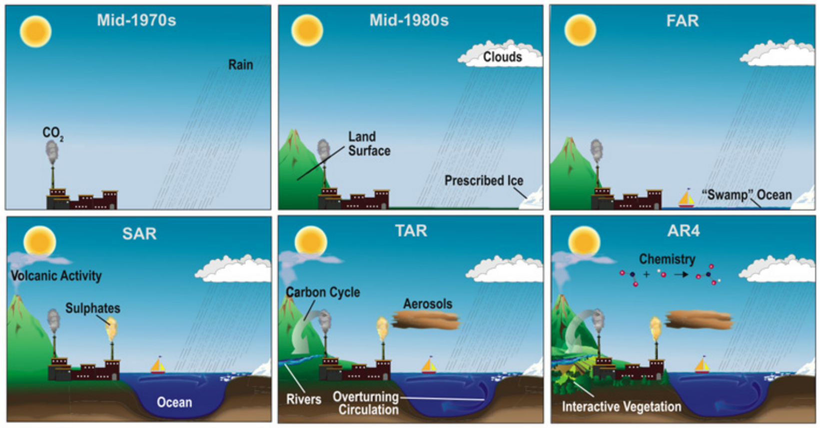

Figure 1-7 Evolution of Climate Models' complexity (Source: IPCC AR4, Chapter 1 page 99 Fig. 1.2)

1.5 Radiative Forcing

Except from internally induced climate variability, which results from internal interactions between components of the climate system, climate variations result from external factors that may be natural (i.e. solar activity, volcanism) and anthropogenic forcings (i.e. atmospheric CO2 concentration, deforestation). When the flow of incoming solar energy at the top of the Earth's atmosphere (Total Solar Irradiance - TSI) is balanced by an equal flow of heat to space, Earth is in radiative equilibrium (Figure 1-8). Anything that increases or decreases the amount of incoming or outgoing energy disturbs Earth's radiative equilibrium. As defined in the AR4 report of the IPCC, radiative forcing is a measure of the influence that one factor has in altering the balance of incoming and outgoing energy in the Earth-atmosphere system and is an index of the importance of the factor as a potential climate change mechanism (Bernstein et al. 2008).

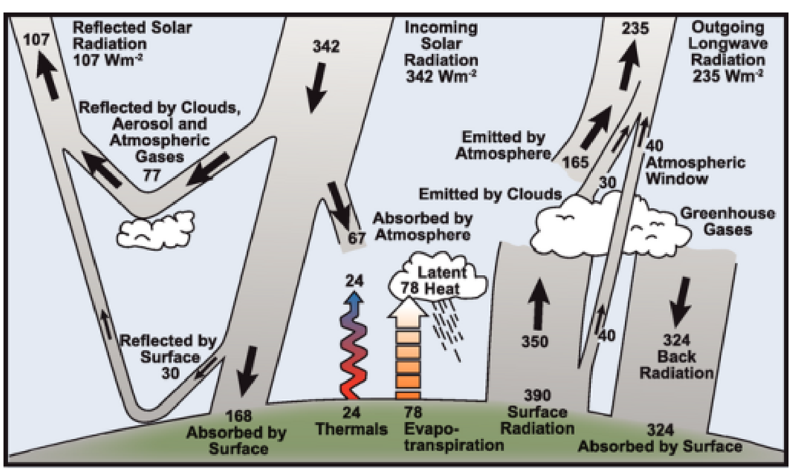

Figure 1-8 Estimate of the Earth's annual and global mean energy balance (Source: Kiehl and Trenberth, 1997)

A proposed mechanism through which solar variability may influence climate involves changes in the amount and composition of energy emitted by the Sun (due to changes in solar activity). This will affect the total amount of solar energy reaching the Earth's atmosphere in a given period of time and therefore induce changes in the Earth's climate by impacting directly the surface temperatures and the hydrological cycle. In addition, changes in solar UV irradiance may lead to heating the upper and middle atmosphere and therefore impact the atmosphere's temperature structure. Another solar forcing factor could be the modulation of energetic charged particle fluxes incident upon the Earth's atmosphere by the Sun in Polar Regions, where they enhance the destruction of stratospheric ozone and therefore impact atmospheric composition and temperatures. Finally, Sun modulates the galactic cosmic rays (GCRs) reaching the Earth and therefore impacts the ionization of lower atmosphere and the cloud condensation nuclei (Haigh 2007; Lockwood 2012), although the climatic relevance of this latter mechanisms is likely very small.

Another important natural external forcing is explosive volcanism: a long known cause for radiative, chemical, dynamic, and thermal perturbations in the climate system. Volcanic eruptions inject sulfuric gases into the lower stratosphere where they oxidize to form sulfate aerosols resulting in an increase of Aerosol Optical Depth (AOD), therefore increasing planetary albedo and reducing downwelling shortwave radiation that consequently results on surface and lower troposphere cooling (Cole-Dai 2010). Even though stratospheric aerosols have a characteristic lifetime of 1-2 years, the climate response may persist for longer (Ding et al. 2014). Although it is considered that the human impact on global temperature since the start of the industrial era (about 1750 AD) very likely exceeds the impact of natural forcings (Change 2014), during the pre-industrial era externally driven climate change is considered to be forced primarily by the variation in solar output and volcanic eruptions (Crowley 2000; Free and Robock 1999; Hegerl et al. 2006). Solar forcing and volcanic forcing likely played a significant role in the Little Ice Age (LIA) epochs of the last millennium, although their significance for the Medieval Warm Period (MWP) still remains not totally clear. Volcanic forcing is important for regional and global climate change, but it appears unlikely to induce sustained multi-decadal regional climate changes that exceed internal (or unforced) variability. In contrast, solar forcing may cause long term regional climate changes that are greater than unforced variability and resemble those seen in proxy based reconstructions of historical temperature change (Shindell et al. 2003).

1.6 Reconstructing Past Radiative Forcing

There are two major types of proxy records to reconstruct past volcanic forcing: ice cores and tree rings. Ice sheets of Antarctica and Greenland preserve the volcanic sulfuric acid fallout in snow layers. The detection of past volcanic eruption signals can be done with measurements of acidity and/or sulfate concentration that involve measurements of electric conductivity on solid ice (ECM) and meltwater (Hammer, Clausen, and Dansgaard 1980), and measurements of sulfates with ion chromatography (Legrand, De Angelis, and Delmas 1984). What limits the quality of the volcanic records derived from conductivity measurements is the presence of other acids (i.e. nitric acid), the neutralization of volcanic acid by alkaline dust and the influence of physical structure and temperature on the conductivity of the solid ice (Delmas et al. 1985; Taylor et al. 1992). The ion chromatography method introduces less noise and errors in the detection and quantification of the volcanic signals, but still the extrapolation of the experimentally measured concentration or flux of the volcanic sulfate to aerosol mass loading and the subsequent conversion to AOD could involve errors, as the relation of the last two may not be linear because of the AOD dependence to aerosol particle size (Timmreck et al. 2009). Tree ring volcanic records are less valuable than ice core records; the sulfate and acidity records measured in ice cores are a direct measure of volcanic forcing, whereas the tree growth parameters reflect the climatic response to volcanic forcing.

Based on the suggested relationship between solar activity and solar irradiance, it is possible to reconstruct solar activity using cosmogenic radionuclides such as 14C, 10Be, and 36Cl which are produced by the interaction of cosmic rays with the atmosphere (Beer 2005). The production rate is modulated by the solar magnetic field. Quantitative reconstruction of solar modulation, sunspot numbers, and solar irradiance has been attempted based on cosmogenic radionuclides (Bard et al. 2000; Solanki et al. 2004; Steinhilber et al. 2012). Even though these reconstructions have been used to assess past temporal variations in TSI and informed us about the existence of the solar 11-year cycle, there is still debate about past solar-activity levels because of differences in the data underlying these reconstructions (Muscheler et al. 2016). An example regarding the uncertainty in the role of solar irradiance variability is that when solar radiative forcing is specified by irradiance time series that were reconstructed using 11-year activity cycles instead of assuming an additional varying background component, the solar radiative forcing of climate is reduced by a factor of 5 suggesting that general circulation model simulations of twentieth century warming may overestimate the role of solar irradiance variability (Lean, Wang, and Sheeley 2002). It is therefore important to constrain the uncertainties of estimations and reconstructions of past external forcing when using paleorecords to estimate climate sensitivity, that is the equilibrated change of global mean temperature change in response to changes of the radiative forcing, because these estimates depend on the estimation of past forcing changes (Hegerl et al. 2006).

The uncertainties in the reconstructions of climate and of past external forcing do not only originate in measurement errors but also from non-climatic noise present in the records, in inadequacies of the reconstruction methods, inadequate understanding of the proxy response to environmental variations and other factors. A number of modeling studies questions the reliability of empirical reconstructions using regression methods that are based on ordinary least squares regression, because they may fail to recover some of the low-frequency climate variability (von Storch et al. 2004). For example tree-ring data, which are primarily used as input in high resolution proxy networks, may not preserve low frequency climate variability unless they are explicitly standardized to do so (Briffa et al. 2001; Esper, Cook, and Schweingruber 2002). Thus, the reliability of reconstruction methods should be tested in the surrogate climate simulated by climate models prior using those methods for the actual climate reconstruction based on real world proxies.

1.7 Constraining reconstruction uncertainties with PPEs

Pseudo-proxy experiments (PPEs) are controlled and systematic experiments that have been extensively used to evaluate the performance of a climate reconstruction method, exploiting most of the times the surrogate climate of model simulations (Mann and Rutherford 2002; Smerdon 2012). The need for PPEs stems from the need to isolate and evaluate the impact of the uncertainty factors that influence climate reconstructions. PPEs have not only been used to test reconstruction methods, but also the density of proxy networks, optimal proxy sites for reconstructions and uncertainties related to proxy temporal resolution and level of noise (Bradley 1996; Rutherford et al. 2003; Von Storch et al. 2004). When climate model simulations are used as the basis for PPEs, instead of the instrumental record (Tingley and Huybers 2010), methodological evaluations can extend to lower frequencies and longer time scales.

The experimental set up of a PPE that aims to test statistical methods that are used to reconstruct climate is the following: 1) pseudo-proxy data are “sampled” from the field of the ESM from locations where real world proxies are sampled; 2) the sampled pseudoproxy data are perturbed with noise to simulate the noise characteristics that are present in the real-world proxies. This noise, for instance non-climatic factors that affect tree-ring growth, is not straight forward to characterize statistically and usually PPE prescribe plausible statistical models and parameters; 3) climate reconstruction methods are applied to the pseudoproxies in order to reconstruct the targeted climatic variable. Finally, the skill of the reconstruction method is evaluated by comparing the derived reconstruction to the known model climate.

1.8 Thesis Objective

The objective of this thesis originates in an EU-funded international collaboration whose scientific goal is to use the shells of very long-lived mollusks as a record of environmental change in the northeast Atlantic Ocean over the past thousand years. The idea behind the ARAMACC project (Annually Resolved Archives of Marine Climate Change) is to develop a network of these shell-based chronologies in the northeast Atlantic Ocean, and at the same time to advance the applications of this kind of research in the fields of biology, climate modelling, proxy development and environmental monitoring.

The overall goal of the thesis is to analyze the amplitude and spatial structure of decadal and multi-decadal climate variability in the North Atlantic region using both the output of climate model simulations and reconstructions of past climate derived by proxy data, aiming to constrain the characteristics of model simulated variability. So far, Climate Field Reconstructions (CFRs), even for the oceanic realm, primarily have used information from terrestrial proxy records (Mann et al., 2008; Anchukaitis et al., 2017). Climate field reconstructions on a global scale derived from individual marine reconstructions were recently published, but lack temporal information on decadal to multi-decadal time scales (McGregor et al., 2015).

The proxy records derived from Arctica islandica are annually resolved, being suitable for the investigation of climate variability on decadal to multi-decadal time scales. For the reconstruction of large scale climate patterns in the North Atlantic basin, the co-variability of these records with the North Atlantic has to be investigated first. In a second step, aiming to combine the local information provided by Arctica islandica into the broader context of large scale climate patterns, different statistical methods have to be assessed. The methods will be assessed with controlled experiments, namely Pseudo Proxy Experiments (PPEs), as described in the Chapter 1.7. A prerequisite to construct a meaningful PPE relates to the climate models ability to represent the spatiotemporal characteristics of the observed climate.

The thesis consists of two main parts: The first part investigates the potential of the network of Arctica islandica to be used for the reconstruction of Sea Surface Temperatures (SSTs) in the North Atlantic basin. Here the analysis is concentrated on suitable methods that could be used in this context and ESMs that could be used in order to assess statistical methods in the controlled environment of a PPE. *The main focus of the first part of the thesis is therefore on the reconstruction of past climate variability in the North Atlantic basin over the past millennium.*

In the second part of the thesis the origin of the North Atlantic SST variability is investigated during the pre-industrial era of the last millennium. In this period, the main external climate forcings are related to volcanic eruptions and changes in solar activity. The overall research questions that I try to answer within the two parts of the thesis are:

a. Does *Arctica islandica* have the potential to be used in CFRs of the SSTs in the NA Ocean?
b. If there is a NA basin signal registered in Arctica's locations, which CMIP5 models can reproduce that signal?
c. Which Climate Reconstruction Techniques are the most suited to reconstruct SSTs based on Arctica islandica?
d. Is the climate model or the statistical reconstruction method more important to evaluate the skill of the reconstruction?
e. Do changes in solar forcing affect summer upper ocean circulation?

1.9 Thesis Outline

The thesis includes an introductory chapter, three main chapters and a chapter with conclusions and outlook. Repetitions might occur throughout the thesis, due to the preparation of the three main chapters for peer review journals. In the following, a brief overview regarding the context of the three main chapters is given:

Chapter 2:

I evaluated eleven coupled climate model simulations regarding the spatial structures of SST variability in the NA Ocean, during the second half of the 20th century. The subset of models includes CCSM4, CSIRO, CanESM and MPI-ESM, participating in the fifth phase of the Climate Model Intercomparison Project (CMIP5). The evaluation was performed to determine the potential of these models to be used at a later stage as test beds for the evaluation of Climate Field Reconstruction methods that will use the extremely long-lived bivalve mollusk Arctica islandica, an outstanding paleoclimate archive for the boreal and temperate North Atlantic (Schöne 2013). Several validation metrics such as the mean bias, variance, spatial and temporal co-variability and trends of the NA summer SSTs showed that some of the models can be used to test paleoclimatic reconstructions. However, most models showed shortcomings in simulating the Atlantic Multidecadal Oscillation (AMO). Concerning the co-variability of summer SSTs between proxy sites and the whole NA SST field, we found that these proxy locations contain a SST signal that might represent a (basin-wide) signal for the north-eastern NA basin. These results indicate that the proxy records of Arctica islandica, i.e. the recorder system in the context of a pseudo proxy system forward modelling concept, have the potential to be used for Climate Field Reconstructions of the north-eastern NA basin.

Chapter 3:

I tested two statistical methods to reconstruct the past SSTs of the North Atlantic Ocean based on annually resolved and absolutely dated marine proxy records of Arctica islandica. The methods were tested in a pseudo-proxy experiment set-up using state-of-the-art climate models (CMIP5 Earth System Models) and observations from the COBE2 SST data set. The multivariate linear regression methods assessed here are Principal Component Regression and Canonical Correlation Analysis. The methods were applied in the virtual reality provided by the global climate simulations to reconstruct the past NA SSTs, using pseudo-proxy records that mimic the statistical characteristics and network extent of Arctica islandica. Differences in the skill of the Climate Field Reconstruction were assessed according to different calibration periods and different proxy locations within the NA basin.

The choice of climate model used as surrogate reality in the pseudoproxy experiment has a more significant effect on the reconstruction skill than the calibration period and the statistical reconstruction method. The differences between the two methods are clearer with the MPI-ESM model, due to its finer spatial resolution in the NA basin. The addition of noise in the pseudo-proxies is important in the evaluation of the methods, as more differences in the spatial patterns of the reconstruction skill are revealed. More profound changes between methods were obtained when the number of proxy records is smaller than five, making the Principal Component Analysis a more appropriate method in this case. Despite the differences, the results show that the marine network of Arctica islandica can be used to skillfully reconstruct the spatial patterns of SSTs at the eastern North Atlantic basin.

Chapter 4:

Although climate signatures due to TSI variability on solar cycle (decadal) timescales are well established, longer term climate influences from the Sun are less well quantified. As long term changes can be more important, because of the more direct influences of the Sun on the Earth’s climate in these time scales and particularly in preindustrial times, we investigated the effects of solar forcing during the preindustrial era of the last millennium. The analysis was performed separately for inter-annual time scales and for longer time scales of 11 years. The region under consideration is the NA basin between 80˚W—30˚E and 21˚N—75˚N, while the climatic parameters analyzed are the geopotential height at 500 hPa and 850 hPa, the pressure at sea level and the sea surface temperature and were obtained from an only solar forced simulation of the MPI-ESM model from the Max Planck Institute.

The regression of TSI to the grid point climatic variables of the NA basin showed that TSI variability has no effect on the SSTs and on the atmospheric circulation of the NA basin during 850—1849 AD. The effect of solar forcing during the MCA and the LIA epochs of the last millennium was also investigated by calculating the mean temporal difference (MCA minus LIA) of the respective atmospheric and oceanic variables between those periods. In this case, TSI was found to induce a profound effect on the summer climate of the NA. The composite technique (superposed epoch analysis) was also employed for the investigation of the hypothesized link between solar activity and the NA summer climate. The composite pattern regarding the SST response to solar forcing is similar to the pattern shown by linear regression. Regarding atmospheric circulation, a West Atlantic-like blocking pattern with negative centers above Scandinavia and on the southwest of Nova Scotia and a positive center that extends from Greenland to the central NA basin, is the result of lower TSI values in inter-annual time scales.

2. Evaluation of CMIP5 models over the northern North Atlantic in the context of forthcoming paleoclimatic reconstructions[1]

In this chapter we evaluated eleven coupled climate model simulations regarding the spatial structures of sea-surface temperature (SST) variability in the North Atlantic, during the second half of the 20th century. The subset of models includes CCSM4, CSIRO, CanESM and MPI-ESM, participating in the fifth phase of the Climate Model Intercomparison Project. The evaluation was performed to determine the potential of these models to be used at a later stage as test beds for the evaluation of Climate Field Reconstruction (CFR) methods that will use the extremely long-lived bivalve mollusk Arctica islandica, an outstanding paleoclimate archive for the boreal and temperate North Atlantic (Schöne 2013). Several validation metrics such as the mean bias, variance, spatial and temporal co-variability and trends of the North Atlantic summer SSTs showed that some of the models can be used to test paleoclimatic reconstructions. However, most models showed shortcomings in simulating the Atlantic Multidecadal Oscillation (AMO). Concerning the co-variability of summer SSTs between proxy sites and the whole North Atlantic SST field, we found that these proxy locations contain a SST signal that might represent a (basin-wide) signal for the north-eastern North Atlantic basin.

2.1 Introduction

Climate reconstructions based on natural archives for which standard calibration and verification procedures are first developed on the inter-annual to decadal time scale (Jones et al. 2009), rely on statistical methods that link proxy records and local climatic variables (e.g. surface air temperature, precipitation, SST, sea level, sea level pressure, salinity). These methods are statistically calibrated using data from periods in which the proxy and instrumental records overlap. Whereas local climate reconstructions usually amount to a relatively simple linear re-scaling of one proxy record, Climate Field Reconstructions (CFRs) are based on a spatial network of proxy records and aim at spatially resolved climate reconstructions over a certain region. The statistical methods that have been applied so far for CFRs can attain a fair degree of sophistication (e.g. Smerdon, 2016 for a review of CFRs in the context of annually resolved proxy records). The properties and performance of the CFRs is sometimes difficult to establish, as the statistical methods are calibrated with data spanning the observational period –usually of the order of 100 years–, which hampers a

[1] Pyrina, M., Wagner, S. & Zorita, E. Clim Dyn (2017). doi:10.1007/s00382-017-3536-x

robust estimation of the skill of the reconstruction methods for multi-centennial or multi-millennial time scales. For the oceanic realm another level of complexity relates to the sparseness of observational data, especially prior to the pre-1950 period.

The CFR methods can, however, be tested using climate simulations as a virtual reality. Although in the ideal case all climate models should be physically consistent, the estimation of the skill of the CFR methods may depend on the climate model used to perform the climate simulation. Differences in the physical parameterizations, spatial resolution and processes incorporated in the model, may result in different assessment of the performance of CFRs. For instance, Dee et al. 2016 found that structural model biases introduce uncertainties that systematically reduce the reconstruction skill of CFRs. Thus, it is advisable to use several climate simulations with different climate models and previously evaluate the performance of these climate models to realistically simulate the observed climate. A practical hurdle in estimating the overall performance of the models does not only include the definition of the evaluation metrics itself, but also the observational basis for the assessment. This issue is problematic even for continental areas in the latter half of the twentieth century (1950–1999) because of the scarcity of meteorological observations over vast continental areas, especially over high latitudes and the tropical and southern hemispheric regions (Hijmans et al. 2005). For the global oceans, even after 1982 when both in situ and satellite data are available (Reynolds et al. 2002), there are still only few observations in high latitudes and especially in regions covered, at least seasonally, with sea ice (Hirahara et al. 2014). This data issue has, therefore, also to be taken into account when evaluating climate models, especially over those regions where the observational basis is inhomogeneous and not extending far back in time.

There are three studies that have assessed CFR methods taking into account the influence of the model used when evaluating these methods. These studies have demonstrated how different model simulations affect the evaluation of the CFR performance, but none of these studies has tested the ability of the models used to realistically simulate the observed climate. The first study is that of Mann et al. (2007). These authors focused on hemispheric annual mean temperature and used two climate models. In the studies of Smerdon et al. (2011) and Smerdon et al. (2016) the influence of choosing a particular model simulation on the CFR results was investigated, but focusing on the spatially resolved surface temperature, covering global scales. They used a multiproxy network that consists mostly of terrestrial and a few oceanic proxies. The aim of the present study is to evaluate the representation of the modeled spatiotemporal characteristics in simulating SSTs of the North Atlantic (NA) Ocean. In a later study we will focus on specific models that can be considered realistic and evaluate CFRs that can be applied to reconstruct SSTs in the NA region, using annually resolved marine proxy records of Arctica islandica.

Arctica islandica is an extremely long-lived bivalve mollusk (225 to over 500 years: Butler et al. 2013; Wanamaker, Heinemaker et al. 2008), suitable for environmental and climate studies (Wanamaker, Scourse et al. 2008). It is found in the NA basin and lives in water depths ranging from approximately 4 m to 500 m (Rowell et al. 1990; Nicol 1951). Compared to other existing records from extratropical oceans (i.e. sediment cores, coralline red algae), Arctica islandica can monitor environmental changes and ecological dynamics of the NA ocean in seasonal to interannual time scales (Butler et al. 2013; Schöne 2013). Annually laminated marine sediments are rarely used to reconstruct high resolution paleoclimatology of the last millennium unless both their chronology and climate sensitivity is well understood (Jones et al. 2009). Moreover, until now, there is no network of marine sedimentary archives of annual resolution in the NA that could be potentially used for CFRs that are not limited to lower frequency domains of multi-decadal to centennial resolution (McGregor et al. 2015; Cunningham et al. 2013). Within the sectioned shell of Arctica islandica (see Mette et al. 2016, their Fig 1) distinct annual (Butler et al. 2009) and even daily (Schöne et al. 2005) growth lines are apparent. The variability in the shells growth increment widths, which are the portions of shell between consecutive growth lines (Schöne 2013), and in the geochemical signature from the shell material (14C, δ18O, δ13C) relates to changes in environmental conditions (Witbaard and Klein 1994; Schöne et al. 2011; Wanamaker et al. 2011). In addition to the high temporal resolution of Arctica islandica, the reconstructions derived from its records can be cross-validated, absolutely dated (Scourse et al. 2006; Butler et al. 2010) and offer significant advantages in evaluating long-term NA marine climate dynamics (Wanamaker et al. 2009). Records of Arctica islandica can be used to reconstruct sea water temperatures (Eagle et al. 2013; Wanamaker et al. 2016), salinity (Gillikin et al. 2006), major NA climate modes like the AMO (Mette et al. 2016), ocean dynamics (see for NAO in Schöne et al. 2003; see for AMOC in Wanamaker et al. 2012), hydrographic changes and ecosystem dynamics (Witbaard 1996; Witbaard et al. 2003).

The second aim of this study is to perform an assessment of the capability of the network of Arctica islandica sites to provide a comprehensive and spatially resolved reconstruction of NA SSTs. The importance of testing already established locations of proxy archives lies in the further application of the local climate reconstruction into the broader concept of CFRs. As CFRs are co-variance-based approaches, we test whether the sites of Arctica islandica sufficiently co-vary with the NA basin. The information derived from the proxy archive could then be used to reconstruct the larger NA SST field using CFR methods. To assess the capability of the network of Arctica islandica sites to provide spatially resolved reconstruction of NA SSTs, we need to assess the capability of state-of-the-art climate models participating in the 5th phase of the Climate Model Intercomparison Project

(CMIP5) to represent the co-variance of the spatially resolved NA SSTs and the SSTs at the Arctica islandica collection sites during the second half of the 20th century.

The reasoning behind evaluating SST patterns of the anthropogenically forced period to reconstruct, in a second step, changes prior to industrialization is supported by other studies. Rutherford et al. 2003 found that it is more important for the reconstruction skill to use a data-rich calibration period with increasing radiative forcing than a data sparse calibration period with relatively stationary forcing. Moreover, exploiting teleconnected locations implicitly assumes that the teleconnected relationship does not significantly depend on the external forcing (Batehup et al. 2015). Coats et al. 2013 found that atmospheric forcing cannot account for the non-stationary teleconnection between tropical Pacific SSTs and 200 mb geopotential height. Gallant et al. 2013 found significant variations through time in teleconnections on near-centennial timescales in model simulations forced by internal dynamics alone, but Batehup et al. 2015 found that using multiple teleconnected regions minimizes any effects of non-stationarities. As these relationships cannot be assessed within the instrumental record, it is crucial to first evaluate CMIP5 models in the 20th century when model output and observations overlap, and additionally test the teleconnections of the proxy sites that will be used in CFRs.

The present study contributes to the evaluation of the CMIP5 models in several aspects. The spatial structure of SST variability simulated by CMIP5 models, with emphasis on the NA ocean, has been evaluated in previous studies (Perez et al. 2014; Liu et al. 2013). Patterns of interdecadal change have also been evaluated zonally (Carton et al. 1996; Kushnir 1994) and regionally (Qu and Huang 2014). However, only a few studies consider the northern part of NA, north of 60˚ N (Ruiz-Barradas et al. 2013; Jones et al. 2013), where one of the Arctica islandica sites tested in this study is located. In most studies, the structure of SST variability was studied using the ensemble of all CMIP5 models (Wang et al. 2014a) or the ensemble mean (Jha et al. 2014), focusing on the mean response rather than the behavior of each individual model. Teleconnection patterns between SSTs of Arctica islandica sites (Dahlgren et al. 2000; Wanamaker et al. 2016) and the NA basin using CMIP5 models have not yet been investigated.

2.2 Data and Methodology

We compare CMIP5 SST patterns with those derived from the Centennial in-situ Observation-Based Estimates COBE2 (Hirahara et al. 2014) to check the consistency over the NA, aiming to use this assessment of the most suitable models as a test-bed for assessing different climate reconstruction techniques used for Arctica islandica in a follow-up study. We focus on the latter half of the twentieth century (1950–1999), a period during which data coverage was substantially more complete than during the late nineteenth and early twentieth centuries. Based on the work of Schleussner et al. (2014) and of Wang et al. (2014), eleven CMIP5 models were used in our analysis (Table 1) and then compared to the COBE2 data set (Table 2) for this 50 year period. For the selection of models we also took into account the horizontal resolution of the oceanic component of the respective Atmosphere-Ocean General Circulation Model (AOGCM). Additionally, we excluded CMIP5 models with known problems in their archived output (http://cmip-pcmdi.llnl.gov/cmip5/errata/cmip5errata.html).

The CMIP5 project design includes suites of simulations of past climates, future climates, and shorter-term hindcasts of the last few decades (http://cmip-pcmdi.llnl.gov/cmip5/). In this study we used the historical simulations, which are part of the long term coupled simulations and cover most of the industrial period (from the mid-19th century to the beginning of the 21st century) and are sometimes referred to as “twentieth century” simulations. They are forced by changes in the total solar irradiance, observed atmospheric composition changes (reflecting both anthropogenic and natural sources) and include time-evolving land cover (Taylor et al. 2012). The models used in this study, as well as their original spatial and temporal resolution and other relevant information, are listed in Table 1. For a better comparison, the models’ original output was re-processed and re-gridded to a regular grid including the reference data sets. In this context the output was re-gridded onto a 1˚×1˚ degree horizontal resolution covering the NA region, between 60˚W–30˚E and 40˚N–70˚N, because most ocean models have a resolution of the order of our target grid. In the following, a summary of the main characteristics of the models is presented.

2.2.1 Models

In CCSM4 (Gent et al. 2011) the atmosphere (CAM4/ Neale et al. 2013), the land (CLM4/ Lawrence et al. 2012) and the sea ice components (CICE4/ Hunke and Lipscomb, 2008) interchange both state information and fluxes through a coupler in every atmospheric time step. The fluxes between atmosphere and ocean (POP2/ Danabasoglu et al. 2012) are calculated in the coupler and communicated to the ocean component once a day. In CSIRO the ice model has been developed in conjunction with the atmospheric model (R21/ Gordon and O’Farrell 1997). The atmospheric fluxes are averaged over two steps and passed to the ocean model (modified MOM2.2/ Gordon et al. 2010). Land surface interactions are parameterized using a soil–canopy model (Kowalczyk et al. 1994). As described in detail in Arora et al. (2011), CanESM2 evolved from the first generation CanESM1. It is composed of atmosphere, ocean, sea ice and carbon cycle models. The calculation of energy and moisture fluxes at the land surface is carried out within the Canadian Land Surface Scheme (CLASS) module (von Salzen et al. 2013), while coupling with terrestrial ecosystem and

Table 1 CMIP5 models used in this study.

(1) Model name (2) Institution	**Historical runs -temporal resolution**	**(1) Atmosphere Horizontal Grid (2) Ocean Horizontal Grid**	**Aerosol Component Type or Name**	**Atmospheric Chemistry Component Name**	**Ocean Biogeochemistry Component Name**
(1) CSIRO Mk3.6 (2) Common Scientific and Industrial Research Organization	Monthly: Jan 1850-Dec 2005	(1)~1.875˚×1.875˚ (2)~0.9˚×1.875˚	Interactive	Not implemented	Not implemented
(1) CanESM2 (2) Canadian Center of Climate Modelling and Analysis	Monthly: Jan 1850-Dec 2005	(1) spectral T63 (2) 256×192	Interactive	Included	CMOC
(1) HadCM3 (2) Met office Hadley Center, UK	Monthly: Jan 1859-Dec 2005	(1) 3.75˚×2.5˚ (2) 1.25˚×1.25˚ N144	Interactive	Not implemented	Not implemented
(1) MPI-ESM-P (2) Max Planck Institute Earth System Model, Germany	Monthly: Jan 1850-Dec 2005	(1)~1.8˚ T63 (2)~1.5˚ GR15	Prescribed	Not implemented	HAMOCC
(1) INM-CM4 (2) Institute for Numerical Mathematics, Russia	Monthly: Jan 1850-Dec 2005	(1) 2˚×1.5˚ (2) 1˚×0.5˚	Prescribed	Not implemented	Included
(1) IPSL-CM5 (2) Institute Pierre Simon Laplace, France	Monthly: Jan 1850-Dec 2005	(1) 1.9˚×3.75˚ (2) 2×2-0.5˚ ORCA2	Semi-interactive	Not implemented	PISCES
(1) MRI-CGCM3 (2) Meteorological Research Institute, Japan	Monthly: Jan 1850-Dec 2005	(1) 320×160 TL159 (2) 1˚×0.5˚	MASINGAR mk-2	Not implemented	Not implemented
(1) NorESM1-M (2) Norwegian Earth System Model	Monthly: Jan 1861-Dec 2005	(1) 1.9˚×2.5˚ (2) 1.125˚ along the equator	CAM4-Oslo	CAM4-Oslo	Not implemented
(1) GFDL-CM2 (2) Geophysical Fluid Dynamics laboratory, USA	Monthly: Jan 1850-Dec 2005	(1) 0.9˚×1.875˚ (2) 1˚ tripolar 360×200L50	Semi-interactive	Not implemented	Not implemented
(1) GISS-E2-H (2) Goddard Institute for Space Studies, USA	Monthly: Jan 1850-Dec 2005	(1) 2˚×2.5˚ (2) 0.2˚ to 1˚×1.875˚	Interactive	G-PUCCINI	HYCOM Ocean
(1) CCSM4 (2) Community Climate System Model, USA	Monthly: Jan 1850-Dec 2005	(1) 0.9˚×1.25˚ (2) 1.25˚ in longitude, variable 0.27-0.64˚ in latitude	Interactive	Not implemented	Not implemented

ocean carbon models enables some important biogeochemical processes to be represented and feedback to the physical climate (Yang and Saenko 2012). The SSTs and sea ice extent, are the central variables through which the atmospheric component (HadAM3/ Pope et al. 2000), the oceanic component (HadOM/ Collins et al. 2001) and the sea ice component (Cattle et al. 1995) are coupled in HadCM3 (Gordon et al. 2000). HadAM3 includes MOSES, a land surface scheme developed by Cox et al. 1999. The INM-CM4 climate model consists of two major blocks representing a model of general circulation of the atmosphere and a model of general circulation of the ocean. When coupling the atmospheric and oceanic models, the heat, freshwater fluxes and wind stress are transmitted from the atmosphere to the ocean, and the surface temperature and sea-ice area are transmitted from the ocean to the atmosphere (Volodin et al. 2010). The IPSL-CM5A model is built around a physical core that includes the atmosphere (GCM LMDZ5A/ Hourdin et al. 2013), land-surface (ORCHIDEE/ Krinner et al. 2005), ocean and sea ice components (NEMOv3.2/ Madec 2008). The atmospheric model has a fractional land-sea mask and each grid point is divided into four sub-surfaces corresponding to land surface, free ocean, sea ice and glaciers, respectively. The OASIS coupler (Valcke et al. 2006) is used to interpolate and exchange the variables, and to synchronize the models (Dufresne et al. 2013). The MRI-CGCM3 model (Yoshimura and Yukimoto 2008) consists of an atmosphere-land model (MRI-AGCM3) and the MRI.COM3 ocean and sea ice model. Each model component uses a simple coupler to exchange data with the other model components. NorESM is largely based on CCSM4 with the main differences being the isopycnic coordinate ocean module in NorESM. In addition, CAM4-Oslo substitutes CAM4 as the atmosphere module. The sea ice and land models in NorESM also include some differences regarding the aerosol calculations. The ocean component of GFDL-CM2 is the MOM4 code (Griffies et al. 2004) and the atmospheric component relates to the AM2p13 model. The land surface component allows for the simulation of the diurnal and seasonal cycles, while the sea ice component may produce five different ice thickness categories and open water at each grid point (Winton 2000). The new version of the GISS climate model used for CMIP5 simulations is called ModelE2. It is similar to the ModelE but with numerous improvements in physics (Schmidt et al. 2006). The atmosphere is coupled to a full dynamic ocean of the HYCOM model for the version GISS-E2-H that is used in this study (Sun and Bleck 2006). In the MPI-ESM model the coupling at the interfaces between atmosphere (ECHAM6/ Stevens et al. 2013) and land processes (JSBACH/ Reick et al. 2013), and between atmosphere and sea ice occurs at the atmospheric time step. The coupling between atmosphere and ocean (MPIOM/ Jungclaus et al. 2013), as well as land and ocean (the latter by river runoff) occurs once a day.

2.2.2 Data

Yasunaka and Hanawa 2011, performed an intercomparison of seven historical SST datasets including the extended reconstruction of global SST (ERSST/ Smith and Reynolds 2004) version 3, the second Hadley Center SST (HadSST/ Rayner et al. 2006), the optimal smoothing analysis by the Lamont-Doherty Earth observatory (LDEO/ Kaplan et al. 2001), the SSTs by the authors at Tohoku University (TOHOKU/ Yasunaka and Hanawa 2002), as well as the Hadley Centre’s sea ice and sea-surface temperature data set (HadISST/ Rayner et al. 2003) version 1, the release 2.1 of the International Comprehensive Ocean-Atmosphere Data Set (ICOADS/ Worley et al. 2005) and the centennial in-situ observation-based estimate of SSTs (COBE/ Ishii et al. 2005). They categorized the datasets into groups of fully interpolated (HadISST, COBE, ERSST, LDEO) and simply averaged data (ICOADS, HadSST, TOHOKU). They found that the latter group has many missing values and it includes extreme values, while the correlation and standard deviation of SST anomalies of ICOADS and HadSST are dependent on the number of observations. Furthermore, all datasets except ICOADS agree in the phases of the AMO index and on the SST global means. In the study of Loder et al. 2015 and in terms of Empirical Orthogonal Functions (EOFs) for the summer means during 1900-2011, it is found that for the data sets HadISST1, ERSST3 and COBE the leading summer EOF patterns show considerable similarities. Regarding the summer SST trends during the period 1950-2011, Loder et al. 2015 found that there are variations on local scales among the gridded datasets that will affect the trends at particular sites, indicating that caution is required regarding the spatial representativeness of the trend values from the gridded datasets. The large-scale patterns of the trends are generally similar for the period 1950-2011 amongst the three datasets, but there are differences particularly for the COBE dataset north of Iceland (see in Loder et al. 2015; Fig 7) due to a suspect abrupt jump in the COBE SSTs in that region around 1979. In our work, the SSTs are detrended prior to the analysis and therefore we do not expect these differences to affect our results.

We used the historical SST data set COBE2, developed at the Japanese Meteorological Agency (Hirahara et al. 2014). The COBE2 data set is a spatially complete SST product, covering the period 1850–2013 AD interpolated to a 1˚x1˚ grid. It combines SST measurements from ICOADS release 2.0, the Japanese Kobe collection, and readings from ships and buoys. Data are gridded using optimal interpolation. Similar to HadISST, data up to 1941 were bias-adjusted using "bucket correction" (Hirahara et al. 2014). Prior to the interpolation analyses, data were also subject to quality control using combined a-priori thresholds and nearby observations. (https://climatedataguide.ucar.edu/climate-data/sst-data-cobe-centennial-situ-observation-based-estimates).

2.2.3 Methodology

For the present analysis we considered the summer time (June-August) mean SST values for each year, covering the period 1950–1999 AD. The summer time SSTs were motivated by the growing season of Arctica islandica, that in both sites that are tested in this study, growth occurs approximately from February to September but it is biased towards summer (Schoene et al. 2005; Schoene et al. 2004). For this reason we calculated the summer mean SSTs of the NA for the eleven CMIP5 models and the dataset COBE2. We then calculated the SST bias as the difference between the CMIP5 and COBE long-term summer mean and the climatological root mean square error (RMSE). The climatological RMSE was calculated from the long-term summer mean squared differences between the CMIP5 models and the COBE2 data. The temporal standard deviation was also calculated to infer information on the performance concerning the amplitude of the (inter-annual) temporal variability.

To assess the spatial co-variability of SST anomalies, EOF analysis (von Storch and Zwiers 1999) is applied. The leading EOF represents spatio-temporal patterns of variability that account for the maximum co-variance between the SST anomaly time series at all pairs of grid points in the data set. The remaining co-variability was subjected to the same decomposition with the additional constraint that the second EOF pattern is orthogonal (e.g., uncorrelated) in both time and space to the leading EOF pattern (Deser et al. 2010).

In a second step we correlated the simulated model time series (1950–1999) in two model regions co-located with proxy sites of Arctica islandica and the NA Ocean (40˚–70˚N and 30˚E–60˚W). The first region is located in the North Sea (NS) at 58.5˚ N, 0.5˚ E and the second north of Iceland (Icelandic Self-IS) at 66.5˚ N, 19.5˚ W. These sites where chosen based on previous collection sites and studies (Wanamaker et al. 2012; Scourse et al. 2006; Butler et al. 2013; Wanamaker, Heinemaker et al. 2008). It is also important that the SST trends calculated by the models over NA share a similar distribution of the observed trends at a certain level of statistical significance. For both calculations of teleconnections and trends we tested the statistical significance at the 1% level, taking into account the effect of serial correlation (Zhang et al. 2000).

Moreover, the AMO index was computed from the modelled data, as it is associated with the NA dominant pattern of SST variability. To obtain the AMO index we linearly detrended the averaged NA SST (0˚–70˚N and 10˚E–80˚W), for the period 1850–2005 AD and calculated a 10-year running mean. AMO's spatial structures in both models and data are determined by linearly regressing the grid point SST onto the AMO index (Zhang and Wang 2013). Additional to the realization r1 of the MPI-ESM model, that has been used for all results presented in this work, we used two more realizations (r2, r3) of the MPI-ESM model to study the AMO. The r1 and r2 experiments are initialized with the same ocean state, but they differ in the standard deviation of the assumed lognormal distribution of the volcanic aerosol size (1.2 μm in r1, 1.8 μm in r2 and r3). The simulations r2 and r3 used the same parameter setting, but are started from different initial conditions (Jungclaus et al. 2014).

2.3 Results

In each of the following figures, we choose to present in most cases the best performing models with respect to each of the validation metrics used in this study. The results regarding all models are shown in the Appendix C2.

2.3.1 RMSE, mean bias and variance

As an initial skill metric on the basis of RMSE (Table 3), the best performing models in terms of summer SST biases are shown in Figure 2-1. The spatial distribution of the differences between the models and the observations share some similar characteristics (Appendix C2 Fig. 12A). Negative SST biases are shown for most models, with maximum values on the southwest of the study region east off Newfoundland (~4 K), except from the GISS model, indicating a widespread overestimation of SSTs over most of the NA Ocean (Appendix C2 Fig. 1A). The simulation of the North Atlantic Current path could be the reason for this SST difference between the observations and the models. The systematic error is located near the tail of Grand Banks, where the Gulf Stream turns north. This phenomenon can be seen for all eleven CMIP5 models used in this study. Discrepancies between the models mainly occur over the northern NA and more specifically on the path of the east Greenland current, were some models underestimate and others overestimate the SSTs, showing a wide spread in SST biases. Finally, the climate models best simulating the climatological mean of the summer SSTs in the period 1950–1999, according to the aforementioned validation metrics, are CSIRO, CCSM4 and GDFL.

Table 2 COBE2 data used in this study.

Reanalysis Data	Spatial Resolution
COBE2_SST	1˚ × 1˚

Although SST biases can represent a measure of skill of the models, it is not the only metric for the evaluation of climate models. Additionally, models should also be able to reproduce the observed pattern of inter-annual variability of the SSTs for the 1950–1999 year period. The observations show (Fig. 2-2a) small standard deviation of SSTs, between 0.2 and 0.4 K, on the path of an arc connecting Greenland and Iberian Peninsula and largest variance, up to 1 K, on the southeast of Newfoundland. Most of the models indicate that the SSTs mainly vary in the west part of the NA (Appendix C2, Fig 12A), so there is large temperature range on the path of the NA current and of the Labrador Current further to the south (Appendix C2, Fig 2A). Therefore, it can be inferred that most of CMIP5 models are not able to simulate the correct position and evolution of the individual ocean currents (Willebrand et al. 2001). The model closest to the geographical distribution of the observed SSTs standard deviation is CCSM4 (Fig. 2-2b).

Table 3 RMSE of the 11 CMIP5 models used in this study.

Model	RMSE	Model	RMSE
GFDL	1.77	INM-CM4	2.29
CCSM4	1.78	GISS	3.00
CSIRO	1.79	IPSL-CM5	3.10
NorESM	1.93	HadCM3	3.28
CanESM2	2.27	MRI- CGCM	2.64
MPI-ESM r1	2.28		

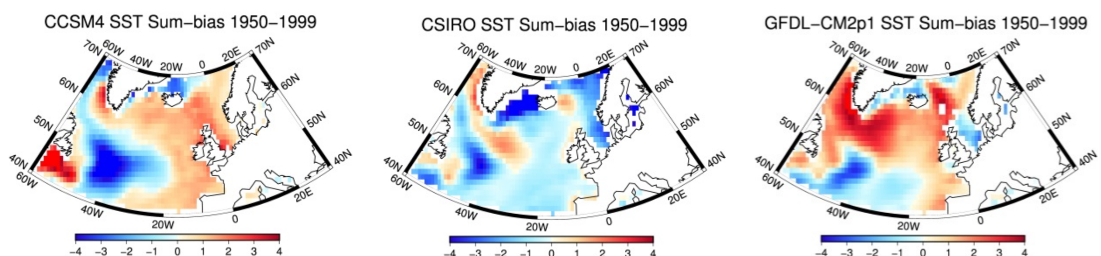

(a) (b) (c)

Figure 2-1 Mean summer SST bias between COBE2 and the CMIP5 models (a) CCSM4, (b) CSIRO and (c) GFDL, for the period 1950-1999.

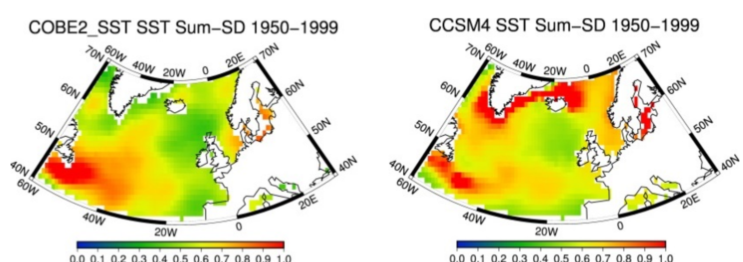

(a) (b)

Figure 2-2 Standard deviation of summer SSTs for (a) COBE2 and (b) CCSM4, for the period 1950-1999.

2.3.2 Leading modes of variability

In addition to investigating the variability pattern in terms of spatially resolved standard deviations, EOFs reveal the main patterns of co-variability in a given region. Therefore in terms of CFRs it is important for the models to simulate an appropriate spatial co-variability structure. Several studies already performed an evaluation related to the spatial co-variability of NA SSTs (Cannaby & Hu 2009; Fan & Schneider 2010), but for our purposes regions north of 60° are also important. Those changes in the geographical domain will ultimately impact on the structure of the individual EOFs (Legates 1991) and therefore it is necessary to carry out a separate EOF analysis for our region of interest.

Figures 2-3 and 2-4 depict the first and second EOF of models and data, respectively. The third EOF pattern is shown in the Appendix C2 (Fig. 5A). The first EOF (Fig. 2-3) represents around 30% of the variance in most simulations, except for the INM, HadCM3 (Appendix C2, Fig. 3A) and MPI models with reduced values around 20%. The corresponding eigenvector map of the COBE2 data describes a zonal dipole of the NA SST anomalies. The amplitude of this dipole is largest in the northern NA, at about 55˚ N and in the southeast of our study area close to the Iberian Peninsula, with SST anomalies of the opposite sign. The EOF maps derived from the models CanESM2 and CCSM4 also depict a zonal dipole, but are different to the one shown by COBE2. The EOF pattern of MPI-ESM shows some similarities to the COBE2 data, with cold SST anomalies north of 55˚ N and to the south and warm SST anomalies in some areas of the subpolar gyre. The EOF pattern of CCSM4 does not display warm anomalies in the area close to the Iberian Peninsula, but it depicts both the northern NA warm anomalies and the cold ones of the subtropical gyre. The CanESM2 model shows similar results as the CCSM4, while the rest of the models show dipole or monopole patterns with different centers. Generally, AMO-like variability is found in the temporal evolution (PC1) of the 1st EOF patterns for both CMIP5 models and the COBE2 data for the period 1950-1999. Assuming that the AMO is externally forced, we expect significant correlations between the PC1 of the models and the observed AMO for the period 1950-1999. Taking into account the effect of serial correlation, significant correlation at the 5% level of r=+ 0.3 is found between the PC1 of the models CanESM2 and CCSM4 when correlated to the COBE2 AMO for the period 1950-1999. These results indicate that the temporal evolution of the AMO in the models CCSM4 and CanESM2, is likely driven to some extent, although not totally, by the external forcing.

The second EOF of SST variability (Fig. 2-4) represents 20% of the variance in almost all models, with the MPI and HadCM3 models again showing reduced values of around 13%. This second EOF for COBE2 shows a dipole centered on the subpolar gyre and the Norwegian coast. This is also shown by the CCSM4 model, but the center of the east pole is located at the south coast of Greenland and of the west pole at the coast of Europe, while

CSIRO and MPI-ESM models also show this relationship between the SSTs of the west and the northeast of the study region. In general almost all models capture the strong center of variability over the south of Greenland, but with a northwestward shift of its center. Finally, the pattern shown by the third EOF (Appendix C2 Fig. 5A) is not realistically represented by any of the models.

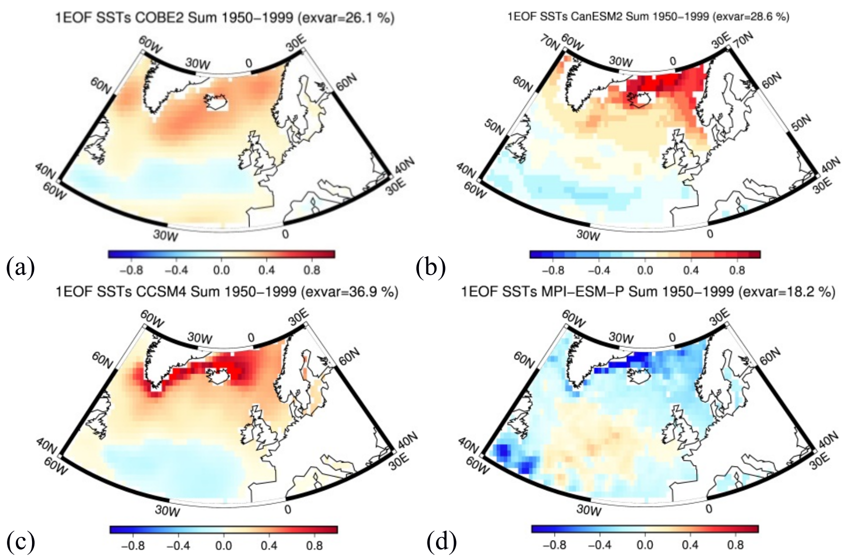

Figure 2-3 1st EOF of the detrended summer SSTs of the period 1950-1999 for (a) COBE2 and the Models (b) CanESM2, (c) CCSM4 and (d) MPI-ESM-P.

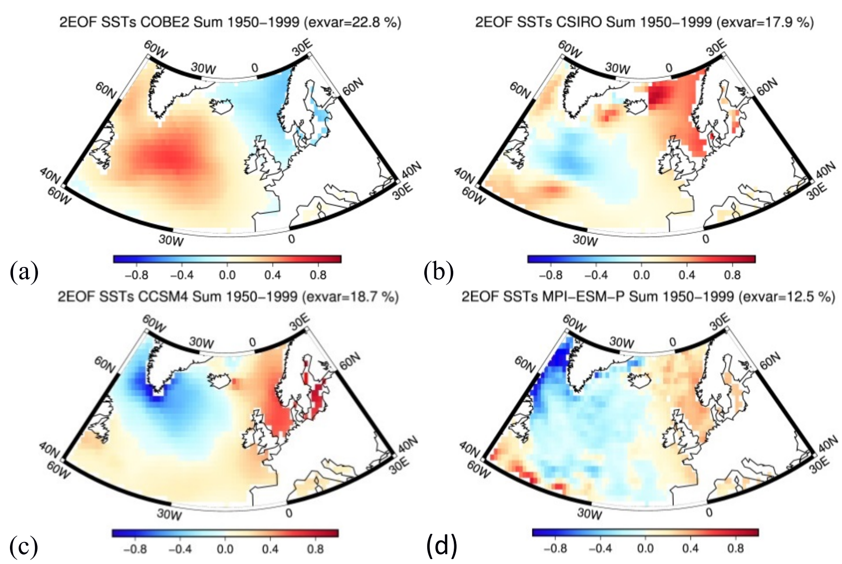

Figure 2-4 2nd EOF of the detrended summer SSTs of the period 1950-1999 for (a) COBE2 and the Models (b) CSIRO, (c) CCSM4 and (d) MPI-ESM-P.

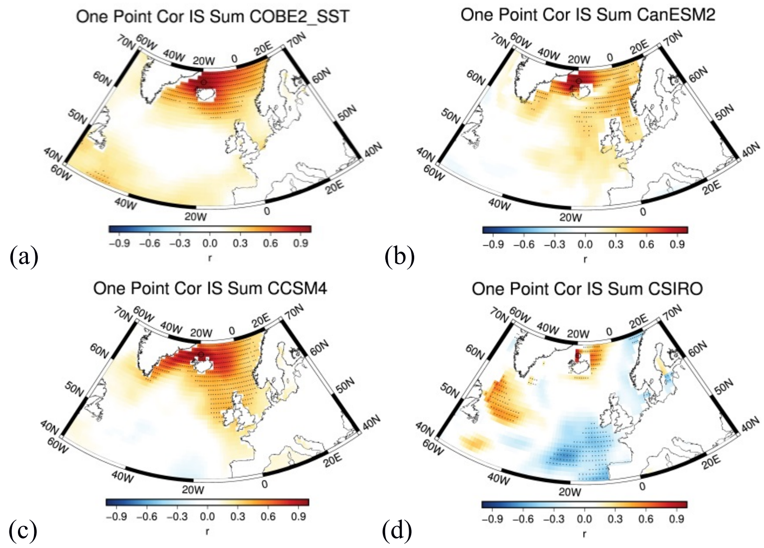

Figure 2-5 Correlation patterns (one-point correlation maps) for the Icelandic Shelf IS summer SSTs, for the period 1950-1999, for (a) COBE2 and the models (b) CanESM2, (c) CCSM4 and (d) CSIRO. Hatched areas indicate values statistically significant at the 1% level according to a statistical test taking into account the effect of serial correlated data.

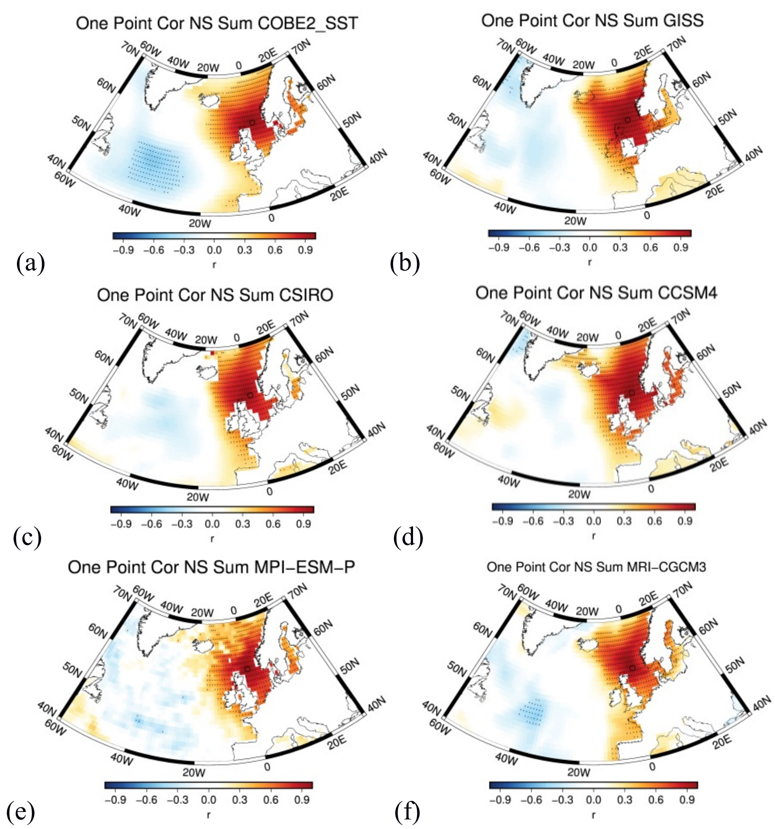

Figure 2-6 As in Figure 2-5, but for (a) COBE2 and the models (b) GISS, (c) CSIRO, (d) CCSM4, e) MPI-ESM-P and f) MRI-CGCM3 for the site in the North Sea (NS).

2.3.3 Correlation patterns of collection sites of Arctica islandica

For an evaluation of the models related to their potential use for paleoclimatic applications and reconstructions using oceanic proxy data, we correlate SSTs in two model regions, co-located with two proxy sites of Arctica islandica in the NA, with all grid-cells SSTs in the study area simulated by the same model. The locations are in the Icelandic Shelf (IS, Fig. 2-5) and in the northern North Sea (NS, Fig. 2-6). The resulting correlation patterns are compared with the derived in the same way for the COBE2 data set. This comparison between COBE2 and the eleven initially chosen models, reveals that the correlation patterns regarding the IS are well represented by most models, with the largest differences over the southern part of the region where some models show anti-correlation with the IS SSTs (Appendix C2, Fig. 6A). CanESM2 and CCSM4 simulate well the spatial distribution shown by COBE2. Statistically significant correlation at 1% level is shown by COBE2 over the area surrounding the collection site of Iceland with positive values between r=+0.7 and r=+1, including the areas of the East Greenland Current and the northern coast of Norway. Even though the CSIRO model was one of the best performing models in terms of RMSE, mean bias, variance and leading modes of variability, it does not show the aforementioned maximum correlation with the areas of the NA indicated by the analysis based on COBE2. A closer look at CSIROs results, regarding the temperatures at the north of Iceland, shows that most of the values are covered by sea ice. Furthermore, the number of grid points between Iceland and Greenland is reduced due to the coarse resolution of CSIRO model (see Table 1) and therefore these areas are mostly represented by sea ice or represent land grid-cells.

According to COBE2, the correlation with the collection site at the North Sea (Fig. 2-6) reveals a dipole pattern between the positive correlated values around NS and the negative correlated values at the east of Newfoundland. The models that can replicate the COBE2 pattern, showing some grid points of negative correlation values in the central Atlantic are CCSM4, MPI-ESM, GISS, MRI and CSIRO. The dipole pattern shown by COBE2 between NS and the central NA is also one of the dominant patterns of SST co-variability, as indicated by the second EOF, but is not reproduced in any of the model simulations. Finally, all models show the influence (i.e. high correlations) of the surrounding waters on the NS location.

2.3.4 Long term trends

SSTs provided by the CMIP5 models are additionally tested on their long-term trends over the second half of the 20th century. In this analysis we calculated the linear trends of the summer SSTs, for the 50 year period from 1950-1999 (Appendix C2, Fig. 8A). COBE2 shows that SSTs along the coast of Europe, along the north coast of Iceland and south of Newfoundland have undergone warming, while the SSTs south of Greenland and on the

Norwegian coast show a negative temperature trend over the 50 year period (Fig. 2-7). As shown in the Appendix C2 in Fig. 8A, none of the eleven CMIP5 models are able to capture the SST trends shown by COBE2 over the NA for this period, but they can capture some of the individual characteristics in specific areas. Nor-ESM and MPI-ESM models show the negative trends along the coast of Norway reaching 0.4˚ C per decade, while GFDL, CCSM4 and GISS the positive trends north of Iceland, with GFDL better approaching the magnitude shown by COBE2 (~0.4˚ C per decade). HadCM3, INM-CM4 and MRI-CGCM3 agree with the results of COBE2 only at the coast of Europe, while CSIRO and IPSL show warming to be dominant in the region of NA. As the external forcing applied in all simulations is similar, the way different processes are represented within each model could be the reason for the disagreement, not only between models and observations, but also amongst the individual models (Taboada and Anadón 2012).

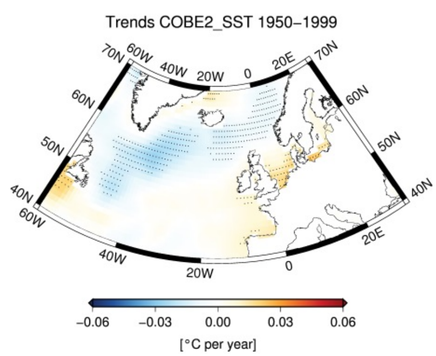

Figure 2-7 Summer SST trends of the period 1950-1999 as calculated with COBE2 SSTs. Hatched areas indicate values statistically significant at the 1% level according to a statistical test taking into account the effect of serial correlated data.

Table 4 Pearson correlation between the 10 year running mean of the CMIP5 and COBE2 AMO. *The AMO for the models GFDL and HadCM3 was calculated for the years 1861-2005 and 1859-2005, respectively.

Model (years 1850-2005)	**Correlation for the AMO 10y running mean**	**Significance (denoted with 1) at the 5% significance level**	**Model (years 1850-2005)**	**Correlation for the AMO 10y running mean**	**Significance (denoted with 1) at the 5% significance level**
*GFDL	0.20	0	MPI-ESM r3	0.60	0
CCSM4	0.60	0	GISS	0.40	0
CSIRO	0.50	0	IPSL-CM5	0.60	1
NorESM	-0.30	0	*HadCM3	0.70	1
CanESM2	0.40	0	MRI- CGCM	0.40	0
MPI-ESM r1	0.30	0	INM-CM4	0.50	0
MPI-ESM r2	-0.03	0			

2.3.5 Atlantic Multidecadal Oscillation

The model representation of the AMO, an important factor of decadal climate variability in the NA realm (Ruiz-Barradas et al. 2013), was also investigated. The AMO was calculated for the eleven CMIP5 models used in this study and also for two additional realizations (r2, r3) of the MPI-ESM model (Appendix C2, Fig 10A). As seen in Figure 2-8, the best performing models in terms of bias and variance do not follow the same AMO index that was calculated using the COBE2 SSTs. The AMO 10 year running mean was calculated and is shown in Figure 2-8, with the black line for COBE2-AMO and with the red line for the Models-AMO. If the AMO variability is externally induced, we can expect strong correlations between the COBE2 data and the CMIP5 models, as the external forcing applied in all simulations is similar. The Pearson correlation of the AMO running mean between data and models is shown in Table 4. Taking into account the effect of serial correlation, the models that exhibit statistically significant correlation at the 5% level are IPSL-CM5 and HadCM3, with correlation coefficients approximately equal to r=+0.6 and r=+0.7, respectively.

The r1, r3 and r2, r3 pairs of realizations of the MPI-ESM model are driven with the same forcing conditions (with a different aerosol forcing uncertainty between r1, r2) and with different initial conditions. Therefore, the ratio of the forced AMO variability to total variability between the pairs of realizations can be estimated by the correlation of their respective AMO time series (Table 5). The correlation coefficient between the different realizations of the MPI-ESM model is not statistically significant at the 5% level, indicating that for the MPI-ESM model the AMO variability is to a large degree unaffected by changes in external forcings. However, this does not generally rule out that the real-world connection is different and it does not imply that other models will show the same behavior.

The effect of large volcanic eruptions (AOD>0.2) can be seen in each modelled AMO, but prior to 1980 the AMO variability is largely model dependent. During the last 20 years it seems that the AMO index from most of the models is closer to observations, suggesting some role of the external forcing in pacing the AMO. Generally, the anomalies vary between ±0.4 ˚C for COBE2 and for most CMIP5 models, indicating that the CMIP5 suite captures the range of observed amplitude of decadal-scale SST variations of the NA area. The spatial structure of AMO, for both models and data, is determined by linearly regressing the grid point SST onto the corresponding modelled or reanalyzed AMO index (Appendix C2, Fig. 9A). Despite the different temporal evolution in the CMIP5 models' AMO, almost all models are consistent in showing a warming across the entire NA as shown by COBE2. This is also shown by Ting et al. 2011 who found a well-defined spatial pattern for AMO in the NA, albeit with differing temporal behavior of the phenomenon between models and observations.

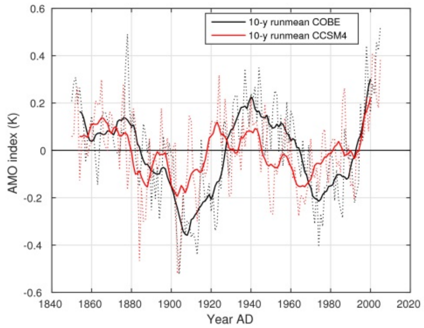

(a)

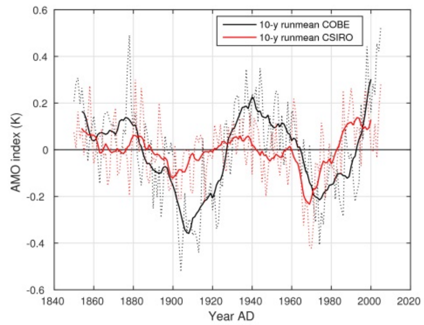

(b)

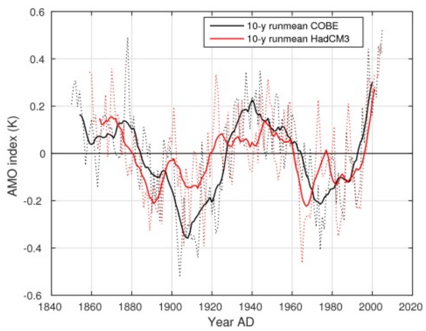

(c)

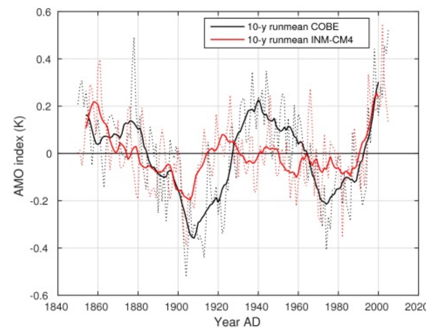

(d)

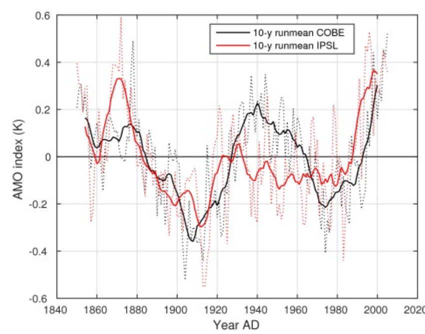

(e)

Figure 2-8 AMO index as calculated from COBE2_SSTs (black dotted line) and from CMIP5 model SSTs (red dotted line). Black and red solid lines are the ten year running mean for the COBE2 and models, respectively.

Table 5 Pearson correlation of the AMO 10-year running mean between the different realizations of the MPI-ESM model.

Realization number	**Correlation for the AMO 10y running mean**	**Significance (denoted with 1) at the 5% significance level**
r1 - r3	0.29	0
r2 - r3	0.16	0

2.4 Discussion

2.4.1 RMSE, mean bias and variance

Most of the CMIP5 models analyzed in this work show a common cold SST bias east of Newfoundland, which is accompanied by a warm bias near the coast (Fig. 2-1). Willebrand et al. (2001) showed that these biases are largely due to the early separation of the Gulf Stream, far too north from the coast of Cape Hatteras, and the turn of the NA Current northward near the mid-Atlantic ridge region and not at the Grand Banks of Newfoundland. MPI-ESM and CanESM2 show relatively large biases in the correct spatial simulation of the path of the Gulf Stream, while the INM models' colder temperatures are expanded to the north (Appendix C2, Fig. 1A). One reason for these dissimilarities might be the different spatial resolution in each model. Previous studies have shown that when ocean models are integrated at higher resolution, the representation of these currents is improved due to the better representation of meso-scale features (Smith et al. 2000; Bryan et al. 2007). This is, however, not necessarily the case for the INM model, which has the highest spatial resolution compared to the other models shown in Figure 2-1. Accordingly, its cold bias is still dominant over most regions of the NA Ocean, and therefore other processes are obviously playing a more important role in explaining differences between these models. One reason might relate to the anthropogenic aerosol concentration changes that influence the simulated spatial response of the NA SSTs. Booth et al. 2012 found that the inclusion of aerosol indirect effects in model simulations allows for a better representation of the spatial structure of NA SST variability. Another cause of discrepancies between models could relate to a somewhat different representation of the Atlantic Meridional Overturning Circulation (AMOC). Wang et al. (2014) found common bias patterns among CMIP5 climate models and attributed them to AMOC and its associated northward heat transport. Negative SST anomalies are shown in the path of East Greenland Current by all models, except by the MPI model, which shows a warm bias compared to the COBE2 SSTs. Model biases are in the order of ±4˚C and the model resolution and physical implementation might still not be realistic enough to represent certain features of this area (i.e. topography, meltwater) that are important for a good match between models and data. In addition to the coarse resolution, the magnitude and large scale patterns of SSTs are also influenced by additional factors such as surface and cloud albedo, and sea ice distribution (Hasumi 2014). Franco et al. (2012), found that most of the 5 km ice sheet topography of southeast Greenland can be reproduced at lower resolutions and that a model resolution of at least 10–15 km is needed to resolve the steep slopes in the vicinity of the ice sheet margin. Discrepancies could also arise by an overestimated transport of momentum, salt and heat diffusion around Iceland within the simulations (Logemann and Harms 2006).

The underestimation of the SST variability in the path of the East Greenland current by almost all models could also have its roots in the observational coverage related to the COBE2 data. For instance, the study of Deser et al. (2010) claims that the observation coverage of SSTs over these areas has increased since 1960. However, approximately during 1950–1979 the coverage, is only around 20-50% compared to the number of measurements south of Iceland. Furthermore, there is a suspect abrupt jump in the COBE SSTs in that region around 1979 (Loder et al. 2015). Additionally, errors could result from a lack of atmospheric processes in the models i.e. an underestimation of low cloud cover is a cause of significant errors in radiative fluxes (Kauker 2003), as the SST response to shortwave radiative forcing is thermally direct (Cheng et al. 2013) and low-level stratiform liquid and mixed-phase clouds are found to be the most important contributors to the Arctic surface radiation balance (Shupe and Intrieri 2004). Another explanation could be the sea ice export and variation, so the changes of albedo and fresh water input of the area, during the 50 years of study (Halvorsen et al. 2015).

To quantify the magnitude of spatial distribution of the summer SST variability, Figure 2-2 shows the standard deviation of the mean summer SSTs of the period 1950–1999 for the CMIP5 models and for COBE2. The COBE2 SSTs show their largest variability reaching ±1˚C in the western boundary current region of the Gulf Stream, coinciding with a region of maximum north-south mean SST gradient (Deser et al. 2010). The large SST variability shown by the data in this region is captured well by the CCSM4 model, while the rest of the models show that the SSTs mostly vary in the west and south parts of the study region. Along the path of the East Greenland Current, the SSTs vary by ±0.4˚C according to COBE and by ±1˚C according to the CMIP5 models. In this case, due to sea ice export from the Arctic Ocean and continental runoff (melt water is only added into the ocean during the summer half of the year), one could expect a larger variability in the observed summer SSTs than the one reproduced by the models. Many studies show that SSTs in the high-latitude Arctic Ocean are largely governed by sea-ice and continental runoff, rather than by evaporation and precipitation controlling low-latitude tropical oceanic variability. In addition, global satellite analyses and models incorporating remotely observed SSTs may be inaccurate due to lack of direct measurements for calibrating satellite data (Bai et al. 2015). On the other hand, due to lack of consistency in time, space and the number of SST measurements north of 60˚ N, the small variance shown by COBE2 on the east coast of Greenland and on the north coast of Iceland must be interpreted with care.

2.4.2 Leading modes of variability

Much of the spatial structure of SST variability is already highlighted by the variance, but it does not provide information on the spatial co-variability of SST variations. One common approach to investigate spatial co-variability is the EOF analysis. The EOF modes are pure geometric deconstructions of the domain, not considering any structure in the SST standard deviation (Wang et al. 2014). The differences between models and data may be a result of the decomposition into the linear combination of orthogonal spatial modes being driven by the large variability of SSTs simulated by the models (Fig. 2-2) along the path of the East Greenland current. Cannaby and Hu (2009) showed a zonal oscillatory mode of the NA SSTs, with amplitude of the eigenvector of the zonal pattern representing only 9% of the summer SST variability, being the 3rd mode derived from the SSTs in the winter months. Other studies found that there are two dominant SST modes in the NA derived from observations in the 20th century: a dipole mode on biennial and decadal time scales and a monopole on interdecadal time scales (Kushnir 1994; Deser and Blackmon, 1993). The dipole becomes a part of a tripole if the domain is extended to the south (Fan and Schneider 2010). An important point when comparing EOF patterns calculated over a different spatial domain relates to the fact that the relative significance of each independent mode of variability is spatially dependent. Therefore, results of EOF analysis depend on the spatial domain of the data on which the analysis is performed. The length of the data set used could influence the ranking of the EOF patterns in terms of explained variance, i.e. the ranking of eigenvalues (Cannaby and Hu, 2009). This is one of the reasons that could explain why the EOF results of our study area are different from those of other studies (e.g. Wang et al. 2014, for the central and southern NA).

The study by Marshall et al. (2001) shows that the leading pattern of SST variability in the NA is a tripole, with two poles in the NA above 40°N and the third pole near the Gulf of Mexico. These findings agree with our results (Fig. 2-4) regarding the second dominant pattern of SST variability in the NA, but due to the southerly limit of our study region, around 40°N, the 3rd pole cannot be seen. Marshall et al. (2001) relates this pattern to a direct response of the ocean to the anomalous air-sea fluxes controlled by the North Atlantic Oscillation (NAO). NAO is a large scale teleconnection pattern of atmospheric variability at sea level pressure, that refers to a reorganization of atmospheric mass between the subtropics of the Atlantic sector and the Arctic (Wallace and Gutzler 1981; Walker and Bliss 1932; Deser et al. 2010). One could argue that because NAO is more active from December to March we should not see this NAO related pattern in our results, as our study is restricted to the summer season. However, Gastineau and Frankignoul (2014) found a summer SST tripole, similar to the traditional SST tripole forced by the NAO during winter, that is lagged by an anticyclone over the subpolar NA.

2.4.3 Correlation patterns of collection sites of Arctica islandica

In Figure 2-5 we present the one-point correlation patterns by correlating SSTs of the Icelandic Shelf for the period 1950–1999 with the entire central and northern NA Ocean. COBE2 shows strong and statistically significant correlations (at 1% level of significance) between the IS and the SSTs north of Iceland, while CanESM2 and CCSM4 models additionally show strong and statistically significant correlations along the coast of Europe (r~0.5) and weak negative correlations over the southern domain of our study region. The positive correlation between these regions can be expected because water mass transformation in the Iceland Sea produces Arctic Intermediate Water, which overflows the Greenland-Iceland and the Iceland-Faroe Ridges and contributes to the North Atlantic Deep Water (Swift and Aagaard 1981). Other models show statistically significant and strong correlations in the south and/or west part of our study region. As mentioned previously, NA SSTs are affected by the NAO and when correlation maps are displayed between SST anomalies and the NAO index they show positive anomalies in high latitudes and the subtropical area and negative anomalies over middle latitudes (Czaja and Frankignoul 2002; Bojariu and Gimeno 2003). NAO differently affects SSTs in different regions and that could be a reason for the negative correlation shown between the temperatures over the high and middle latitudes by some models in Figure 2-5. Another interesting fact relates to the comparison of each graph of Figure 2-3 and Figure 2-5. Here we can see that for COBE2, and for most models, the dominant mode of variability of the NA summer SSTs is the spatial pattern shown by the correlation of SSTs with the ones of the Icelandic Shelf. The correlation between the summer SSTs of the NA and a location in the northern North Sea is shown in Figure 2-6. COBE2, CSIRO, MPI-ESM and the GISS model show a dipole between the east and west NA SSTs. This dipole seems to represent the correlation pattern between SST anomalies and NAO shown by Wanner et al. (2001).

2.4.4 Long term trends

A calculation of the NA local SST trends was performed (Figure 2-7) to compare the observed and model simulated temperature change for the period 1950-1999. CSIRO, GISS and the IPSL model show a basin wide SST warming trend that reaches 0.6 ˚C per decade, while the rest of the CMIP5 models show both cooling and warming trends in different areas. The COBE2 data show a statistically significant cooling, approximately equal to 0.4 ˚C per decade at high latitudes and a warming trend on the coast of Europe south of the Scandinavian Peninsula. In the work of Knutson et al. (2006) the annual regional surface temperature trends in observations and models were assessed for the period 1949–2000, using the GFDL model. Similar to our results, model and observations do not agree, as the ensemble mean trend map shows a warming trend around 0.1 ˚C per decade in the region of NA and the observed trend shows cooling approximately equal to 0.2 ˚C per decade. Possible reasons for the disagreement between the CMIP5 models and between models and data could be the models internal climate variability (Knutson et al. 2006), the sparse data in high latitudes before 1970 (Smith et al. 1996) that affect the overall trend of the regions in the northern NA of the second half of the 20th century, and uncertainties in the historical forcing, climate sensitivity and the rate of heat uptake by the ocean (Stott et al. 2000). Even though it is not a part of this study, the additional comparison of SSTs with available SST reconstructions could fill the gaps in the data sets based on space-time statistical methods and provide a better understanding of the differences between data and models.

2.4.5 Atlantic Multidecadal Ocsillation

Positive AMO anomalies are shown by COBE2 (black line) during the 30 year periods 1850-1880, 1940-1970. All models exhibit AMO-like fluctuations (Appendix C2, Fig. 10A) and some of the models agree on the timing of the positive phases of AMO that the observed data show, but it is not clear whether that is internally generated by these models or they truly represent an externally forced signal. Several modeling studies have questioned the response of NA temperature variations to the ocean's internal variability. Lohmann et al. (2015) found the highest correlation coefficients between the AMO index and the NA SSTs in the tropical and subtropical regions, where the SSTs are mostly influenced by the external (volcanic, solar) radiative forcing (Otterå et al. 2010). The opposite picture is evident in several General Circulation Models (GCMs), which produce the AMO in the absence of external forcing (Knight et al. 2005). Ting et al. 2009 separated the externally forced component and the internally varying component of the NA SST variations and found that during the 20th century the NA displayed an internal oscillation of considerable magnitude. Thus, the AMO cannot be fully explained by the radiative forcing (Ting et al. 2014; DelSole et al. 2011; Zhang and Wang 2013). The models' errors regarding the representation of AMO may suggest that their ability to simulate and predict at decadal time scales is compromised, because it could possibly mean that they do not incorporate the mechanisms associated to the generation of the AMO (or any other source of decadal variability like the PDO) and in turn incorporate or enhance variability at other frequencies (Ruiz-Barradas et al. 2013).

As the externally forced part of the AMO can be estimated from simulations and meaningfully compared to other empirically reconstructed AMO indices based on oceanic proxy data like Arctica islandica, we focused our analysis on the models ability to reveal the externally forced part of the AMO by comparing the observed and simulated AMO evolution, acknowledging the ongoing uncertainties regarding the forced and internal nature of the AMO. This analysis could give more confidence to the models' output regarding longer time scales such as the last millennium, as it could be assumed that if some of the models can reveal the externally forced part of the AMO during a period manifested by anthropogenic forcing, then it is plausible that the same models can capture the externally forced part of the AMO during the preindustrial period.

2.5 Conclusions

The estimation of the skill of the CFR methods largely depends on the model used to evaluate the CFR method and the locations of the proxy network used to perform the spatially resolved CFR. Therefore, we first investigated the robustness of the CMIP5 simulated summer SSTs in the NA, compared to COBE2 data, for the second half of the 20th century. Regarding the representation of the spatiotemporal characteristics of the NA SSTs we found that even though the second dominant pattern of NA SST co-variability is captured to a certain degree by most models evaluated in this study, the first dominant EOF pattern is well represented by the models CanESM2, CCSM4 and represented to a certain degree by the models MPI-ESM and HadCM3. We can, therefore, expect that these models will provide with a better representation of the NA region's co-variability that is important for CFRs. Uncertainties will be introduced in a potential application of CFR by any of the models, as most of them suffer biases that coincide with regions of maximum model inter-annual variability. The models with the highest climatological error distributions are found to be GISS, IPSL-CM5, HadCM3 and MRI-CGCM. The simulated AMO reveals similar evolutions in the 2nd half of the 20th century within the models, but presents a prominent source of uncertainty for reconstructions.

To assess the capability of Arctica islandica collection sites to provide a good spatially resolved reconstruction, we tested the models ability to represent the co-variance of the spatially resolved NA SSTs and the SSTs at two of the Arctica islandica collection sites. Both the COBE2 data and the CMIP5 models showed that the IS and NS sites of Arctica islandica are promising sites that can be used to reconstruct the SSTs of the north-east Atlantic. The IS site does not provide any information about the central Atlantic, but it provides information about the northern NA, north of 60°N. A number of CMIP5 models, such as CanESM2, CCSM4, MPI-ESM and IPSL-CM5 can reproduce the IS teleconnection pattern shown by the COBE2 data. The site in the North Sea seems promising not only for the eastern NA basin but for the central Atlantic as well, as COBE2 shows a significant anti-correlation between the NS site and the central Atlantic. Some of the CMIP5 models can capture the NS teleconnection pattern shown by COBE2, while most of the models can capture the co-variance of the NS site SSTs to the surrounding waters. Therefore, we can expect that the given proxy record will contain a strong SST signal that might represent a basin-wide signal for the north-east Atlantic, which is an important result in the context of using CMIP5 models to paleoclimate reconstructions based on the proxy sites of Arctica islandica. The models that are found to simulate well most of the spatiotemporal characteristics of the NA SSTs and the co-variance of the SSTs of the two Arctica islandica collection sites are CanESM2, CCSM4 and MPI-ESM. In a forthcoming study we will assess the uncertainties relevant to paleoclimate reconstructions by using the best performing CMIP5 models, as evaluated in the context of this work, to test different CFR methods.

3. Pseudo-proxy evaluation of Climate Field Reconstruction methods of North Atlantic climate based on annually resolved marine proxy network

I tested two statistical methods to reconstruct the past SSTs of the North Atlantic Ocean based on annually resolved and absolutely dated marine proxy records of Arctica islandica. The methods were tested in a pseudo-proxy experiment set-up using state-of-the-art climate models (CMIP5 Earth System Models) and observations from the COBE2 SST data set. The multivariate linear regression methods assessed here are Principal Component Regression and Canonical Correlation Analysis. The methods were applied in the virtual reality provided by the global climate simulations to reconstruct the past NA SSTs, using pseudo-proxy records that mimic the statistical characteristics and network extent of Arctica islandica. Differences in the skill of the Climate Field Reconstruction were assessed according to different calibration periods and different proxy locations within the NA basin.

I found that the choice of climate model used as surrogate reality in the pseudoproxy experiment has a more profound effect on the evaluation of the reconstruction skill than the calibration period or the statistical reconstruction method. The differences between the two methods are clearer within the MPI-ESM model, due to its finer spatial resolution in the NA basin. The addition of noise in the pseudo-proxies is important in the evaluation of the methods, as more differences in the spatial patterns of the reconstruction skill are revealed. More profound changes between methods were obtained when the number of proxy records is smaller than five, making the Principal Component Regression a more appropriate method in this case. Despite the differences, the results show that the marine network of Arctica islandica can be used to skillfully reconstruct the spatial patterns of SSTs at the eastern North Atlantic basin.

3.1 Introduction

Several studies have targeted to reconstruct hemispheric or global average temperature from networks of proxy records (Mann and Jones 2003; Marcott et al., 2013; Moberg et al., 2005), as well as spatial patterns of past temperature changes at global (Rutherford et al., 2005; Wahl and Ammann 2007) and regional scale during the last millennium (Xoplaki et al., 2005; Luterbacher et al., 2004; Ahmed et al., 2013). Most of these studies have primarily used terrestrial proxy records, with very little marine proxies that could contain information about the vast ocean areas, e.g. over the North Pacific and the North Atlantic Ocean that cannot be represented by the terrestrial proxies. In the context of marine proxy networks, reconstructions of global Sea Surface Temperatures (SSTs) for the past 2000 years derived from individual marine reconstructions were recently published as a global synthesis of SST for the Common Era (CE), (McGregor et al., 2015). Due to the diversity of marine proxies used, McGregor et al., 2015 averaged each SST reconstruction into 200-yr bins, providing a synthesis of proxy data representative for global variations, yet loosing temporal information on decadal-to-multidecadal time scales. Other studies have targeted reconstructions of spatial patterns of SST changes using marine proxies, but mostly regarding regions in the tropics and subtropics (Evans et al., 2000; Wilson et al., 2006; Dowsett and Robinson 2009; Tierney et al., 2015). Regarding the North Atlantic (NA) Ocean, Gray et al., 2004 reconstructed the Atlantic Multidecadal Oscillation since 1567 AD using tree ring records, while Marshal et al., 2002 used sediment cores to locally reconstruct upper ocean temperature during the Holocene (10-0 ka B.P.).

In the present study, I test the potential of using a high-resolution marine proxy collected in the NA Ocean to reconstruct spatially resolved SST fields for the last millennium, and further test whether Climate Field Reconstruction (CFR) methods are appropriate for that specific marine proxy network. The proxy that motivates my pseudo proxy experiments is Arctica islandica. It is an absolutely dated (Scourse et al., 2006) annually resolved (Butler et al., 2009) and long lived bivalve mollusk (Butler et al., 2013; Jr et al., 2008) that can serve as a proxy archive for the Atlantic marine climate (Reynolds et al., 2017; Wanamaker Jr et al., 2012). It can be found in various regions in the North Atlantic including locations north of 60°N (Dahlgren et al., 2000) and, amongst others, it can be used to reconstruct SSTs (Eagle et al., 2013) and major NA climate modes like the AMO (Mette et al., 2015). Arctica's proxy collection sites have been found to contain a NA SST basin signal (Pyrina et al., 2017) which renders this proxy archive suitable for Climate Field Reconstructions.

Numerous reconstructions of large scale mean climate have employed CFR approaches which assimilate proxy records into reconstructions of the underlying spatial patterns of past climate change (Riedwyl et al., 2008; N Riedwyl et al., 2009; Touchan et al., 2005; Zhang et al., 2016). These methods use the covariance between the proxy series and the instrumental series during a calibration period in which the two series overlap. However, observational environmental records span only the past 150 years so that it is not assured that the covariance structure estimated at inter-annual timescales is also valid at decadal and multidecadal timescales. The magnitude of the reconstruction uncertainties will generally vary with the time scales (Briffa et al., 2001) and can possibly be underestimated if in prior analysis steps the proxy records have been previously screened according to their high covariance with instrumental records. Since a large number of proxy records is usually screened, this high proxy-observation covariance could be due to chance

(Osborn and Briffa 2006). Another reason that could lead to an underestimation of the reconstruction uncertainties is the possible long term inhomogeneities or deterioration back in time existing in the proxy records, which cannot be identified within the calibration period (Jones et al., 2009).

The CFR methods can, however, be tested using climate simulations as a test bed. In the virtual world of a climate simulation all variables are known at all times. CFR methods can be recreated in this world by producing pseudo-proxies, using the simulated temperature at the grid-cell level and contaminate these records with statistical noise, so that the link between pseudo-proxies and grid-cell temperature resembles the observed link between proxy-records and instrumental temperature. A very important assumption underlying all CFR methods relates to the general ability of the climate models to realistically simulate the spatial co-variance structure of the variable under consideration. This is difficult to assess, especially in the oceanic realm that offers only a sparse observational network prior to the 1950’s. Taking into account the available re-analysis products, efforts can be undertaken to at least test the plausibility of state-of-the-art climate models in correctly simulating present-day ocean circulation and related quantities (Pyrina et al., 2017).

Given a realistic simulation of the variable under consideration, the CFR methods can be then applied to those pseudo-proxy records to estimate a target variable, for instance the global, hemispheric or regional temperature. The pseudo-reconstruction can be then compared to the simulated target variable. The differences between the pseudo-reconstructed and simulated target variables can give information about the deficiencies of the statistical CFR. Pseudo-proxy experiments (PPEs) also allow testing the sensitivity of the pseudo-reconstructions to changes in the density and location of the pseudo-proxy network.

The performance of CFRs has been tested using PPEs by a number of studies (Rutherford et al., 2003; von Storch et al., 2004). Given the importance of the spatial information estimated in CFRs a growing number of studies has explicitly evaluated the spatial performance of CFRs (Smerdon et al., 2008; Li and Smerdon 2012; Wang et al., 2014; Dannenberg and Wise 2013; Evans et al., 2014), though only a few studies have tested the differences in the spatial performance of CRF methods according to the modeled climate that forms the basis of the PPE (Mann et al., 2007; Smerdon et al., 2011; Smerdon et al., 2016). These studies tested the spatial skill of CFR methods using information from a composite network including mostly terrestrial proxies. As CFRs depend on the characteristics of the proxy network used, such as proxy temporal resolution, growth season, character and level of noise, in my analysis I test CFR methods in the context of the annually resolved marine proxy network of Arctica islandica. The multivariate linear regression techniques tested are Principal Component Regression (PCR) and Canonical

Correlation analysis (CCA). PCR has been previously used to reconstruct climate using only marine proxy records (Evans et al., 2002; Marchal et al., 2002), while both methods have been commonly applied in the context of CFRs using annually resolved proxies (Smerdon et al., 2016; Smerdon et al., 2011; Gómez-Navarro et al., 2015). A fundamental assumption of PPEs is that the models can realistically simulate the spatiotemporal characteristics of the observed climate. Therefore, the models that are used in this analysis were chosen based on their ability to simulate the spatiotemporal characteristics of the observed NA SSTs and have been previously evaluated in the context of paleoclimate reconstructions (Pyrina et al., 2017).

3.2 Data

I performed a pseudo-proxy experiment using modeled and observed grid point SSTs co-located with proxy sites of Arctica islandica. The grid point SSTs were taken from the General Circulation Models (GCMs) CCSM4 and MPI-ESM-P, as well as the centennial in-situ observation-based estimate of SSTs, COBE2 (Hirahara et al., 2014). The SSTs represent the summer period (June-August) of the NA region between 60˚W — 30˚E and 40˚N — 75˚N, motivated by the growing season of the bivalve shell Arctica islandica (Schöne et al., 2004; Schöne et al., 2005). The pseudo-proxy sample sites are based on 5 real world proxy sites of Arctica islandica, that include collection sites in the North Sea (NS: 1˚E, 58.5˚N) (Witbaard et al., 1997), the Irish Sea (IrS: 5˚W, 52.5˚N) (Butler et al., 2009), the coast of Scotland (Sct: 7˚W, 56.5˚N) (Reynolds et al., 2013), the North Icelandic Shelf (IS: 20˚W, 66.5˚N) (Butler et al., 2013) and a location at Ingoya Island (InI: 24˚E, 71.5˚N) (Mette et al., 2015).

3.2.1 Observational and Proxy Data

I used the fully interpolated spatially complete observational data set COBE2 (Hirahara et al., 2014). The COBE2 data set was developed at the Japanese Meteorological Agency, covers the period 1850–2013 AD and has a spatial resolution of 1˚x1˚ grid. COBE2 data pass first quality control using combined a-priori thresholds and nearby observations and are later gridded using optimal interpolation. Data up to 1941 were bias-adjusted using "bucket correction" (Hirahara et al., 2014). COBE2 combines SST measurements from the release 2.0 of the International Comprehensive Ocean-Atmosphere Data Set, ICOADS (Worley et al., 2005), the Japanese Kobe collection, and readings from ships and buoys. The proxy data of Arctica islandica used in this analysis were downloaded from the National Centers for Environmental Information (NOAA, https://www.ncdc.noaa.gov/data-access/paleoclimatology-data/datasets) and refer to the 1357-year Arctica islandica reconstructed chronology from Butler et al., 2013. The multicentennial absolutely dated chronology was reconstructed using annual growth increments in the shell of Arctica islandica and spans from 649 AD to 2005 AD.

3.2.2 Models

I employed two climate models in this study, the CCSM4 model and the MPI-ESM-P model, which are part of the 5th phase of the Climate Model Intercomparison Project (CMIP5/ http://cmip-pcmdi.llnl.gov/cmip5/). The models' original output was re-processed and re-gridded to a regular grid to match the COBE2 data set. Therefore, the output was re-gridded onto a 1˚×1˚ degree horizontal resolution. The output of the models used in this study includes the combination of the past1000 runs and the historical runs, so that the period used spans from 850 AD to 1999 AD.

The CCSM4 (Gent et al., 2011) uses the atmosphere component Community Atmosphere Model, version 4 (CAM4) (Neale et al., 2013) and the land component Community Land Model, version 4 (CLM4) (Lawrence et al., 2012). Both components share the same horizontal grid (0.9˚ latitude × 1.25˚ longitude). The CCSM4 ocean component model (POP2) is based on the "Parallel Ocean Program", version 2 (Smith et al., 2010). The ocean grid has 320 × 384 points with nominally 1˚ resolution except near the equator, where the latitudinal resolution becomes finer, as described in (Danabasoglu et al., 2006). CICE4, the CCSM4 sea ice component model is based on version 4 of the Los Alamos National Laboratory "Community Ice Code" sea ice model (Hunke et al., 2008). The atmosphere, land, and sea ice components communicate both state information and fluxes through the coupler in every atmospheric time step. The fluxes between atmosphere and ocean are calculated in the coupler and communicated to the ocean component only once a day. The CCSM4 simulation starts at 850 and continues to 1850, where it matches up and is extended as an additional ensemble member of the CCSM4 twentieth century simulations that ends in December 2005 (Landrum et al., 2013). The forcings and boundary conditions follow the protocols of PMIP3 as discussed by (Schmidt et al., 2012) (https://pmip3.lsce.ipsl.fr/wiki/doku.php/pmip3:design:lm:final). For the volcanic forcing the ice core based index of Gao et al., 2008 is used, where several large volcanic eruptions have significantly larger aerosol optical depths compared to the Crowley et al. (2008) alternate reconstruction for PMIP3. Stratospheric aerosols are prescribed in the model as a fixed single-size distribution in the three layers in the lower stratosphere above the tropopause. Changes in total solar irradiance (TSI) are prescribed using the Vieira et al. (2011) reconstruction merged to Lean et al. (2005) at 1834 to have a smooth transition to twentieth-century CCSM simulations. The Pongratz et al. (2008) reconstruction of land use, proposed by PMIP3, is merged with that of Hurtt et al. (2009) used in the CCSM4 twentieth-century simulations to give a consistent and smoothly evolving land use change.

In MPI-ESM-P the atmosphere model ECHAM6 (Stevens et al., 2013) is run at a horizontal resolution of spectral truncation T63 (1.875), while the ocean/sea-ice model MPIOM (Marsland et al., 2003) features a conformal mapping grid with nominal 1.5 resolution. There is one grid pole over Antarctica and one grid pole over Greenland, which leads to considerably higher resolution in the North Atlantic. For land and vegetation the component JSBACH (Reick et al., 2013) is used and for the marine biogeochemistry the HAMOCC5 (Ilyina et al., 2013). The coupling at the interfaces between atmosphere and land processes, and between atmosphere and sea ice occurs at the atmospheric time step, which is also the time step of the land processes, except for the dynamic vegetation, which is updated once a year. The coupling between atmosphere and ocean as well as land and ocean occurs once a day. In the past1000 runs a prescribed CO2 is used. For volcanic aerosol optical depth and effective radius the Crowley and Unterman reconstruction (Crowley and Unterman 2013) is employed and the Pongratz et al. (2008) reconstruction of global land-cover and agricultural areas. For solar radiation is used the combined Vieira et al. (2011) total solar irradiance (TSI) reconstruction over the Holocene with the Wang et al. (2005) data set that provides the recommended solar forcing for the CMIP5 20th-century (1850–2005) simulations. In this work I used three experiments of the MPI-ESM model. The r1 and r2 experiments were initialized with the same ocean state, but they differ in the standard deviation of the assumed lognormal distribution of the volcanic aerosol size, while the simulations r2 and r3 use the same parameter setting but are started from different initial conditions (Jungclaus et al., 2014). For the historical simulations the applied boundary conditions follow the CMIP5 protocol, except for land-cover-changes, where the Pongratz et al. (2008) data set is used.

3.3 Methodology

Based on five proxy locations of Arctica islandica I reconstructed the summer SST evolution of the NA region during the preindustrial (850-1849 AD) and industrial (1850-1999 AD) periods of the last millennium, using two CFR methods. In both approaches the goal is to reconstruct the temperature and this is the variable considered as predictand. The predictors are the proxy indicators. To test the stationarity assumption of the calibration coefficients, I repeated the reconstruction of the summer SSTs by calibrating the regression models over different calibration periods. The calibration periods include time spans during a) the medieval period (1000-1049 AD), b) the little ice age (1650-1699 AD), c) the industrial period (1850-1999 AD), d) the preindustrial period (850-1849 AD) and c) recent years (1950-

1999 AD). The fields' inter-annual anomalies were reconstructed using the COBE2 reanalyzed SSTs and the CMIP5 modeled SSTs. To conclude whether the usage of different models or of reanalysis data has an effect on the reconstruction I correlated the original modeled or reanalyzed inter-annual anomalies of the NA field with the reconstructed modeled or reanalyzed inter-annual anomalies, respectively.

3.3.1 Principal Component Regression

The first step of the pseudo-proxy experiment is the estimation of the NA SST field co-variances for the different calibration periods using PCA (Equation 1). Each eigenvector is associated with a spatial pattern (EOF, empirical orthogonal function) and its temporal evolution (PC, principal component). In Equation 1, $\vec{x}_t$ is the field vector of the NA SST anomalies and i the number of eigenvectors. In our analysis I kept the first 10 eigenvectors, as they represent more than 90% of variability. The time, t, depends on the calibration period that I refer to.

$\vec{x}_t = \sum_{i=1}^{10} PC_{i,t}\overrightarrow{EOF_i}$ (Equation 1)

For the 5 sampled SST time series ($\mathrm{Proxy}_{j,t}$ with j representing the respective proxy location) I calibrated the regression model (Equation 2) against the PCs estimated during the calibration period and predicted the calibration coefficients, $\hat{\alpha}$, using PCR.

$PC_{i,t} = \sum_{i=1}^{10} \hat{\alpha}_{i,j} Proxy_{j,t} + \varepsilon$ (Equation 2)

In this approach I assume that the PCs are linearly related to the pseudo-proxies, so that they represent large-scale climate variations. This relationship is modeled through a disturbance term or error variable ε. The error could be an unobserved random variable that adds noise to the linear relationship between the dependent variable (PC) and the regressors (Proxy SSTs). Based on Principal Component Regression (Equation 3) I then predict the principal components $\widehat{\mathrm{PC}}_{i,t}$ during the reconstruction period, assuming that the calibration coefficients calculated in Equation 2, are stationary in time. In this case the time, t, depends on the reconstruction period that I refer to.

$\widehat{PC}_{i,t} = \sum_{i=1}^{10} \alpha_{i,j} Proxy_{j,t}$ (Equation 3)

Assuming that the dominant patterns of climate variability are similar in recent and past centuries, I predict the $\vec{\hat{x}}_t$ field vector of the NA SST anomalies for the reconstruction period, using the predicted $\widehat{PC}_{i,t}$ and the $\overrightarrow{EOF_i}$ patterns calculated in Equation 1. This stationarity assumption holds at least for multi-decadal timescales and allows us to deduce back in time the surface temperature patterns (Mann et al., 1998).

3.3.2 Canonical Correlation Analysis

The first step of the pseudo-proxy experiment using CCA is the eigenvalue decomposition and subsequent truncation of the NA SST field and the proxy SST field (Equation 1), during the calibration interval. The key feature of this analysis involves concatenating the pseudo-proxy SST time series, or in other words the predictor data, so that I can define both the time and space evolution of the climate system. After the transformation of the data to EOF coordinates I retained five empirical orthogonal functions, for each field, that were subsequently used to calculate the pairs of Canonical Correlation Patterns (CCP^{NA}, CCP^{pr}) and their time depended coefficients (CC^{NA}, CC^{pr}), as shown in Equations 4 and 5 for the NA SST field and the proxy SST field, respectively. The CC patterns are estimated when the correlation between their time depended coefficients is maximized and not correlated with the CC coefficients of another pair of patterns. Therefore, the CC coefficients fulfill the condition of orthogonality.

$$\vec{x}_t = \sum_{i=1}^{5} CC_{i,t}^{NA} \overrightarrow{CCP}_i^{NA} \text{ (Equation 4)}$$
$$\overrightarrow{Proxy}_t = \sum_{i=1}^{5} CC_{i,t}^{pr} \overrightarrow{CCP}_i^{pr} \text{ (Equation 5)}$$

The steps following, are the same as the ones used in the method PCR, but instead of regressing and predicting the PCs I use the $CC_{i,t}^{pr}$. To reconstruct the $\vec{\hat{x}}_t$ field vector of the NA SST anomalies I used the predicted $\widehat{CC}_{i,t}^{pr}$ and the $\overrightarrow{CCP}_i^{NA}$ patterns calculated in Equation 4.

3.3.3 Noise Addition

The pseudo-proxy experiments were conducted using idealized pseudo-proxies and noise-contaminated pseudo-proxies. Idealized pseudo-proxies are the raw grid point SSTs, from simulations or reanalysis, co-located with the collection sites of the bivalve shell *Arctica islandica*, while in the case of the noise-contaminated pseudo-proxies the grid point temperatures are deteriorated by adding statistical noise in order to mimic more realistically the real world proxy records of *Arctica islandica*. The exact level of non-climatic noise in the real proxies is usually not known and could be strongly dependent on the nature of the proxy indicator (von Storch et al., 2009).

The dynamics of many physical processes can be approximated by first or second order ordinary linear differential equations, whose discretized versions can be represented by autoregressive processes (von Storch and Zwiers 2001). An autoregressive processes of order k=0, where k is the time lag, is white noise (Z_t). An autoregressive processes of order k=1, or AR(1), represents a discretized first order linear differential equation and can be written as:

$$X_t = a_1 X_{t-1} + Z_t \text{ (Equation6)}$$

where α_1 is the damping coefficient and Z_t represents a random variable uncorrelated in time. The Yule-Walker equations can be used to derive the first k+1 elements of the autocorrelation function and for an AR(1) process they give $\alpha_1=\rho_1$, where ρ_k is the autocorrelation for lag k. For a positive damping coefficient, an AR(1) process is unable to oscillate. Its 'spectral peak' is located at frequency $\omega=0$ and therefore the variation X_t behaves as red noise. Furthermore, the stationarity condition for an AR(1) process implies that $|\alpha_1|<1$. Therefore, to approximate the variation of noise in *Arctica islandica* the autocorrelation function of an *Arctica islandica* chronology located at the Icelandic shelf was calculated and found equal to 0.4 at lag 1 year. Assuming that the relative amount of noise is constant for all the noise-contaminated pseudo-proxies, red noise pseudo-proxies were constructed by fitting the parameters of the AR(1) process to the simulated grid-point temperatures.

3.4 Results

3.4.1 Ideal Pseudo-proxies

In this section the results are based on 5 ideal pseudo-proxies co-located to Arctica islandica sites that are "sampled" from the SST output fields of 3 realizations of the MPI-ESM model, the CCSM4 model and the COBE2 data set. The correlation between the reconstructed and the original SST-anomaly evolution of the NA field is calculated for two reconstruction periods (preindustrial and industrial) and for the two different reconstruction methods. The methods are calibrated during the Medieval period, the Little Ice Age, the recent period, the industrial period and the preindustrial period and the results are shown in the Appendix C3 (Figures 1S-5S). The results shown here regard the reconstruction of the industrial period when the regression models are calibrated during the recent period and LIA (Figures 3-1 and 3-2 respectively), and are shown for the CCSM4 model, the realization r1 of the MPI-ESM model and the COBE2 data. Verification experiments were performed to test how well the calibration coefficients work when the reconstruction interval is the same as the calibration interval; see in the Appendix C3 the first and third columns of Figure 4S and the second and fourth columns of Figure 5S.

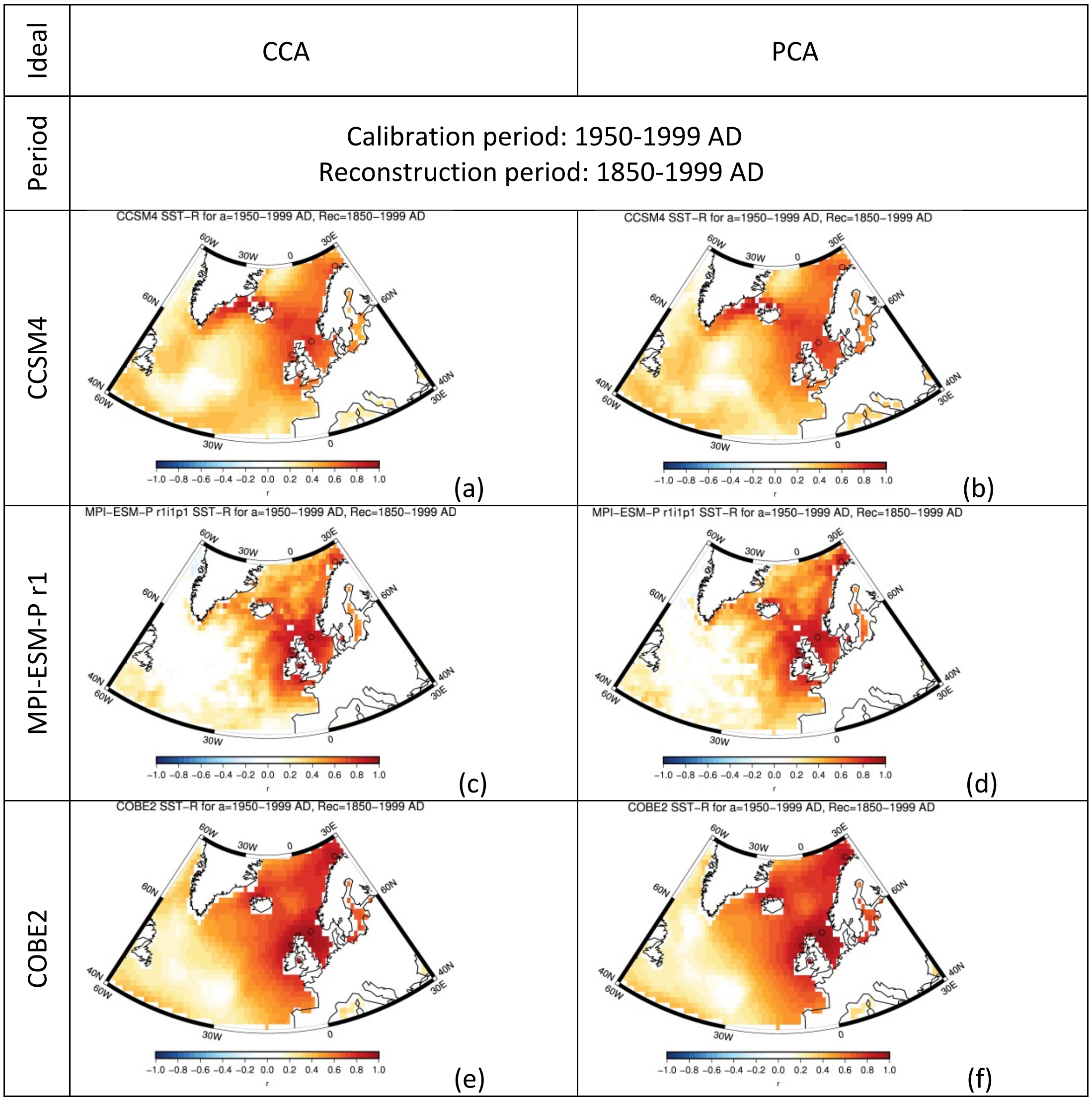

Figure 3-1 Correlation coefficient between the reconstructed and the original SST-anomaly evolution of the NA field during the preindustrial era. The results are given for the recent calibration period (1950—1999 AD) and for the two different reconstruction methods (left column CCA, right column PCA) for the models CCSM4 (first row) and MPI-ESM-P r1 (second row) and the reanalysis data COBE2 (third row).

Looking at the results of the same model simulation and method but for different calibration periods we can see that the spatial skill of the reconstruction does not significantly change according to the period where the regression models were calibrated, therefore the calibration coefficients can be considered stationary. Additionally, the patterns shown by the correlation maps do not significantly change when a different method is applied, indicating that with both methods the SST evolution of the eastern NA basin can be reconstructed using the 5 proxy locations of Arctica islandica. More pronounced differences are found between the pseudo-reconstructions conducted with each model and also with the pseudo-reconstruction using the reanalysis. For instance, when the industrial period is reconstructed using the recent calibration period (Figure 3-1), according to COBE2 and MPI-ESM-P the SSTs west of Ireland and in the North Sea can be skillfully reconstructed with a correlation coefficient equal to r=+1, but according to CCSM4 the skill is reduced over the same regions. Another interesting finding is that the SSTs along the south-east coast of Greenland can be reconstructed with a good skill using the CCSM4 model (r~+0.9), while the reconstruction skill drops according to COBE2 (r~+0.8) and the MPI-ESM model (r~+0.5). The correlation maps given by the CCSM4 model and the COBE2 data are smoother that the ones given by the MPI-ESM-P model. The areas that exhibit correlation values higher than r=+0.6 are larger in COBE2 compared to MPI-ESM-P and CCSM4.

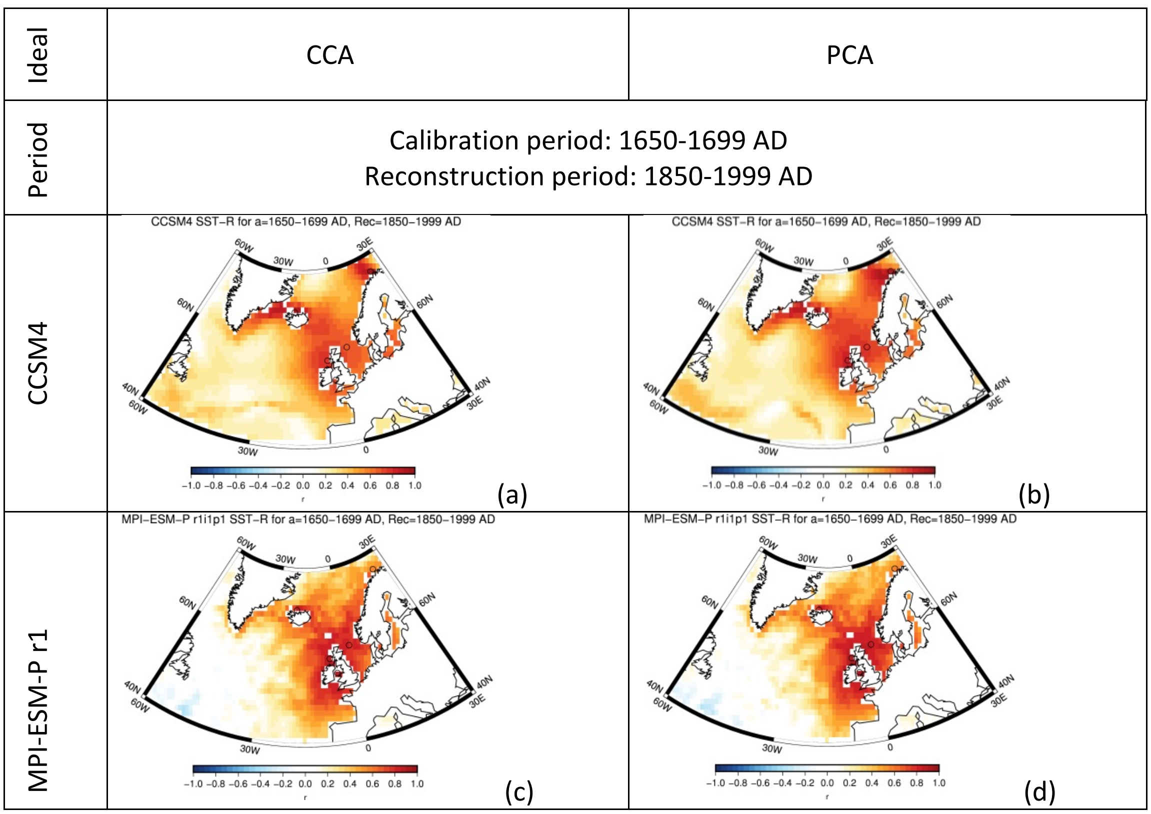

Figure 3-2 Correlation coefficient between the reconstructed and the original SST-anomaly evolution of the NA field during the preindustrial era. The results are given for the LIA calibration period (1650—1699 AD) and for the two different reconstruction methods (left column CCA, right column PCA) for the models CCSM4 (first row) and MPI-ESM-P r1 (second row).

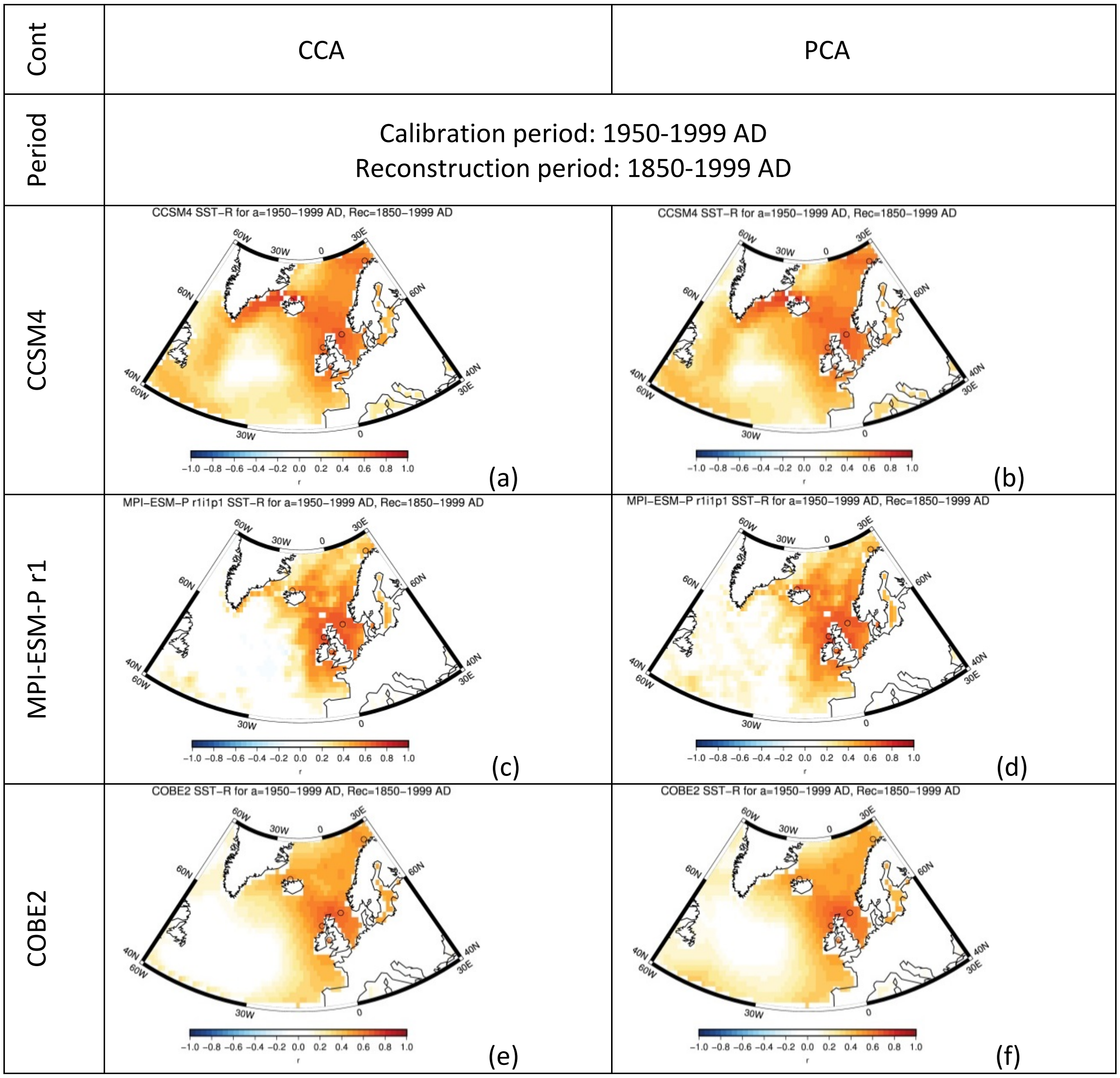

Figure 3-3 Same as in Figure 3-1, but for the noise contaminated pseudo-proxies.

3.4.2 Noise contaminated pseudo-proxies

The results of this section are illustrated as in section 3.4.1, but the calculations were performed with noise-contaminated pseudo-proxies. The methods calibrated during the recent period and LIA are shown in Figures 3-3 and 3-4 respectively for the CCSM4 model, the realization r1 of the MPI-ESM model and the COBE2 data. Compared to the results regarding the ideal pseudo-proxies, the reconstruction skill has decreased with the maximum correlation between the reconstructed and the original SST-anomaly evolution of the proxy sites reaching r=+0.8, depending on the model used and the pseudo-proxy location (Appendix C3, Figures 6S-10S). The areas that exhibit correlation with values higher than r=+0.6 are more limited in extent when compared to the ideal pseudo-proxy experiment. According to both methods, the east part of the NA can be skillfully reconstructed with the proxy sites of Arctica islandica. The differences amongst models are more profound than the differences between the different calibration periods.

<table>
<tr><td>Cont</td><td>CCA</td><td>PCA</td></tr>
<tr><td>Period</td><td colspan="2">Calibration period: 1650-1699 AD
Reconstruction period: 1850-1999 AD</td></tr>
<tr><td>CCSM4</td><td>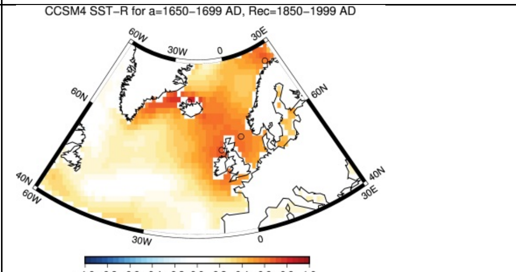

(a)</td><td>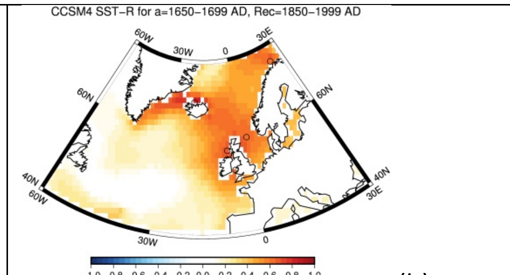

(b)</td></tr>
<tr><td>MPI-ESM-P r1</td><td>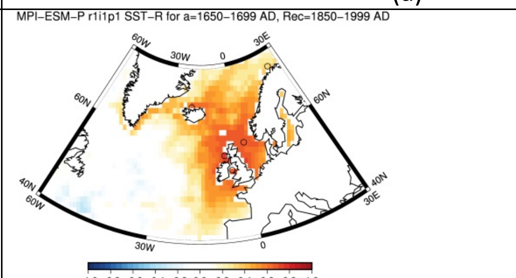

(c)</td><td>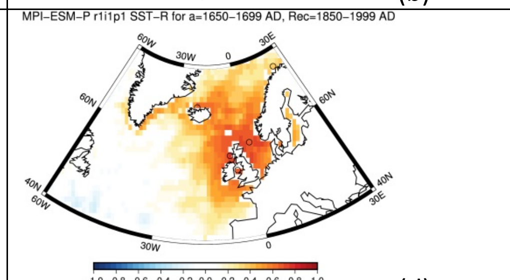

(d)</td></tr>
</table>

Figure 3-4 Same as in Figure 3-2, but for the noise contaminated pseudo-proxies.

Whilst in most cases the results regarding the reconstruction of the eastern Atlantic basin do not significantly change according to the calibration period, the 1st realization of the MPI-ESM model and the CCSM4 model show that this aspect plays an important role. When we compare the pseudo-results of those models during the LIA (1650-1699 AD) calibration period (Appendix C3, Figure 7S) to the results calculated during the rest of the calibration periods (Appendix C3, Figures 6S-10S), the skill of the reconstruction of the east Atlantic basin appears higher in the Appendix Figure 7S. These results are not apparent with the ideal pseudo-proxy experiment. Moreover, for the LIA calibration period there is an anti-correlation of around r~-0.4, shown by all realizations of the MPI-ESM-P model, on the west Atlantic basin; an aspect shown also in the ideal pseudo-proxy experiment (Appendix C3, Figure 2S).

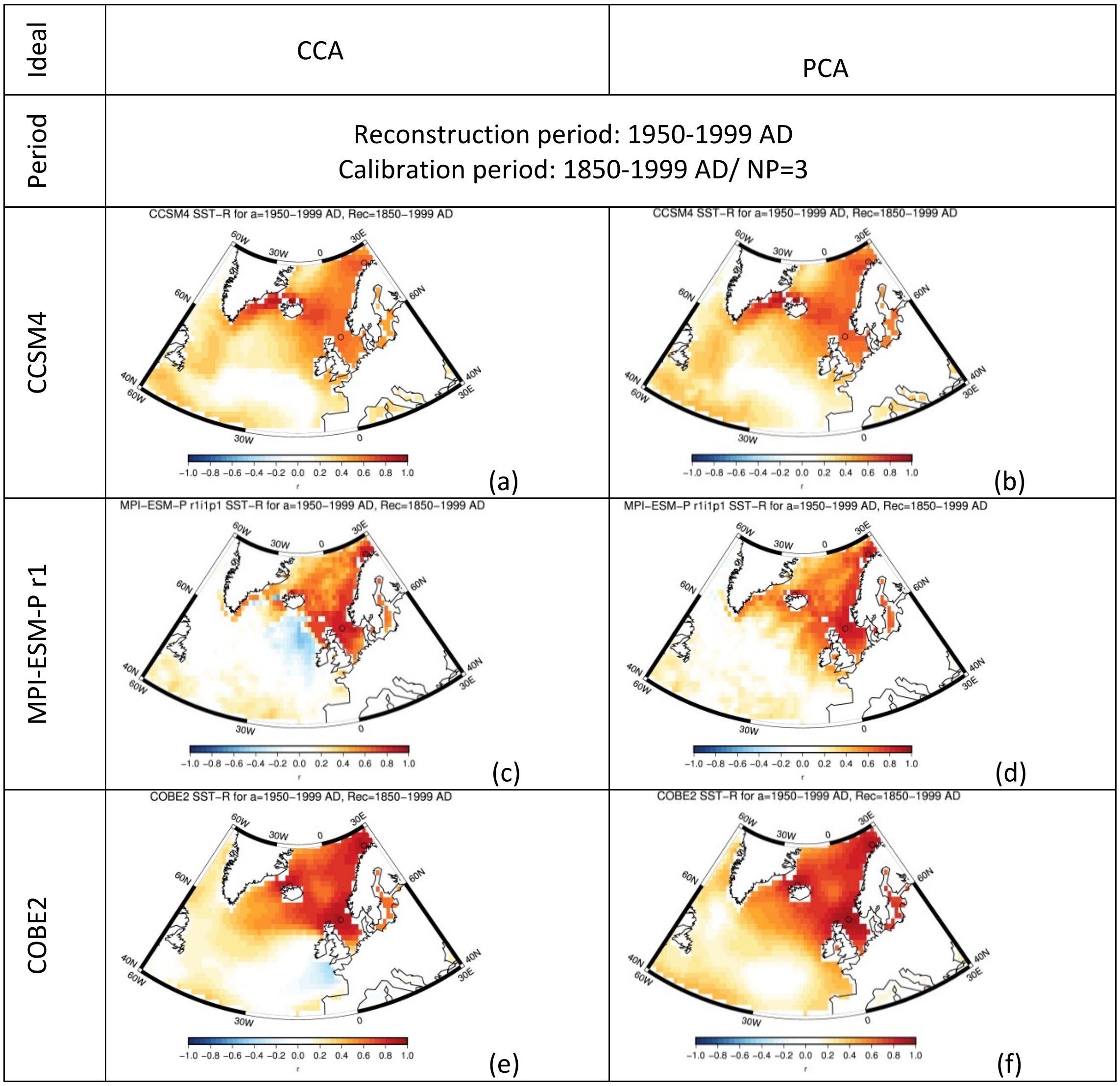

Figure 3-5 Correlation coefficient between the reconstructed and the original SST-anomaly evolution of the NA field during the preindustrial era, when the number of proxy locations used is NP=3. The results are given for the recent calibration period (1950—1999 AD) and for the two different reconstruction methods (left column CCA, right column PCA) for the models CCSM4 (first row) and MPI-ESM-P r1 (second row) and the reanalysis data COBE2 (third row).

3.4.3 Test of proxy locations

I tested the contribution of the different Arctica islandica proxy sites on the reconstruction skill. I reconstructed the NA SSTs during the industrial period and calibrated our regression models during the recent period, according to a) the sites on the Icelandic Shelf and North Sea (figures with NP=2) and b) the sites on the Icelandic Shelf, North Sea and Ingoya Island (figures with NP=3). The reconstruction is performed for both methods, using ideal proxies (Appendix C3, Figure 11S) and noise contaminated proxies (Appendix C3,

Figure 12S). In Figure 3-5 and Figure 3-6 the results using three Arctica islandica sites are shown for ideal proxies and noise contaminated proxies, respectively.

Cont	CCA	PCA
Period	Calibration period: 1950-1999 AD Reconstruction period: 1850-1999 AD/ NP=3	
CCSM4	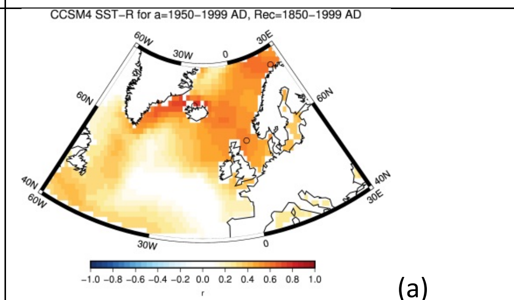	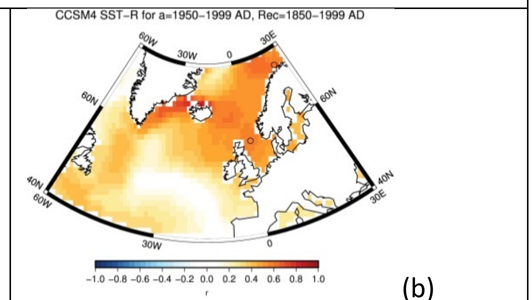
MPI-ESM-P r1	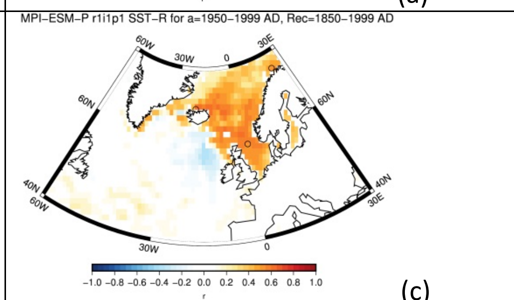	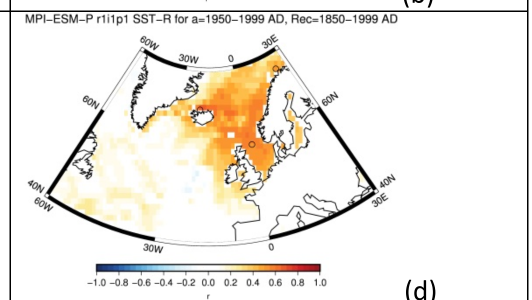
COBE2	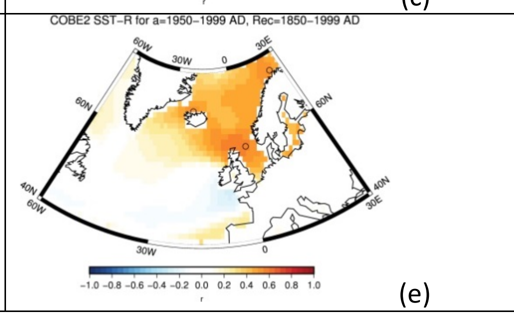	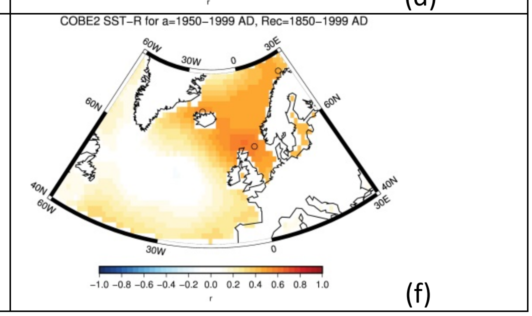

Figure 3-6 As in figure 3-5 but for the noise contaminated pseudo-proxies.

Regarding the ideal experiment, for the COBE2 data and for all models (Appendix C3, Figure 11S) the PCA method results indicate a greater reconstruction skill than the CCA method, in both cases for two and three proxy locations. Anti-correlation between the reconstructed and original SST evolution occurs with the CCA method, mostly when only two proxy sites are used and especially for the COBE2 data (Appendix C3, Figure 11S). Additionally, the differences amongst models and between models and data are more profound for the CCA method than for the PCA, because the number of CCPs that can be used for the CFR are limited by the number of proxies used (two CCPs for NP=2 and three CCPs for NP=3). Comparing the results of Figure 3-5, regarding the reconstruction using three Arctica sites, to the according results of Figure 3-1 that are based on the reconstruction using five Arctica sites, we see that the sites in the Irish Sea and the coast of Scotland do not only contribute to the reconstruction of the SSTs on their surrounding waters but they additionally increase the reconstruction skill of the east Atlantic basin.

Regarding the noise contaminated pseudo-proxy experiment (Figure 3-6), the differences of the reconstruction skill according to the two methods are more obvious when compared to the differences shown by the respective idealized experiments (Figure 3-5). Generally, the results of the PCA show a greater reconstruction skill, while when the CCA method is used, regions of anti-correlation are apparent in the results of the r1 and r3 realizations of the MPI-ESM model and of the COBE2 data (Appendix C3, Figure 12S). The addition of the sites in the Irish Sea and at the coast of Scotland also results in an increase of the reconstruction skill of the east Atlantic basin for all models and data, and for both methods. The reason that the sites in the Irish Sea and at the coast of Scotland increase the overall reconstruction skill is that the oceanographic variability of the western British Isles is dominated by the northward transport of warm saline waters derived from the North Atlantic Current (Inall et al., 2009).

3.5 Discussion

3.5.1 Stationarity of the calibration coefficients

Both methods showed that the spatial skill of the reconstruction does not profoundly change according to the period during which the regression models were calibrated, even when the calibration period used is the recent period (1950-1999 AD), a period dominated by anthropogenic forcing. This result is robust amongst models and amongst models and observational data and could be an indication that the NA basin leading modes of SST variability remain stationary during periods of the last millennium for different climatic background states. However, changes in teleconnections on multi-decadal to centennial time scales in control model simulations or externally forced simulations have been proposed by several studies (Gallant et al. 2013; Müller and Roeckner 2008). Regarding the NA basin, non-stationary AMO-like variability emerges in climate simulations and proxy-data covering the last half millennium (Enfield and Cid-Serrano 2006). Apparent non-stationarity in multidecadal to centennial (and even longer) AMO fluctuations is found in a multi-millennial unforced climate simulation (Zanchettin, Rubino, and Jungclaus 2010). In contrast, for longer time scales, Zanchettin et al., 2013 investigated the basin-scale leading modes of SST variability for the extra-tropical NA in a five-member full-forcing ensemble simulation covering the period 800–2005 AD and in a multi-millennial control run describing an unforced climate and found that the simulated SST modes during such long time intervals describe regional SST variability patterns in the NA consistent with those simulated and observed over the last 160 years.

Another reason that could potentially explain the similarities of the reconstruction skill amongst different calibration periods could be that the relationship of the SSTs of the regions where the proxies are located and the modes of variability that influence the NA basin remain unchanged. Lohmann et al. (2005) found that during 1900—1998 AD the Arctic Oscillation-related (AO) temperature teleconnections show weak decadal variations in some regions of the North Atlantic. The AO signature in climate variables was also detectable during the spring season, which is of practical relevance as the climate information obtained from most terrestrial and marine proxy archives is more linked to the growing season rather than to winter (Cook, D'Arrigo, and Mann 2002). The NA regions that Lohmann et al. (2005) identified with stable teleconnections include almost all the proxy locations used in our study (see Figure 4; Lohmann et al., 2005), but their analysis regards only the recent period and decadal variations. Regarding the North Atlantic Oscillation (NAO), variable teleconnections have been detected in coupled ocean-atmosphere model simulations (Zorita and González-Rouco 2002; Raible et al. 2001). Moreover, model inaccuracies in the representation of the mean NA climate, NAO and other modes of climate variability that influence the NA SSTs could lead to a poor representation of the NA regions. However, as CFRs are covariance-based approaches, a poor representation would lead to a generally low reconstruction skill in the NA basin, which is not consistent with the results of this study. Therefore, a more plausible reason that explains the similarities of the reconstruction skill amongst different calibration periods is that the possibly existing non-stationarities have been minimized due to the usage of proxy sites from multiple regions (Batehup et al., 2015).

3.5.2 Model and method dependent spatial skill

More profound spatial differences in the reconstruction skill are found for the different model simulations rather than for the different periods in the last millennium that were used to calibrate the regression models. The pseudo-proxy results of the CCSM4 model are found to be closer to the pseudo-proxy results of COBE2 rather than those of the MPI-ESM-P model. In the study of Pyrina et al. (2017), and in terms of Empirical Orthogonal Functions (EOFs) for the summer means during 1950-1999 for the NA, it was found that the leading patterns of SST variability as given by the COBE2 show more similarities to the ones calculated by the CCSM4 model than the ones calculated by the MPI-ESM-P model. Moreover, the teleconnection patterns of the IS and NS proxy sites to the SSTs of the NA basin were evaluated and the CCSM4 model was again found to be closer to the teleconnection maps shown by COBE2 in terms of both, resemblance of magnitude and spatial patterns. Therefore, as the large scale SST variability of NA basin of the CCSM4 model was found to be closer to the observational data, this could be the reason for the resemblance of the COBE2 reconstruction skill by the CCSM4 model. Another interesting finding relates to the fact that the SSTs on the path of the east Greenland current can be reconstructed with a good skill only with the CCSM4 model and this is one of the points where the CCSM4 model does not agree with the COBE2 data (Figure 3-1, Figure 3-3). The reason in this case could be the COBE2 data set, as there is a suspect abrupt jump in the SSTs of the regions north of Iceland in the COBE2 dataset (see in Loder et al. 2015; Fig 7).

The usage of MPI-ESM-P generally leads to less spatially homogenous correlation maps. Even though the ocean component of the CCSM4 model has globally finer spatial resolution than the MPI-ESM-P, in the NA Ocean the ocean component of the MPI-ESM-P model has considerably higher spatial resolution on the original curve-linear model grid. That technical characteristic could explain the more heterogeneous results of the MPI-ESM-P in the NA area. Differences between the two models could also arise from the slightly different volcanic forcing used. Booth et al. (2012) found that aerosol concentration changes influence the simulated spatial response of the SSTs. In addition, differences between the two models could also arise from the implementation of the aerosol component which is prescribed in the MPI-ESM model but interactive in the CCSM4. Rotstayn et al. (2010) found an improvement of the Australian mean seasonal climate by including in the CSIRO model an interactive aerosol scheme. The effect to the reconstruction skill due to a change in the standard deviation of the volcanic forcing can be seen by the comparison between the ensemble members r1 and r2 of the MPI-ESM model. These members are integrated with the same model version, started with the same ocean state, but with standard deviation of the distribution of volcanic aerosol size equal to 1.2 μm in r1 and 1.8 μm in r2. Comparing the results of r1 to r2 we see that for both reconstruction methods and in all the calibration periods the reconstruction skill of the r2 simulation is lower (Appendix C3, Figures 6S-10S).

The differences of the reconstruction skill according to CCA or PCR can be better identified in the case of the MPI-ESM model, because of the less spatially homogenous correlation maps between the original and the reconstructed SST anomalies. For the reconstruction of the NA SSTs using the PCR method, we take advantage of the dominant patterns of SST variability of the NA basin, while with the usage of the CCA method we exploit only those patterns with time histories related to the time histories of the proxy network. In the case of five proxy locations, and even worse in the case of three and two, I see that this method is problematic because of the information lost due to the limited number of CCP^{pr} that can be derived from our small sized proxy network. Moreover, the differences in the methods can be better seen when I use the noise contaminated pseudo-proxies, as in this case the loss of information is greater, because the noise contaminated pseudo-proxies do not explain 100% of the SST signal.

3.6 Conclusions

From the PPEs derived herein I have demonstrated that a small sized proxy network of the marine bivalve mollusk Arctica islandica (five proxy locations) can produce skillful spatial SST reconstructions of the eastern NA basin. The tested CFR methods can alter the spatial skill of the reconstruction especially when noise contaminated pseudo-proxies are used. Therefore, it is important to assess CFR methods with contaminated proxies, rather than with ideal ones. Even though the CCA method is problematic when a significantly low number of proxies is used (two and three proxies), the spatial skill of the reconstruction using CCA and five proxy locations is similar to the results calculated with the PCR method. The calibration period does not significantly affect the reconstruction, while the most profound changes in the spatial skill of the reconstruction are caused by the model simulation used.

4. Signature of solar forcing on the North Atlantic basin during the preindustrial era in summertime

I investigated the effects of solar forcing on the North Atlantic Dynamics during the preindustrial era of the last millennium in a climate simulation with the Earth System Model of the Max-Planck-Institute for Meteorology, MPI-ESM-P, driven only by variations in Total Solar Irradiance (TSI). The analysis was performed separately for inter-annual time scales and for time scales longer than 11 years. The region under consideration is the North Atlantic (NA) basin between 80˚W—30˚E and 21˚N—75˚N, while the climatic parameters analyzed are the geopotential height at 500 hPa and 850 hPa, the pressure at sea level and the sea surface temperature (SST).

A regression analysis of the inter-annual variations of TSI and the grid cell climatic variables in the NA basin could not identify an effect of TSI variability on the SSTs and on the atmospheric circulation of the NA basin during 850—1849 AD. The solar-forcing-only simulation shows climate periods that resemble the Medieval Climate Anomaly (MCA) and Little Ice Age (LIA). The effect of solar forcing during these periods of the last millennium was also investigated by calculating the mean temporal difference (MCA minus LIA) of the respective atmospheric and oceanic variables. In this case, TSI was found to induce a profound effect on the summer climate of the NA. The composite technique (superposed epoch analysis) was also employed to investigate the possible link between solar activity and the NA summer climate. The composite pattern of SST response to solar forcing is similar to the pattern shown by linear regression but with prominent differences in magnitude. Regarding atmospheric circulation, a West Atlantic-like blocking pattern with positive centers above Scandinavia and on the southwest of Nova Scotia and a negative center that extends from Greenland to the central NA basin, is the result of lower TSI values.

4.1 Introduction

It has been repeatedly suggested that changes in Total Solar Irradiance (TSI) may influence the Earth’s climate. The effect of TSI changes has been identified by earlier works (Eddy et al. 1976) and confirmed with more recent studies (Haigh 2007; Ineson et al. 2011; Ermolli et al 2013). However, the relationship between changes in solar activity and the Earth’s climate are more complicated, hampering a proper evaluation of the Sun-climate relationship (Lockwood 2012). In this context, Scafetta and West (2007) argued that solar change contributed to a 60% temperature rise since the pre-industrial times, but it might be that these authors exploited a feature in the TSI data that turned out to be an instrumental artefact (Lockwood and Fröhlich 2008). Therefore, a proper null hypothesis testing should be formulated in order to check the consistency of results (Legras et al. 2010). Santer et al. (2001) and Lockwood (2008) have used regression analysis to investigate climatic effects of solar forcing, but several studies have demonstrated how regression analysis is prone to yielding spurious results (Ingram 2007, Benestad and Schmidt 2009, Stott and Jones 2009). Possible reasons for the occurrence of spurious results could be the non-Gaussian Distribution of the variations in TSI, the high temporal autocorrelation in the TSI record and a lack of mechanistic explanation of the statistical correlation of the solar-climate relationship.

Composite analysis, also referred as superposed epoch analysis or conditional sampling, is useful for isolating low amplitude signals within data where background variability would otherwise obscure the signal detection (Laken and Čalogović 2013). With this non-parametric approach I can take advantage of spatially resolved climate characteristics due to TSI responses and therefore it has been used by several studies. Camp and Tung 2007 obtained a globally averaged air surface warming of almost 0.2° K during solar maximum as compared to solar minimum, which is consistent with other studies using the composite technique (Labitzke et al. 2002; Van Loon at al. 2007). Some studies have examined the climate response to solar irradiance changes by analyzing the mean difference between two different periods. In this way, the magnitude and role of external forcings might be more distinguishable. Shindell et al. (2001) used a General Circulation model (GCM) to examine the winter response of surface temperature to TSI changes between the late 17th century Maunder Minimum and the late 18th century. They found that global average temperature changes are about 0.3° to 0.4°C with respect to the aforementioned periods. This response is similar to the annual average North Hemisphere (NH) 1680-minus-1780 temperature change of about –0.2° ± 0.2° C calculated from proxy data (Mann et al. 1999). Crowley (2000), used an energy balance model forced with TSI changes of around 0.25% from the 14th century to the 20th century to calculate the mean annual temperature response of the period 1000—1850 AD to TSI changes. He found that the mean annual North Hemisphere temperature response to that magnitude of solar variations is on the order of 0.2°C.

The physical mechanisms involved in the interaction of solar activity and a tropospheric climatic variable are still uncertain. For instance, in 1997, Friis-Christensen and Svensmark suggested an important role of cloud-radiation interactions modulated by the output of solar particles. Also, ozone is a radiative active gas, the concentration of which varies in concert with TSI changes and therefore it is vital to include this effect in model simulations (Palmer et al. 2004). In the MPI-ESM-P model configuration, the ozone dependency on solar irradiance is represented and therefore mechanisms related to the interaction of solar activity and a tropospheric climatic variable could be represented as well. Shindell et al. (1999) found that increases in ozone abundance and incoming UV radiation lead to greater UV absorption and hence greater solar heating during solar maximum. Meehl et al. (2009) investigated the winter response of the Pacific basin to TSI changes and found that the top-down stratospheric response of ozone to fluctuations of shortwave solar forcing and the bottom-up coupled ocean-atmosphere surface response act together to lower the eastern equatorial Pacific SSTs during peaks in the 11-year solar cycle, and reduce low-latitude clouds to amplify the solar forcing at the surface.

In my analysis I focus on the spatial climatic response during summer, of the North Atlantic (NA) basin due to TSI changes. I analyze a simulation of the preindustrial period in the last millennium with the Earth System Model of the Max-Planck-Institute for Meteorology, MPI-ESM-P, driven only by variations in solar forcing. Changes due to volcanic, aerosol, land-use and greenhouse gas are not considered in this simulation. For the shake of discussion I additionally analyze, for the same period, a fully forced simulation of the preindustrial period conducted with the MPI-ESM-P model. For my investigation I contrast the results of composite analysis to linear regression methods and we additionally test the effect of solar forcing on the climate during the Medieval Climate Anomaly (MCA) versus the Little Ice Age (LIA) epochs of the last millennium.

In this chapter I concentrate on lower-tropospheric dynamics and on SSTs over the North Atlantic realm. I assume that the simulated changes in solar output are integrated into the lower troposphere and therefore might affect directly and indirectly sea surface temperatures. I also acknowledge that our model study can only capture those effects that are realistically simulated and parameterized by the Earth System model I use. The MPI-ESM model is run over a comparably high resolution of the stratosphere and also includes changes in the ozone chemistry, depending on changes in solar activity (see section 2.2) (Giorgetta et al. 2013).

Another important issue for the investigation of changes in simulated climate and solar activity relates to the reconstruction of the solar constant over multi-decadal to centennial time scale over the last millennium, and in particular of the amplitude of the reconstructed variations. This amplitude can ultimately affect the amplitude and the spatial extent of tropospheric climate changes caused by changes in solar activity. In the early 2000 it was generally accepted that a long-term change in solar activity between the mean state of the sun during the Maunder Minimum, a period with low solar activity (Zorita et al. 2004), and the present-day climate, a period with presumably higher solar output, is about 0.3% (Fligge and Solanki 2000). The amplitude of TSI variations has been subsequently revised and following the PMIP3 protocol (Paleoclimate Modelling Inter-comparison Project phase 3), this scaling was reduced to approximately 0.1% (Vieira et al. 2011; Wang at al.

2005). Currently, only the reconstruction of Shapiro et al. (2011) shows a maximum amplitude of TSI change of 0.6% over the past millennium, but this large amplitude is not compatible with the reconstructed climate evolution over the last millennium and the sensitivity of present climate models to changes in TSI (Schurer at al. 2014).

4.2 Data and Methodology

I investigate the effects of TSI on the summer climate (June-July-August) of the NA basin during the pre-industrial era of the last millennium, using a fully forced (R1) and an only solar forced (R4) simulation of the MPI-ESM-P model. The region under consideration lies between 80˚W—30˚E and 21˚N—75˚N, while the climatic parameters analyzed are the geopotential height at 500 hPa (geo500) and 850 hPa (geo850), the pressure at sea level (psl) and the sea surface temperature (SST).

4.2.1 Methods

The analyses was performed separately for inter-annual time scales and for eleven year low pass filtered series, thereafter referred to as decadal timescales. The decadally filtered series were obtained by filtering the climatic parameters in the spectral domain (cut off frequency=1/11) using the low-pass filtering technique described in Schulzweida et al. (2012). It must be noted that even though the TSI series are provided as one value per year, the physical resolution of the reconstructed TSI record is decadal (Vieira et al. 2011), due to the resolution of the ice-core records. Therefore, the TSI series were not low-pass filtered. The analysis was performed for two different time scales because the variability of the climatic variables changes with time scales so that the detection of a solar signal in these variables may depend on the time scales considered.

To identify the effects of TSI forcing on NA climate, I used three methods. The first method identifies the linear dependence between variables, using techniques such as Pearson Correlation and Linear Regression and taking into account the full pre-industrial period, 850—1849 AD. The second method compares two climatically different periods during the last millennium, namely the Medieval Climate Anomaly (MCA) and the Little Ice Age (LIA). In the present study I define the MCA as the period from 1088 to 1187 AD and as LIA the period spanning from 1500 to 1599 AD. My definition of the periods is based on a random choice of 100 years within a low solar activity period that has been linked to cooling during the Little Ice Age epoch of the last millennium (1450—1850 AD) and a warm period that could be possibly caused by high solar activity during the Medieval Climate Anomaly (950—1250 AD). Even though high (low) solar activity periods are evident in the TSI series during the MCA (LIA) periods (Figure 4-1a), the average surface warming (cooling) in the NA basin during these periods is not simulated by the only solar forced simulation R4 of the MPI-ESM-P model (Appendix C3, Figure 5K-b). The third method used is Composite Analysis. With Composite Analysis I focus on the effect of the most prominent TSI periods with high and low TSI. Periods of high TSI were defined as those with positive TSI anomalies exceeding twice standard deviation. Periods with low TSI were defined as those with negative TSI anomalies exceeding in magnitude 1.4 times the standard deviation. These asymmetric requirements were set in order to have approximately the same amount of selected cases with positive and negative extreme TSI, as the TSI distribution is not Gaussian but positively skewed (Figure 4-1b).

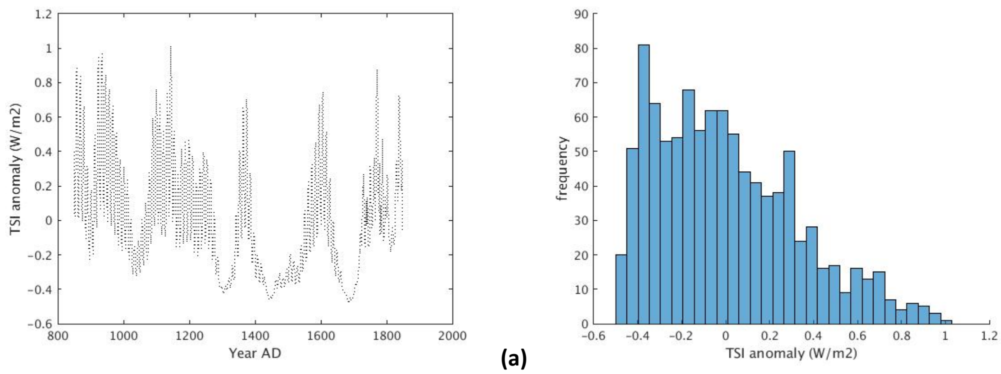

(a) (b)

Figure 4-1 Inter-annual TSI anomalies for the period 850—1849 AD presented in (a) as a function of time and in (b) as a function of frequency.

4.2.2 Model simulations

The model employed in this study, MPI-ESM, is the Max Planck Institute Earth System Model and a part of the 5th phase of the Climate Model Intercomparison Project (CMIP5/ http://cmip-pcmdi.llnl.gov/cmip5/). We used the simulations conducted with MPI-ESM-P, which is the configuration for paleo-applications (see in Jungclaus et al., 2014 for a detailed description). In this configuration the atmosphere has a T63/1.9° horizontal resolution and 47 hybrid sigma pressure levels (ECHAM6/ Stevens et al. 2013), and the ocean grid is a bipolar grid with 1.5° resolution (near the equator) and 40 z-levels (MPIOM/ Jungclaus et al. 2013). The L47 grid extends to 0.01 hPa in the vertical direction, where the center of the topmost level in the upper mesosphere is set. This vertical extension of the atmospheric grid includes for the first time the stratosphere in CMIP simulations at MPI-M (Giorgetta et al. 2013). The solar spectrum is split into 14 spectral bands and therefore temporal variations of solar irradiance depend on the wavelength, but the relative variations among spectral bands is prescribed, since the information provided by the ice-core records cannot differentiate between spectral bands (Kinne et al. 2013). The monthly average ozone concentrations for the period 850–1849 AD are prescribed and were calculated using the 1850–1860 monthly climatology of ozone concentrations from the AC&C/SPARC Ozone Database as a basis. The ozone dependency on solar irradiance is represented through regression coefficients between historical ozone concentrations and the annual 180.5 nm solar flux (Jungclaus et al. 2014).

The realization R1 of the MPI-ESM-P model is a part of the past1000 runs and follows the PMIP3 protocol regarding the external forcings used. The Crowley and Unterman reconstruction (2013) is used for volcanic aerosol optical depth and effective radius, while the Pongratz et al. (2008) reconstruction is used to prescribe global land-cover and agricultural areas. For solar radiation the Vieira et al. (2011) total solar irradiance reconstruction over the Holocene is employed, with an increase in TSI of 0.1% from the 17th century Maunder Minimum to present time (Lohmann et al. 2015). The second simulation analyzed in this study is the R4 simulation of the MPI-ESM-P model, which is forced only by changes in TSI. This simulation is not a part of the CMIP5 project. For both R1 and R4 simulations the original output was re-processed and re-gridded to a regular grid (1˚×1˚ degree horizontal resolution).

4.3 Results

4.3.1 Linear Methods

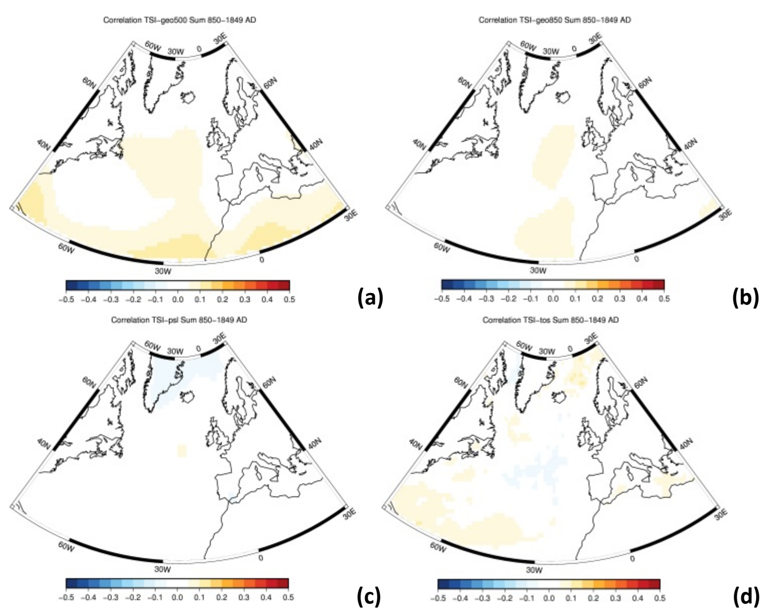

Figure 4-2 Spatial correlation between the TSI anomalies and the a) geo500 hPa, b) geo850 hPa, c) psl and d) SST for the period 850—1849 AD and the realization R4.

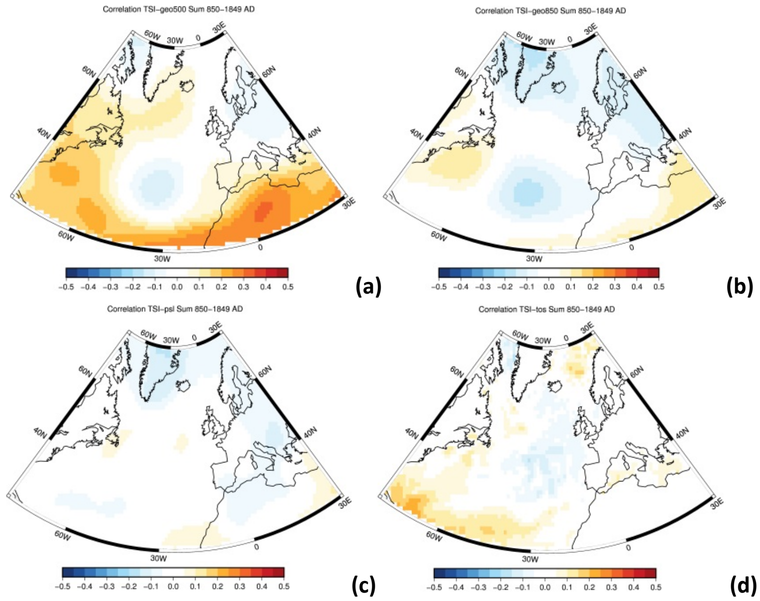

Figure 4-3 Spatial correlation between the TSI anomalies and the a) geo500 hPa, b) geo850 hPa, c) psl and d) SST for the period 850—1849 AD and the realization R4, after 11 year low pass filtering.

The TSI time series were correlated to atmospheric and oceanic variables, based on the realization R4 of the MPI-ESM-P, at each grid point of the NA basin for the period 850—1849 AD. The Pearson correlation coefficient is shown in Figure 4-2 and Figure 4-3 for inter-annual time scales and decadal time scales, respectively. In the case of inter-annual time scales the correlation coefficient does not exceed values around r≈±0.1, while in the case of decadal time scales changes in TSI seem to have a stronger effect on the four climatic variables analyzed in this study. However, even for decadal time scales, the TSI signal is generally weak reaching a maximum correlation of about r≈±0.3 when TSI is correlated to geo850 (Figure 4-3b), to psl (Figure 4-3c) and to SSTs (Figure 4-3d). For geo500 maximum values are around r≈+0.4 (Figure 4-3a). Therefore, only a low fraction of the total variance of the lower tropospheric variable can be explained by changes in TSI using linear methods and taking into account the full pre-industrial period.

The TSI anomalies were standardized to a standard deviation (SD) equal to one, and subsequently regressed at each grid point of the NA basin to the inter-annual values (Figure 4-4) and the decadally filtered values (Figure 4-5) of the atmospheric and oceanic variables studied herein. During the period 850—1849 AD and for inter-annual time scales, TSI forcing results in an increase of the atmospheric variables in the central NA basin and in a decrease of the atmospheric variables above Greenland (Figure 4-4 a-b-c). Regarding SSTs (Figure 4-4d), TSI changes have a warming effect of approximately +0.1 K per one SD of TSI over the Nordic Seas and regions of the subtropical gyre and a cooling effect of -0.1 K per one SD of TSI over regions of the central NA basin and the west coast of Greenland.

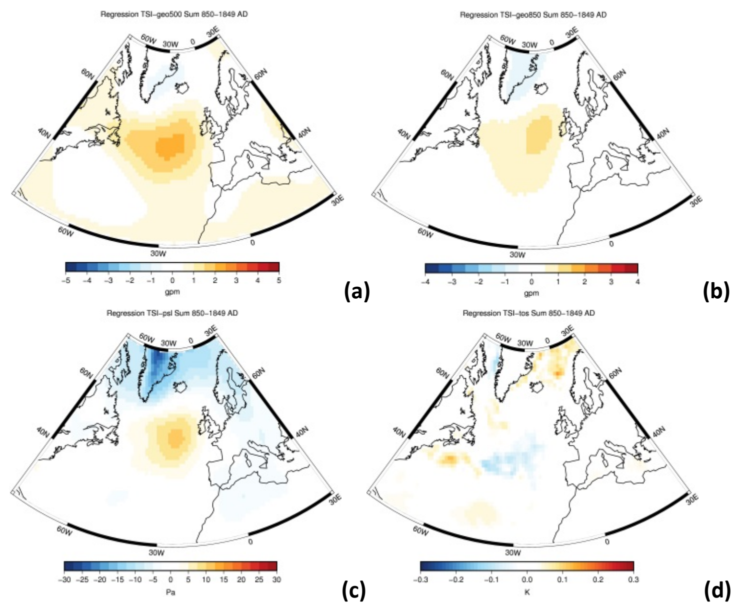

Figure 4-4 Regression of the TSI anomalies to the a) geo500 hPa, b) geo850 hPa, c) psl and d) SST for the period 850—1849 AD and the realization R4. The units refer to changes of 1 standard deviation in TSI.

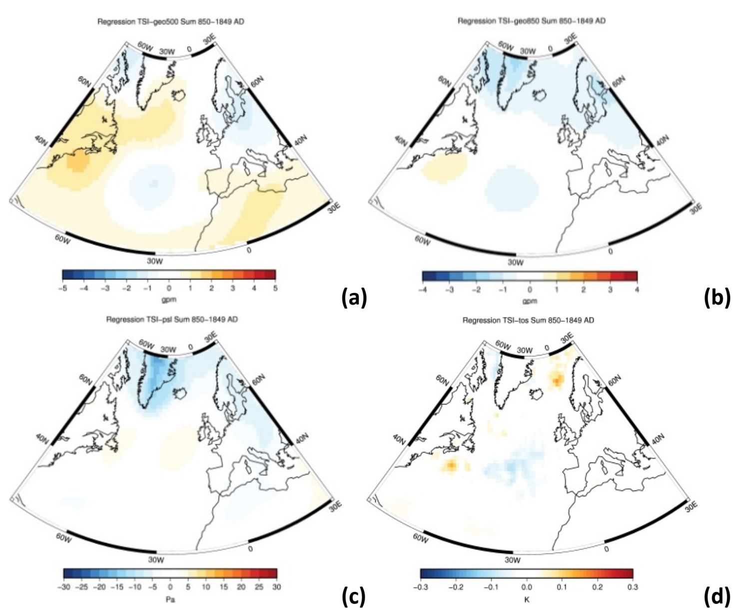

Figure 4-5 Regression of the TSI anomalies to the a) geo500 hPa, b) geo850 hPa, c) psl and d) SST for the period 850—1849 AD and the realization R4, after 11 year low pass filtering. The units refer to changes of 1 standard deviation in TSI.

The SST pattern given by the regression of TSI to the inter-annual SST values is consistent with the pattern shown for decadal time scales (Figure 4-5d), but a change of ±0.1 K can be considered not profound when the long term mean SST values of the period 850—1849 AD vary from 280 to 297 K, depending on the region (Appendix C4, Figure 1K-d). The pattern that results from the regression of TSI to psl has the same structure for inter-annual and 11-year time scales (Figures 4-4c and 4-5c, respectively), but it is weaker in magnitude in the case of the 11-year filtered results. Due to TSI forcing, psl decreased by approximately 0.20 hPa above Greenland and increased by approximately 0.07 hPa or 0.15 hPa above the central NA basin, depending on the time scales under consideration. Changes in geopotential height at 500 hPa and 850 hPa, due to TSI forcing, do not share the same spatial patterns between the two different time scales.

4.3.2 MCA vs LIA

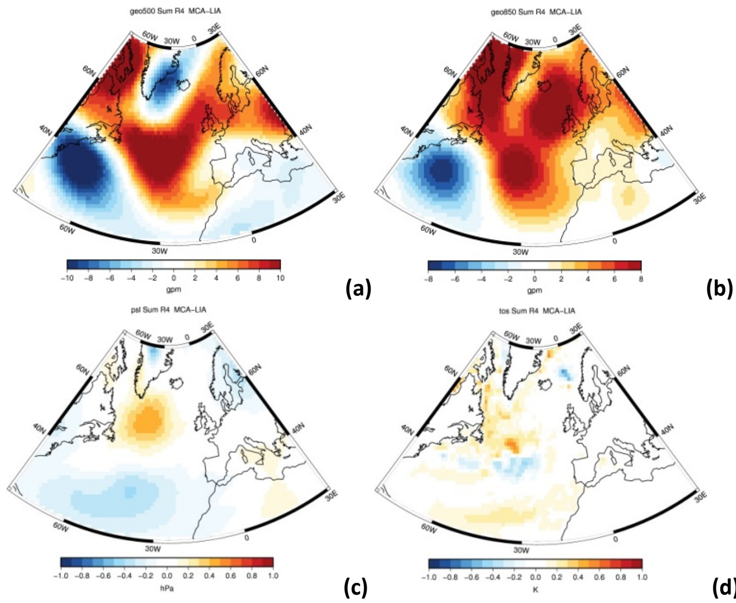

Figure 4-6 Difference of the mean a) geo500 hPa, b) geo850 hPa, c) psl and d) SST of the period MCA minus LIA for the realization R4.

Another method to investigate whether climate responds to changes in TSI is to compare the response of climatic variables between periods during which TSI values are considerably different from the mean solar constant. Therefore, we selected a period of 100 years within the MCA and a period of 100 years within the LIA epochs of the last millennium and calculated the mean temporal difference (MCA minus LIA) of the respective atmospheric and oceanic variables between those periods. The results are shown in Figure 4-6. During the LIA the geo500 (Figure 4-6a) is higher by approximately 10 gpm above Greenland and south of Nova Scotia, while it is lower by approximately 10 gpm in a V-shape area covering the mid and high latitudes. The increase of geopotential height south of Nova Scotia seems to persist in geo850 (Figure 4-6b), while the geo850 of the rest of our study region is lower during the LIA. There are three regions where psl has risen and two regions where psl has declined by approximately 0.20 to 0.50 hPa. The regions with higher sea level pressure are located above Greenland, Scandinavia and the subtropics, while the regions with lower sea level pressure are located above the Mediterranean and on regions of the subpolar gyre. During the LIA the SSTs north of Iceland and of regions in the subtropics and the subpolar gyre are cooler around -0.7 K. Warmer SSTs by approximately +0.6 K are found northeast of Iceland and on the central NA around 40 °N.

4.3.3 Composite Analysis

Within composite analysis, periods with higher TSI and periods with lower TSI are selected out from the period 850—1849 AD. The response of each atmospheric and oceanic variable analyzed in this study was estimated by subtracting the mean of the atmospheric and oceanic variables in the low TSI from the respective atmospheric and oceanic variables of the periods with high TSI. The thresholds to detect the high-TSI and low-TSI periods were 2 times the standard deviation and -1.4 times the standard deviation, respectively. The composite difference maps are given in Figure 4-7. As seen in Figure 4-7d, the patterns of SST change which result from composite analysis due to TSI forcing are similar to the ones obtained by linear regression (Figure 4-4d and 4-5d). Lower values of TSI are linked to warmer SSTs over the central NA and the west coast of Greenland, and with colder SSTs over most parts of the NA basin north of 60 °N and regions in the subtropics. A West Atlantic-like blocking pattern, with negative centers above Scandinavia and on the southwest of Nova Scotia and a positive center that extends from Greenland to the central NA basin is the result of lower TSI values according to composite analysis (Figure 4-7 a-b-c). This pattern describes the atmospheric circulation at sea-level, 850 mb and 500 mb and resembles the 3rd dominant pattern of geo500 variability in the NA basin (Appendix C4, Figure 2K-c).

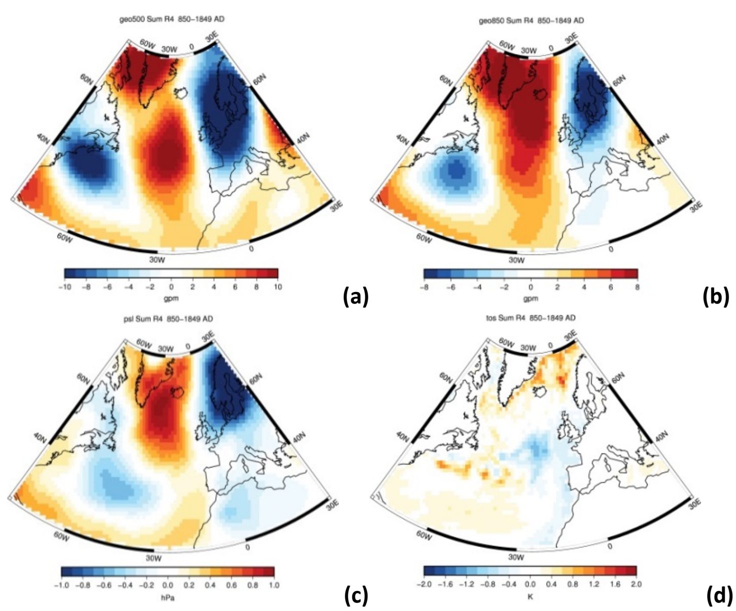

Figure 4-7 Difference of the mean a) geo500 hPa, b) geo850 hPa, c) psl and d) SST during TSI maxima minus TSI minima for the realization R4.

4.4 Discussion

In the results section several techniques estimating the relationship and potential impact of TSI changes to lower tropospheric circulation and SSTs were investigated for the summer season. We stress this point because former studies have mostly concentrated on changes of winter circulation and the according impact in the context of TSI changes. The selection of summer season will allow a future comparison of our results to oceanic proxy data, such as the annually resolved bivalve mollusk Arctica islandica (Butler et al. 2009). This proxy archive grows during summer (Schoene et al. 2005) and that might be important for the test of the results based on our modelling study.

4.4.1 Linear methods

According to Pearson correlation, TSI seems to explain larger portion of the climate variance on decadal time scales, with the strongest signal in the NA basin being on the geo500 at the subtropics (Figure 4-3a). In contrast, such strong signal on the geo500 on the tropics is not revealed by linear regression (Figure 4-5a). Moreover, according to Pearson correlation and for decadal time scales, TSI correlates with an r≈+0.3 to the NA subtropical SSTs (Figure 4-3d). Even though a correlation of r≈+0.3 is statistically significant at the 95% level for a 1000 year time series, we cannot see an SST change greater than 0.05 K per one SD of TSI, at the same regions, according to the linear regression technique (Figure 4-5d).

Generally, according to linear regression, the response of summer SSTs in the NA basin does not exceed ±0.15 K per 1 TSI standard deviation, which corresponds to ±0.05 K per W/m^2. Other studies have also found that the magnitude of temperature response to solar irradiance changes is small. Ammann et al. (2007) calculated the spatial pattern of solar-induced surface temperature changes with only solar-forced simulations over the period from 850 AD to 1849 AD, by using linear regression of local yearly mean temperature and solar irradiance anomalies. The spatial pattern of solar-induced SST changes that these authors found is different compared to our work, as they investigate non seasonal SSTs, but their results confirm the small SST response (~0.3°C maximum spatial response for each W/m^2 of irradiance change).

Another important question is whether the NA SSTs during the pre-industrial era (850—1849 AD) were driven towards warming or cooling by changes in TSI. Swingedouw et al. (2009) used an externally forced simulation (solar forcing and volcanic forcing) to calculate the impact of TSI variations on surface temperatures. From the regression of TSI to the grid point surface temperature for the period 1001–1860, these authors concluded that maximum temperature warming occurs in the Greenland Sea while a general SST warming occurs throughout the NA basin as a result of TSI variations. We have additionally regressed

TSI to the grid point SSTs that were simulated by the externally forced simulation R1 of the MPI-ESM model (Appendix C4, Figure 3K). The effect of TSI in the NA SSTs when the modeled climate is driven by both solar and volcanic changes is a NA basin warming with maximum values occurring in the Greenland Sea and being approximately equal to +0.4 K per 1 TSI standard deviation, which corresponds to +0.1 K per W/m^2. The temperature patterns that we obtain look similar to those derived by Swingedouw et al. (2009). When climate variations are externally driven only by changes in TSI, then the effect of TSI is comparably less SST warming in the Greenland Sea and cooling in the central Atlantic (Figure 4-5d). A possible reason for the differences between Figure 4-5d and the Appendix C4 Figure 3K might not be TSI, as the regression suggests, but that volcanoes actually convolve solar variability effects due to the fact that TSI minima coincide to periods with volcanic eruptions during the last millennium (Appendix C4, Figure 4K). Volcanic eruptions are known to produce a warming in some areas of the NH extra tropics due to the intensification of the Arctic Oscillation (Shindell et al. 2003) and thus counteract the effect of changes in TSI in those regions. The results of the linear regression method are contaminated by the (comparably to TSI) large signal caused by volcanic outbreaks. Another reason for the differences between Figure 4-5d and Appendix C4 Figure 3K, might be the model’s internal variability which was not investigated in our study.

4.4.2 MCA vs LIA

The SSTs’ response to TSI changes could be evidenced by the changes between MCA and LIA (Figure 4-6d). According to the realization R4 of the MPI-ESM model, during the LIA the SSTs of the NA basin have undergone changes of maximum |0.7| K. That is a large impact considering that the observed warming for the first half-decade of the 21st century relative to 1951–1980 climatology shows that the SSTs of the NA basin have undergone a warming of maximum +1.2 K (Hansen et al. 2006). Our results show that SSTs are warmer during the LIA at the northeast of Iceland and in regions around 40° N, while the SSTs have undergone cooling on the path of the east Greenland current, in the Labrador Sea, in regions of the subpolar gyre and in the south of our study region around 20° N.

The SST cooling located at the west coast of Greenland, in the Labrador Sea and in regions of the subpolar gyre is expected, as periods of increased southward transport of polar water masses by the East Greenland Current (EGC) increase the export of drift ice and promote colder conditions on those regions (Moffa-Sánchez et al. 2014). Moffa-Sanchez et al. (2014) presented multi-decadally resolved proxy reconstructions of the surface eastern Labrador Sea spanning the last millennium. These authors found colder conditions in the Labrador Sea at ~1400 AD and reduced deep convection. Furthermore, a recent paleoceanographic reconstruction suggested that the subpolar gyre weakened between the

MCA and the LIA transition (Copard et al. 2012). Moreno-Chamarro et al. (2016) employed the MPI-ESM-P model to study the mechanisms of decadal to centennial variability during 850—1849 AD. According to MPI-ESM model relatively fresh conditions in the Labrador Sea are related to a weaker subpolar gyre. Häkkinen et al. (2011) analyzed surface drifter tracks in the North Atlantic Ocean from the time period 1990 to 2007 and found that a continual weakening of the North Atlantic subpolar gyre allows the increase of the penetration of warm subtropical waters toward the Nordic Seas. These results could explain the warming seen on the Northeast of Iceland in the present study.

4.4.3 Composite analysis

Figure 4-7 displays the geo500, geo850, psl and SST composite difference maps between periods with high and low TSI. The response of the summer atmospheric circulation of the NA basin to TSI forcing during the preindustrial period is a West Atlantic-like blocking pattern that persists from sea level until 500 hPa geopotential height. Even though our results regard only the summer atmospheric circulation, they agree with the findings of Barriopedro et al. (2008) who investigated the blocking response to the 11-year solar cycle for 44 winters (1955–1999) and found that although North Hemisphere blocking frequency is not affected by the level of solar activity, blocking persistence increases when the solar activity is low. Ineson et al. (2011) found that the modeled winter psl response at the solar minimum is a North Atlantic Oscillation-like pattern, but Adolphi et al. (2014) conclude from the analysis of a high resolution ice core record from Greenland that solar minima could have induced changes in the stratosphere that favor the development of high-pressure blocking systems located to the south of Greenland. Davini et al., (2012) used reanalysis data for the winter (DJF) season from 1951 to 2005 to compute the Greenland blocking and its coupling to NAO. When blocking occurs for less than 15 days per year over Greenland, they found that the resulting psl pattern is not the NAO but a West Atlantic-like blocking pattern that represents 33% of the variability. In this case the blocking frequency is high along the coast of Europe. That might be a reason that explains the warming of the NA SSTs shown in Figure 4-8d, as the blocking might push the westerlies to the south and therefore warm the central Atlantic.

Even though the magnitude of the induced SST changes due to the effect of TSI cannot be compared between the Composite method and the MCA-LIA method, as the changes in TSI are different, the SST patterns share similarities regarding the western Atlantic basin. However, each method shows a different SST pattern on the eastern Atlantic basin. With composite analysis we contrast two periods with high TSI and low TSI, but with the method MCA—LIA we contrast two randomly selected periods within the MCA and the LIA epochs of the last millennium. Even though the MCA (LIA) epoch is supposed to represent predominantly warm (cold) phases, this does not necessarily imply that TSI is constantly above (below) its mean value. Moreover, the predominantly warm (cold) phases during the MCA (LIA) epoch of the last millennium are not evident by the average summer temperature of the NA basin as simulated by the only solar forced simulation R4 of the MPI-ESM-P model (Appendix C4, Figure 5K-b). Therefore, this method is expected to provide a more heterogeneous climatic response compared to the Composite method. We calculated the mean difference of TSI between the MCA and LIA, as defined in this study, and found a difference of 0.35 W/m^2 that means 0.03% change in the total values. Many empirical studies use the MCA—LIA method to draw conclusions about the effect of TSI changes to climate, but the climatic response that they find is too large to be explained solely by changes in solar forcing.

4.5 Conclusions

I investigated the effects of TSI forcing to the summer climate of the NA basin during the pre-industrial era of the last millennium, using three different methods. The results according to the linear methods show small signals of the TSI forcing to the atmospheric and climatic variables, signals that could be in the limits of model errors. In contrast, the method MCA vs LIA shows temperature difference by a magnitude that is close to the observed warming for the first half-decade of the 21st century, relative to 1951–1980 climatology. With composite analysis we contrast the effect of TSI during periods of high TSI and low TSI. We found that low TSI induces cooling in most of the NA basin except in regions close to the European coast, where warmer SSTs are found. Moreover, a West Atlantic-like blocking pattern seems to dominate the atmospheric circulation during periods with reduced solar activity. We did not investigate the effect of internal variability in our results. Therefore, to establish core conclusions related to the effects of TSI during the preindustrial era, we need to extend our investigation in future work including ensemble runs of solar forced simulations.

5. Conclusions and Outlook

In order to understand the role of the coupled atmosphere-ocean mechanisms in climate variability and identify the causal relationships, uncertainties related to reconstructions of past climate need to be assessed and the different sources of uncertainty investigated. In this study I addressed three points in this context: First, the bias of current earth system models in simulating mean climate and its variability over the North Atlantic Ocean. Second, uncertainties that are stemming from methods currently used to reconstruct past climate variability. A third issue that is indirectly related to uncertainty in the context of the impact of changes in external forcings relates to the response of the upper ocean circulation and lower atmosphere to changes in solar activity.

This thesis has investigated to what extent variations of the North Atlantic circulation can be reconstructed from the evidence provided by marine proxy data, and assessed current state-of-the-art climate models in their capability to simulate the upper ocean circulation variability. We focused on molluscan-based proxy records, and specifically the bivalve mollusk shell Arctica islandica, as a tool for analyzing and reconstructing the amplitude and spatial structure of decadal and multi-decadal climate variability in the NA region (40°–70°N and 30°E–60°W) during the last millennium.

1.

As spatial networks of high resolution marine proxy archives are limited and valuable for the reconstruction of past marine climate, in the first part of the thesis I investigate the potential of the Arctica islandica network to be used for the reconstruction of the SSTs in the North Atlantic basin. Additionally, climate field reconstruction techniques that would be appropriate to reconstruct climate based on the Arctica network were tested using pseudo-proxy experiments. In order to construct meaningful pseudo-proxy experiments current earth system models are evaluated in simulating the mean climate and its variability over the North Atlantic Ocean. The questions answered within the first part of the thesis are the following:

a. Does Arctica islandica have the potential to be used in CFRs of the SSTs in the NA Ocean?

One important factor that determines whether the network of Arctica islandica has the potential to be used for CFRs is the covariance of the Arctica islandica collection sites with the NA basin. The reason is that CFR methods are covariance based approaches and therefore if the proxy sites describe local signals rather than basin signals, then the skill of the CFR will be reduced. If the network of Arctica islandica indeed co-varies with the entire NA basin, then the information derived from the individual local proxy archives could be successfully used to reconstruct the larger NA SST field using CFR methods. This question was answered with the usage of COBE2 reanalysis data during the second half of the 20th century (1950-1999).

Two Arctica islandica collection sites were tested and found to have the potential in terms of reconstructing the SSTs of the north-east Atlantic basin. According to COBE2, the SSTs of the Arctica islandica site located in the North Sea (NS - 58.5°N, 0.5°E) correlate significantly with the Northeast Atlantic basin and show a statistically significant anti-correlation (alpha=0.05) to the SSTs of the central Atlantic, albeit with very low values. Therefore, the NS site seems promising not only for the reconstruction of the SSTs of the eastern Atlantic but also of the central Atlantic. The site located on the Icelandic Shelf (IS-66.5°N, 19.5°W) is found to not provide any information about the central Atlantic, but statistically significant correlation (alpha=0.05) is found at the eastern and northern NA, north of 60°N. That is an important result in terms of reconstructing oceanic climate over high latitudes were only few observations are available.

b. *If there is a NA basin signal registered in Arctica islandica locations, which CMIP5 models can reproduce that signal?*

Another factor that will influence the estimated skill of the CFR is the climate model simulation used for the estimation of the NA SSTs co-variance. Therefore, I assessed the capability of state-of-the-art climate models participating in the 5th phase of the Climate Model Intercomparison Project to represent the co-variance of the spatially resolved NA SSTs, as well as the SSTs at the Arctica islandica collection sites during the second half of the 20th century (1950-1999). The robustness of eleven CMIP5 models was investigated by comparing the simulated SSTs to COBE2 reanalysis data. The teleconnection pattern of the IS site can be reproduced by a number of CMIP5 modes. Most of the models can realistically simulate the co-variance pattern of the NS site SSTs to the surrounding waters, while some of them capture the NS teleconnection pattern shown by COBE2. Not only COBE2 data but also CMIP5 models showed that there is a NA basin signal registered in Arctica's locations. The models that can reproduce that signal and simulate robustly most of the spatiotemporal characteristics of the NA SSTs relate to CanESM2, CCSM4 and MPI-ESM.

c. Which Climate Reconstruction Techniques are the most suited to reconstruct SSTs based on Arctica islandica?

CFR techniques should be tested in the context of the annually resolved marine proxy network of Arctica islandica, because the skill of the climate reconstruction depends on the characteristics of the proxy network used, such as proxy temporal resolution, growth season, character and level of noise. As the estimation of the skill of the CFR methods depends also on the climate model used to evaluate the CFR method, to answer this question I used the best performing models (according to my evaluation metrics that include one-point map correlations and variances), as evaluated in Question b, in terms of realistically simulating the spatiotemporal characteristics of the NA SSTs and the teleconnections of the Arctica islandica collection sites.

Two widely used CFR techniques were tested, namely Principal Component Regression and Canonical Correlation Analysis. We found that even though the CCA method is problematic when a considerably low number of proxy locations is used (two and three proxies), the spatial skill of the reconstruction using CCA and five proxy locations is similar to the results calculated with the PCR method. In any case, the tested CFR methods altered the spatial skill of the reconstruction and therefore it is important to assess CFR methods prior to reconstructing past climate.

d. Is the climate model or the statistical reconstruction method more important to evaluate the skill of the reconstruction?

Even though the spatial skill of the reconstruction does not profoundly change between the two methods when more than three proxy locations are used, notable changes are seen in the spatial skill of the reconstruction when a different model simulation is used. Pseudo-proxy experiments were performed using the simulated NA SST field of the CCSM4 model, three ensemble members of the MPI-ESM model (r1, r2, r3) and the reanalyzed NA SST field of the COBE2 data set. The pseudo-proxy results based on the CCSM4 model are closer to the ones calculated using the COBE2 reanalysis data, with the main differences lying on regions of the east Greenland current. The skill of the reconstruction is found lower according to the pseudo-proxy results for the MPI-ESM model and especially when the realization r3 is used. The choice of the climate model used as the surrogate reality in the PPE has therefore a more profound effect on the evaluation of the reconstruction skill than the statistical reconstruction method.

2.

The externally forced part of climate variability is the part that can be estimated from model simulations and meaningfully compared to the empirically reconstructed climate variability based on oceanic proxy data like Arctica islandica. Therefore, the second part of the thesis focused on the investigation of the impact on the NA climate of one of the naturally occurring external forcing factors, namely solar forcing. The question that I seek to answer is:

e. Do changes in solar forcing affect summer upper ocean circulation?

To answer whether changes in solar forcing affect summer ocean circulation I had to investigate the response of climate models and marine proxy archives to solar forcing. Therefore, we investigated the summer climate response (June-July-August) of the NA basin to total solar irradiance changes, during the pre-industrial era of the last millennium, using an only solar forced (r4) simulation carried out with the MPI-ESM-P model. In this analysis three methods were used. For the first method I took into account the full period, 850—1849 AD, and used techniques that measure the linear dependence between variables. The second method relates to the comparison of two climatically different periods during the last millennium, namely the Medieval Climate Anomaly (MCA/1088—1187) and the Little Ice Age (LIA/1500—1599). The third method used was Composite Analysis, with which we focus on the separate effect of the most prominent TSI maxima and minima during the 1000 year period.

Signals of solar forcing were detected on the simulated summer climate of the NA basin with the two last methods, while linear methods were found to be inadequate to detect changes in the climatic variables studied herein. The comparison of MCA to LIA indicates that TSI changes affect the NA climate in both inter-annual and longer time scales of 11 years, changing the SSTs by maximum |0.7| K on the northeast of Iceland and on the central NA around 40 °N. According to composite analysis, the solar effect signature on the pre-industrial atmospheric circulation at inter-annual time scales is a west Atlantic-like blocking pattern that persists from sea level until 500 hPa geopotential height. TSI changes during the pre-industrial era seem to induce warming of the central Atlantic SSTs and cooling of the SSTs of the Nordic Seas and of regions of the subtropical gyre.

Within this work I have identified a highly resolved marine proxy, Arctica islandica, with its network being suitable for the reconstruction of large scale climate in the northeast Atlantic basin. Moreover, I assessed different statistical methods that can be applied for climate field reconstructions based on the network of Arctica islandica. The assessment of statistical methods is an important methodological step, as the quality of past climate reconstructions largely depends on the statistical method applied. It is found that only a subset of current state-of-the-art models is appropriate to be used as a pseudo-proxy test bed. This requires a rigorous evaluation of the models ability prior to the setup of the PPEs and according model-proxy comparison studies. In order to obtain a better understanding on the impact of changes in external forcings, the origin of the North Atlantic sea surface temperature variability is investigated during the preindustrial era of last millennium. These results indicate that phases with lower solar activity could be linked to blocking-like atmospheric circulation in the North Atlantic basin.

Outlook

In the first part of the thesis I evaluated statistical methods that could be used for the reconstruction of NA past climate. In future work, principal component regression could be a method applied on the $\delta^{18}O$ series of Arctica islandica for the reconstruction of the SSTs of the east-Atlantic basin.

How are changes in solar forcing registered in paleoclimate models and proxy archives like Arctica islandica?

To answer the Outlook Question, I would need to find the mechanisms responsible for the in-homogenous effects of TSI changes on the regional climate of the NA basin, starting with the effects of blocking patterns to ocean circulation in decadal to centennial time scales. To reach robust conclusions in both the Outlook Question and Question e, I should additionally investigate the response of marine proxies collected in regions where model simulations suggest that TSI changes induce changes in the local SSTs. Moreover, the study of an only solar forced ensemble, instead of a single simulation, would be advantageous in order to establish core conclusions regarding the effect of solar forcing versus internal variability. The MPI-ESM model does not provide an ensemble of solar forced simulations but in a follow—up analysis I intend to use the CCSM4 solar forced simulations for the investigation of solar induced changes in the ocean circulation of the NA basin. Additionally, atmospheric proxies such as tree rings could be used to study the response of atmospheric variability to TSI changes. In this way a connection could be possibly established between atmospheric and oceanic circulation.

Abbreviations

AMO	Atlantic Multidecadal Oscillation
AMOC	Atlantic Meridional Overturning Circulation
AO	Arctic Oscillation
AOD	Aerosol Optical Depth
AOGCMs	Atmosphere Ocean General Circulation Models
AR4	Assessment Report 4
ASUW	Atlantic Subarctic Upper Water
CCA	Canonical Correlation Analysis
CFR	Climate Field Reconstruction
CMIP5	Coupled Model Inter-comparison Project phase 5
ECM	Electric Conductivity Measurements
EGC	East Greenland Current
ENACW	Eastern North Atlantic Central Water
EOF	Empirical Orthogonal Function
ESMs	Earth System Models
FAR	First Assessment Report
GCRs	Galactic Cosmic rays
IPCC	Intergovernmental Panel on Climate Change
IS	Icelandic Shelf
LIA	Little Ice Age
MCA	Medieval Climate Anomaly
NA	North Atlantic
NAC	North Atlantic Current
NADW	North Atlantic Deep Water
NH	North Hemisphere
NS	North Sea
PCA	Principal Component Analysis
PCR	Principal Component Regression
PMIP3	Paleoclimate Modelling Intercomparison Project, phase 3
PPE	Pseudo-proxy Experiments
RMSE	Root Mean Square Error
SACW	South Atlantic Central Water
SAR	Second Assessment Report
SST	Sea Surface Temperature
TAR	Third Assessment Report
THC	Thermohaline Circulation
TSI	Total Solar Irradiance
WNACW	Western North Atlantic Central Water

List of Publications

Pyrina M, Wagner S, Zorita E (2017) Evaluation of CMIP5 models over the northern North Atlantic in the context of forthcoming paleoclimatic reconstructions. Climate Dynamics:1-19, doi:10.1007/s00382-017-3536-x

Pyrina M, Wagner S, Zorita E (2017) Pseudo-proxy evaluation of Climate Field Reconstruction methods of North Atlantic climate based on an annually resolved marine proxy network, Climate of the Past Discussions, doi:10.5194/cp-2017-61

Pyrina M, Wagner S, Zorita E: Signature of solar forcing on the North Atlantic basin during the preindustrial era in summertime, Under preparation

Bibliography

Adolphi F, Muscheler R, Svensson A, Aldahan A, Possnert G, Beer J, Sjolte J, Björck S, Matthes K, Thiéblemont R (2014) Persistent link between solar activity and Greenland climate during the Last Glacial Maximum. Nature Geoscience 7:662-666

Ahmed M, Anchukaitis KJ, Asrat A, Borgaonkar H, Braida M, Buckley BM, Büntgen U, Chase BM, Christie DA, Cook ER (2013) Continental-scale temperature variability during the past two millennia. Nature Geoscience 6:339-346

Alley R (2004) GISP2 Ice Core Temperature and Accumulation Data. IGBP PAGES/World Data Center for Paleoclimatology Data Contribution Series# 2004-013. NOAA/NGDC Paleoclimatology Program Boulder, CO, USA

Ammann, Caspar M, Fortunat Joos, David S Schimel, Bette L Otto-Bliesner, and Robert A Tomas. 2007. 'Solar influence on climate during the past millennium: Results from transient simulations with the NCAR Climate System Model', Proceedings of the National Academy of Sciences, 104: 3713-18.

Arora VK, Scinocca JF, Boer GJ, et al. (2011) Carbon emission limits required to satisfy future representative concentration pathways of greenhouse gases. Geophysical Research letters 38: 3–8. doi:10.1029/2010GL046270

Bai Y, Cai WJ, He X, Zhai W, Pan D, Dai M, Yu P (2015) A mechanistic semi-analytical method for remotely sensing sea surface pCO2 in river-dominated coastal oceans: A case study from the East China Sea. Journal of Geophysical Research: Oceans 120: 2331-2349. doi:10.1002/2014JC010632

Bard E, Raisbeck G, Yiou F, Jouzel J (2000) Solar irradiance during the last 1200 years based on cosmogenic nuclides. Tellus B 52:985-992

Barriopedro D, García-Herrera R, Huth R (2008) Solar modulation of Northern Hemisphere winter blocking. Journal of Geophysical Research: Atmospheres 113

Batehup R, McGregor S, Gallant A (2015) The influence of non-stationary teleconnections on palaeoclimate reconstructions of ENSO variance using a pseudoproxy framework. Climate of the Past 11:1733-1749

Beer J (2005) Solar variability and climate change. MEMORIE-SOCIETA ASTRONOMICA ITALIANA 76:751

Benestad R, Schmidt G (2009) Solar trends and global warming. Journal of Geophysical Research: Atmospheres 114

Bernstein L, Bosch P, Canziani O, Chen Z, Christ R, Davidson O, Hare W, Huq S, Karoly D, Kattsov V (2008) Climate change 2007: Synthesis report: An assessment of the intergovernmental panel on climate change.

Bjerknes V (1906) Fields of force: supplementary lectures, applications to meteorology; a course of lectures in mathematical physics delivered December 1 to 23, 1905, Vol. The Columbia university press

Bjerknes V (1910) Dynamic meteorology and hydrography, Vol. Carnegie

Bojariu R, Gimeno L (2003) Predictability and numerical modelling of the North Atlantic Oscillation. Earth-Science Reviews 63: 145–168. Available at: http://dx.doi.org/10.1016/S0012-8252(03)00036-9

Böning CW, Scheinert M, Dengg J, Biastoch A, Funk A (2006) Decadal variability of subpolar gyre transport and its reverberation in the North Atlantic overturning. Geophysical Research Letters 33

Booth BB, Dunstone NJ, Halloran PR, Andrews T, Bellouin N (2012) Aerosols implicated as a prime driver of twentieth-century North Atlantic climate variability. Nature 484:228-232

Booth BBB, Dunstone NJ, Halloran PR, Andrews T, Bellouin N (2012) Aerosols implicated as a prime driver of twentieth-century North Atlantic climate variability. Nature 484: 228-232. doi:10.1038/nature10946

Bradley RS (1996) Are there optimum sites for global paleotemperature reconstruction? In: Climatic variations and forcing mechanisms of the last 2000 years. Springer

Briffa KR, Osborn TJ, Schweingruber FH, Harris IC, Jones PD, Shiyatov SG, Vaganov EA (2001) Low-frequency temperature variations from a northern tree ring density network. Journal of Geophysical Research: Atmospheres 106:2929-2941

Bryan FO, Hecht MW, Smith RD (2007) Resolution convergence and sensitivity studies with North Atlantic circulation models. Part I: The western boundary current system. Ocean Model. 16: 141–159. doi:10.1016/j.ocemod.2006.08.005

Butler PG, Richardson CA, Scourse JD, Wanamaker AD, Shammon TM, Bennell JD (2010) Marine climate in the Irish Sea: analysis of a 489-year marine master chronology derived from growth increments in the shell of the clam Arctica islandica. Quat. Sci. Rev. 29: 1614–1632. doi:10.1016/j.quascirev.2009.07.010

Butler PG, Richardson CA, Scourse JD, Witbaard R, Schöne BR, Fraser NM, Wanamaker AD, Bryant CL, Harris I, Robertson I (2009) Accurate increment identification and the spatial extent of the common signal in five Arctica islandica chronologies from the Fladen Ground, northern North Sea. Paleoceanography 24

Butler PG, Scourse JD, Richardson CA, Wanamaker AD, Bryant CL, Bennell JD (2009) Continuous marine radiocarbon reservoir calibration and the 13 C Suess effect in the Irish Sea: Results from the first multi-centennial shell-based marine master chronology. Earth Planet. Sci. Lett. 279: 230–241. doi:10.1016/j.epsl.2008.12.043

Butler PG, Wanamaker AD, Scourse JD, Richardson CA, Reynolds DJ (2013) Variability of marine climate on the North Icelandic Shelf in a 1357-year proxy archive based on growth increments in the bivalve Arctica islandica. Palaeogeography, Palaeoclimatology, Palaeoecology 373:141-151

Camp CD, Tung KK (2007) Surface warming by the solar cycle as revealed by the composite mean difference projection. Geophysical Research Letters 34

Cannaby H and Hüsrevoğlu YS (2009) The influence of low-frequency variability and long-term trends in North Atlantic sea surface temperature on Irish waters. ICES Journal of Marine Science: Journal du Conseil 66: 1480-1489. doi:10.1093/icesjms/fsp062

Carton JA, Cao X, Giese BS, Da Silva AM (1996) Decadal and Interannual SST Variability in the Tropical Atlantic Ocean. Journal of Physical Oceanography 26: 1165–1175. doi:10.1175/1520-0485(1996)026<1165:DAISVI>2.0.CO;2

Cattle H, Crossley J, Drewry DJ. (1995) Modelling arctic climate change [and discussion]. Philosophical Transactions of the Royal Society of London A: Mathematical, Physical and Engineering Sciences 352:201-13. doi:10.1098/rsta.1995.0064

Change IPoC (2014) Climate Change 2014–Impacts, Adaptation and Vulnerability: Regional Aspects, Vol. Cambridge University Press

Cheng W, Chiang JCH, Zhang D (2013) Atlantic meridional overturning circulation (AMOC) in CMIP5 Models: RCP and historical simulations. Journal of Climate 26: 7187–7197. doi:10.1175/JCLI-D-12-00496.1

Coats S, Smerdon JE, Cook BI, Seager R (2013) Stationarity of the tropical pacific teleconnection to North America in CMIP5/PMIP3 model simulations. Geophysical Research Letters 40: 4927-32. doi:10.1002/grl.50938

Cole-Dai J (2010) Volcanoes and climate. Wiley Interdisciplinary Reviews: Climate Change 1:824-839

Collins M, Tett SFB, Cooper C (2001) The internal climate variability of HadCM3, a version of the Hadley Centre coupled model without flux adjustments. Climate Dynamics 17: 61–81. doi:10.1007/s003820000094

Cook ER, D'Arrigo RD, Mann ME (2002) A well-verified, multiproxy reconstruction of the winter North Atlantic Oscillation Index since ad 1400*. Journal of Climate 15:1754-1764

Copard K, Colin C, Henderson G, Scholten J, Douville E, Sicre M-A, Frank N (2012) Late Holocene intermediate water variability in the northeastern Atlantic as recorded by deep-sea corals. Earth and Planetary Science Letters 313:34-44

Cox PM, Betts RA, Bunton CB, Essery RLH, Rowntree PR, Smith J (1999) The impact of new land surface physics on the GCM simulation of climate and climate sensitivity. Climate Dynamics 15: 183–203. doi:10.1007/s003820050276

Crowley T, Unterman M (2013) Technical details concerning development of a 1200 yr proxy index for global volcanism. Earth System Science Data 5:187-197

Crowley TJ (2000) Causes of climate change over the past 1000 years. Science 289:270-277

Crowley TJ, Lowery TS (2000) How warm was the medieval warm period? AMBIO: A Journal of the Human Environment 29:51-54

Crowley TJ, Zielinski G, Vinther B, Udisti R, Kreutz K, Cole-Dai J, Castellano E (2008) Volcanism and the little ice age. PAGES news 16:22-23

Cunningham LK, Austin WE, Knudsen KL, Eiríksson J, Scourse JD, Wanamaker AD, Butler PG, Cage AG, Richter T, Husum K, Hald M (2013) Reconstructions of surface ocean conditions from the northeast Atlantic and Nordic seas during the last millennium. The Holocene 23: 921-35. doi:10.1177/0959683613479677

Czaja A and Frankignoul C (2002) Observed Impact of Atlantic SST Anomalies on the North Atlantic Oscillation. Journal of Climate 15: 606-623. Available at: http://dx.doi.org/10.1175/1520-0442(2002)015<0606:OIOASA>2.0.CO;2

Dahlgren TG, Weinberg JR, Halanych KM (2000) Phylogeography of the ocean quahog (Arctica islandica): influences of paleoclimate on genetic diversity and species range. Marine Biology 137: 487–495. doi:10.1007/s002270000342

Danabasoglu G, Bates SC, Briegleb BP, et al. (2012) The CCSM4 ocean component. Journal of Climate 25: 1361–1389. Available at: http://dx.doi.org/10.1175/JCLI-D-11-00091.1

Danabasoglu G, Large WG, Tribbia JJ, Gent PR, Briegleb BP, McWilliams JC (2006) Diurnal coupling in the tropical oceans of CCSM3. Journal of climate 19:2347-2365

Dannenberg MP, Wise EK (2013) Performance of climate field reconstruction methods over multiple seasons and climate variables. Journal of Geophysical Research: Atmospheres 118:9595-9610

Davini P, Cagnazzo C, Neale R, Tribbia J (2012) Coupling between Greenland blocking and the North Atlantic Oscillation pattern. Geophysical Research Letters 39

Dee SG, Steiger NJ, Emile-Geay J, Hakim GJ (2016) On the utility of proxy system models for estimating climate states over the common era. Journal of Advances in Modeling Earth Systems. doi:10.1002/2016MS000677

Delmas RJ, Legrand M, Aristarain AJ, Zanolini F (1985) Volcanic deposits in Antarctic snow and ice. Journal of Geophysical Research: Atmospheres 90:12901-12920

DelSole T, Tippett MK, Shukla J (2011) A significant component of unforced multidecadal variability in the recent acceleration of global warming. Journal of Climate 24: 909–926. Available at: http://dx.doi.org/10.1175/2010JCLI3659.1

Deser C, Alexander MA, Xie SP, Phillips AS (2010) Sea surface temperature variability: Patterns and mechanisms. Annual Review of Marine Science 2: 115-43. doi:10.1146/annurev-marine-120408-151453

Deser C, Blackmon ML (1993) Surface Climate Variations over the North Atlantic Ocean during Winter: 1900–1989. Journal of Climate 6: 1743–1753. doi:10.1175/1520-0442(1993)006<1743:SCVOTN>2.0.CO;2

Ding Y, Carton JA, Chepurin GA, Stenchikov G, Robock A, Sentman LT, Krasting JP (2014) Ocean response to volcanic eruptions in Coupled Model Intercomparison Project 5 simulations. Journal of Geophysical Research: Oceans 119:5622-5637

Douglass DH, Clader BD (2002) Climate sensitivity of the Earth to solar irradiance. Geophysical Research Letters 29

Dowsett HJ, Robinson MM (2009) Mid-Pliocene equatorial Pacific sea surface temperature reconstruction: a multi-proxy perspective. Philosophical Transactions of the Royal Society of London A: Mathematical, Physical and Engineering Sciences 367:109-125

Druffel ER (1997) Geochemistry of corals: Proxies of past ocean chemistry, ocean circulation, and climate. Proceedings of the National Academy of Sciences 94:8354-8361

Dufresne JL, Foujols MA, Denvil S, et al. (2013) Climate change projections using the IPSL-CM5 Earth System Model: from CMIP3 to CMIP5. Climate Dynamics 40: 2123–2165. doi:10.1007/s00382-012-1636-1

Eagle R, Eiler JM, Tripati AK, Ries J, Freitas P, Hiebenthal C, Wanamaker AD, Taviani M, Elliot M, Marenssi S (2013) The influence of temperature and seawater carbonate saturation state on 13C-18O bond ordering in bivalve mollusks. Biogeosciences 10

Eagle RA, Eiler JM, Tripati AK, et al. (2013) The influence of temperature and seawater carbonate saturation state on 13C-18O bond ordering in bivalve mollusks. Biogeosciences 10. Available at: https://doi.org/10.5194/bg-10-4591-2013

Eddy JA, Gilman P, Trotter D (1976) Solar rotation during the Maunder Minimum. Solar physics 46:3-14

Edwards PN (2011) History of climate modeling. Wiley Interdisciplinary Reviews: Climate Change 2:128-139

Enfield DB, Cid-Serrano L (2006) Projecting the risk of future climate shifts. International Journal of Climatology 26:885-895

Ermolli I, Matthes K, Dudok de Wit T, Krivova NA, Tourpali K, Weber M, Unruh YC, Gray L, Langematz U, Pilewskie P (2013) Recent variability of the solar spectral irradiance and its impact on climate modelling. Atmospheric Chemistry and Physics 13:3945-3977

Esper J, Cook ER, Schweingruber FH (2002) Low-frequency signals in long tree-ring chronologies for reconstructing past temperature variability. science 295:2250-2253

Evans M, Smerdon JE, Kaplan A, Tolwinski-Ward S, González-Rouco JF (2014) Climate field reconstruction uncertainty arising from multivariate and nonlinear properties of predictors. Geophysical research letters 41:9127-9134

Evans MN, Kaplan A, Cane MA (2000) Intercomparison of coral oxygen isotope data and historical sea surface temperature (SST): Potential for coral-based SST field reconstructions. Paleoceanography 15:551-563

Evans MN, Kaplan A, Cane MA (2002) Pacific sea surface temperature field reconstruction from coral δ18O data using reduced space objective analysis. Paleoceanography 17

Fan M and Schneider EK (2010) Observed Decadal North Atlantic Tripole SST Variability. Part I: Weather Noise Forcing and Coupled Response. Journal of the Atmospheric Sciences 69: 35-50. Available at: http://dx.doi.org/10.1175/JAS-D-11-018.1

Flato G, Marotzke J, Abiodun B, Braconnot P, Chou SC, Collins WJ, Cox P, Driouech F, Emori S, Eyring V (2013) Evaluation of Climate Models. In: Climate Change 2013: The Physical Science Basis. Contribution of Working Group I to the Fifth Assessment Report of the Intergovernmental Panel on Climate Change. Climate Change 2013 5:741-866

Flato GM (2011) Earth system models: an overview. Wiley Interdisciplinary Reviews: Climate Change 2:783-800

Fligge M, Solanki S (2000) The solar spectral irradiance since 1700. Geophysical Research Letters 27:2157-2160

Franco B, Fettweis X, Lang C, Erpicum M (2012) Impact of spatial resolution on the modelling of the Greenland ice sheet surface mass balance between 1990–2010, using the regional climate model MAR. Cryosph. 6: 695–711. doi:10.5194/tc-6-695-2012

Free M, Robock A (1999) Global warming in the context of the Little Ice Age. Journal of Geophysical Research: Atmospheres 104:19057-19070

FRIIS-CHRISTENSEN E, LASSEN K (1991) Length of the Solar Cycle: An Indicator of Solar Activity Closely Associated with Climate. Science 254:698-700

Friis-Christensen E, Svensmark H (1997) What do we really know about the sun-climate connection? Advances in Space Research 20:913-921

Gallant AJ, Phipps SJ, Karoly DJ, Mullan AB, Lorrey AM (2013) Nonstationary Australasian teleconnections and implications for paleoclimate reconstructions. Journal of Climate 26:8827-8849

Gao C, Robock A, Ammann C (2008) Volcanic forcing of climate over the past 1500 years: An improved ice core-based index for climate models. Journal of Geophysical Research: Atmospheres 113

Gastineau G and Frankignoul C (2014) Influence of the North Atlantic SST Variability on the Atmospheric Circulation during the Twentieth Century. Journal of Climate 28: 1396–1416. doi:10.1175/JCLI-D-14-00424.1

Gent PR, Danabasoglu G, Donner LJ, Holland MM, Hunke EC, Jayne SR, Lawrence DM, Neale RB, Rasch PJ, Vertenstein M (2011) The community climate system model version 4. Journal of Climate 24:4973-4991. doi:10.1175/2011JCLI4083.1

Gillikin DP, Dehairs F, Lorrain A, Steenmans D, Baeyens W, André L (2006) Barium uptake into the shells of the common mussel (Mytilus edulis) and the potential for estuarine paleo-chemistry reconstruction. Geochimica et Cosmochimica Acta 70: 395–407. Available at: http://dx.doi.org/10.1016/j.gca.2005.09.015

Giorgetta MA, Jungclaus J, Reick CH, Legutke S, Bader J, Böttinger M, Brovkin V, Crueger T, Esch M, Fieg K (2013) Climate and carbon cycle changes from 1850 to 2100 in MPI-ESM simulations for the Coupled Model Intercomparison Project phase 5. Journal of Advances in Modeling Earth Systems 5:572-597

Gómez-Navarro JJ, Werner J, Wagner S, Luterbacher J, Zorita E (2015) Establishing the skill of climate field reconstruction techniques for precipitation with pseudoproxy experiments. Climate Dynamics 45:1395-1413

Gordon C, Cooper C, Senior CA, et al. (2000) The simulation of SST, sea ice extents and ocean heat transports in a version of the Hadley Centre coupled model without flux adjustments. Clim. Dyn. 16: 147–168. doi:10.1007/s003820050010

Gordon HB, O'Farrell S, Collier M, et al. (2010) The CSIRO Mk3. 5 climate model. CSIRO and Bureau of Meteorology.

Gordon HB, O'Farrell SP (1997) Transient climate change in the CSIRO coupled model with dynamic sea ice. Mon. Weather Rev 125: 875–908. Available at: http://dx.doi.org/10.1175/1520-0493(1997)125<0875:TCCITC>2.0.CO;2

Gray ST, Graumlich LJ, Betancourt JL, Pederson GT (2004) A tree-ring based reconstruction of the Atlantic Multidecadal Oscillation since 1567 AD. Geophysical Research Letters 31

Griffies SM, Harrison MJ, Pacanowski RC, Rosati A (2004) A technical guide to MOM4. GFDL Ocean Group Tech. Rep. 5: 371

Haigh JD (2007) The Sun and the Earth's climate. Living Reviews in Solar Physics 4:1-64

Häkkinen S, Rhines PB, Worthen DL (2011) Warm and saline events embedded in the meridional circulation of the northern North Atlantic. Journal of Geophysical Research: Oceans 116

Halvorsen MH, Smedsrud LH, Zhang R, Kloster K (2015) Fram Strait spring ice export and September Arctic sea ice. Cryosphere Discuss 9: 4205–4235. doi:10.5194/tcd-9-4205-2015

Hammer CU, Clausen HB, Dansgaard W (1980) Greenland ice sheet evidence of post-glacial volcanism and its climatic impact. Nature 288:230-235

Hansen J, Sato M, Ruedy R, Lo K, Lea DW, Medina-Elizade M (2006) Global temperature change. Proceedings of the National Academy of Sciences 103:14288-14293

Hasumi H (2014) A review on ocean resolution dependence of climate biases in AOGCMs. CLIVAR Exch. 65: 7–9.

Hegerl GC, Crowley TJ, Hyde WT, Frame DJ (2006) Climate sensitivity constrained by temperature reconstructions over the past seven centuries. Nature 440:1029-1032

High relation: CMIP5 model study. Clim. Dyn. 45: 273–289. doi:10.1007/s00382-014-2285-3

Hijmans RJ, Cameron SE, Parra JL, Jones G, Jarvis A (2005) Very high resolution interpolated climate surfaces for global land areas. International Journal of Climatology 25: 1965-78. doi:10.1002/joc.1276

Hirahara S, Ishii M, Fukuda Y (2014) Centennial-Scale Sea Surface Temperature Analysis and Its Uncertainty. Journal of Climate 27: 57–75. doi:10.1175/JCLI-D-12-00837.1

Hood L, Schimanke S, Spangehl T, Bal S, Cubasch U (2013) The surface climate response to 11-yr solar forcing during northern winter: observational analyses and comparisons with GCM simulations. Journal of Climate 26:7489-7506

Hourdin F, Foujols MA, Codron F, et al. (2013) Impact of the LMDZ atmospheric grid configuration on the climate and sensitivity of the IPSL-CM5A coupled model. Climate Dynamics 40: 2167–2192. doi:10.1007/s00382-012-1411-3

Hunke E, Lipscomb W, Turner A, Jeffery N, Elliott S (2008) CICE: the Los Alamos sea ice model, documentation and software, version 4.0. Los Alamos National Laboratory Tech. Rep. In. LA-CC-06-012

Hurtt GC, Chini LP, Frolking S, Betts R, Feddema J, Fischer G, Goldewijk KK, Hibbard K, Janetos A, Jones C (2009) Harmonisation of global land-use scenarios for the period 1500–2100 for IPCC-AR5.

Ilyina T, Six KD, Segschneider J, Maier-Reimer E, Li H, Núñez-Riboni I (2013) Global ocean biogeochemistry model HAMOCC: Model architecture and performance as component of the MPI-Earth system model in different CMIP5 experimental realizations. Journal of Advances in Modeling Earth Systems 5:287-315

Ineson S, Scaife AA, Knight JR, Manners JC, Dunstone NJ, Gray LJ, Haigh JD (2011) Solar forcing of winter climate variability in the Northern Hemisphere. Nature Geoscience 4:753-757

Ingram W (2007) Detection and attribution of climate change, and understanding solar influence on climate. In: Solar variability and planetary climates. Springer

Ishii M, Shouji A, Sugimoto S, Matsumoto T (2005) Objective analyses of sea-surface temperature and marine meteorological variables for the 20th century using ICOADS and the Kobe collection. International Journal of Climatology 25: 865–879. doi:10.1002/joc.1169

Jha B, Hu ZZ, Kumar A (2014) SST and ENSO variability and change simulated in historical experiments of CMIP5 models. Climate Dynamics 42: 2113–2124. doi:10.1007/s00382-013-1803-z

Jones GS, Stott PA, Christidis N (2013) Attribution of observed historical near–surface temperature variations to anthropogenic and natural causes using CMIP5 simulations. Journal of Geophysical Research: Atmospheres, 118: 4001-4024. doi:10.1002/jgrd.50239

Jones P, Briffa K, Barnett T, Tett S (1998) High-resolution palaeoclimatic records for the last millennium: interpretation, integration and comparison with General Circulation Model control-run temperatures. The Holocene 8:455-471

Jones P, Briffa K, Osborn T, Lough J, Van Ommen T, Vinther B, Luterbacher J, Wahl E, Zwiers F, Mann M (2009) High-resolution palaeoclimatology of the last millennium: a review of current status and future prospects. The Holocene 19:3-49

Jones P, Osborn T, Briffa K (2001) The evolution of climate over the last millennium. Science 292:662-667

Jr ADW, Heinemeier J, Scourse JD, Richardson CA, Butler PG, Eiríksson J, Knudsen KL (2008) Very long-lived mollusks confirm 17th century AD tephra-based radiocarbon reservoir ages for North Icelandic shelf waters. Radiocarbon 50:399-412

Jungclaus JH, Fischer N, Haak H, et al. (2013) Characteristics of the ocean simulations in the Max Planck Institute Ocean Model (MPIOM) the ocean component of the MPI-Earth system model. J. Adv. Model. Earth Syst. 5: 422–446. Available at: http://doi.wiley.com/10.1002/jame.20023. doi:10.1002/jame.20023

Jungclaus JH, Lohmann K, Zanchettin D (2014) Enhanced 20th-century heat transfer to the Arctic simulated in the context of climate variations over the last millennium. Climate of the Past 10: 2201–2213. doi:10.5194/cp-10-2201-2014

Kaplan A, Cane MA, Kushnir Y (2001) Reduced space approach to the optimal analysis of historical marine observations: Accomplishments, difficulties and prospects. WMO Guide to the Applications of Marine Climatology.

Kauker F (2003) Variability of Arctic and North Atlantic sea ice: A combined analysis of model results and observations from 1978 to 2001. J. Geophys. Res. 108. doi:10.1029/2002JC001573

Kiehl JT, Trenberth KE (1997) Earth's annual global mean energy budget. Bulletin of the American Meteorological Society 78:197-208

Kinne, Stefan, Declan O'Donnel, Philip Stier, Silvia Kloster, Kai Zhang, Hauke Schmidt, Sebastian Rast, Marco Giorgetta, Tom F Eck, and Bjorn Stevens. 2013. 'MAC-v1: A new global aerosol climatology for climate studies', Journal of Advances in Modeling Earth Systems, 5: 704-40.

Knight JR, Allan RJ, Folland CK, Vellinga M, Mann ME (2005) A signature of persistent natural thermohaline circulation cycles in observed climate. Geophys. Res. Lett. 32: 1–4. doi:10.1029/2005GL024233

Knutson et al. (2005) Assessment of Twentieth-Century Regional Surface Temperature Trends Using the GFDL CM2 Coupled Models. Journal of Climate 19: 1624-51. Available at: http://dx.doi.org/10.1175/JCLI3709.1

Kowalczyk EA, Garratt JR, Krummel PB (1994) Implementation of a soil-canopy scheme into the CSIRO GCM-regional aspects of the model response. CSIRO

Krinner G, Viovy N, de Noblet-Ducoudré N, Ogée J, Polcher J, Friedlingstein P, Ciais P, Sitch S, Prentice IC (2005) A dynamic global vegetation model for studies of the coupled atmosphere-biosphere system. Global Biogeochemical Cycles 19. doi:10.1029/2003GB002199

Kushnir Y (1994) Interdecadal Variations in North Atlantic Sea Surface Temperature and Associated Atmospheric Conditions. Journal of Climate 7: 141–157. doi:10.1175/1520-0442(1994)007<0141:IVINAS>2.0.CO;2

Labitzke K, Austin J, Butchart N, Knight J, Takahashi M, Nakamoto M, Nagashima T, Haigh J, Williams V (2002) The global signal of the 11-year solar cycle in the stratosphere: observations and models. Journal of atmospheric and solar-terrestrial physics 64:203-210

Laken BA, Čalogović J (2013) Composite analysis with Monte Carlo methods: an example with cosmic rays and clouds. Journal of Space Weather and Space Climate 3:A29

Landrum L, Otto-Bliesner BL, Wahl ER, Conley A, Lawrence PJ, Rosenbloom N, Teng H (2013) Last millennium climate and its variability in CCSM4. Journal of Climate 26:1085-1111

Lawrence DM, Oleson KW, Flanner MG, Fletcher CG, Lawrence PJ, Levis S, Swenson SC, Bonan GB (2012) The CCSM4 land simulation, 1850-2005: Assessment of surface climate and new capabilities. Journal of Climate 25:2240-2260

Lean J, Beer J, Bradley RS (1995) Reconstruction of solar irradiance since 1610: Implications for climate cbange. Geophysical Research Letters 22

Lean J, Rottman G, Harder J, Kopp G (2005) SORCE contributions to new understanding of global change and solar variability. In: The Solar Radiation and Climate Experiment (SORCE). Springer

Lean JL, Wang YM, Sheeley N (2002) The effect of increasing solar activity on the Sun's total and open magnetic flux during multiple cycles: Implications for solar forcing of climate. Geophysical Research Letters 29

Legates DR (1991) The effect of domain shape on principal components analyses. Int. J. Climatol. 11:135-146. doi:10.1002/joc.3370110203

Legrand M, De Angelis M, Delmas R (1984) Ion chromatographic determination of common ions at ultratrace levels in Antarctic snow and ice. Analytica chimica acta 156:181-192

Legras B, Mestre O, Bard E, Yiou P (2010) On misleading solar-climate relationship. Clim Past Discuss 6:767-800

Li B, Smerdon JE (2012) Defining spatial comparison metrics for evaluation of paleoclimatic field reconstructions of the Common Era. Environmetrics 23:394-406

Liu H, Wang C, Lee SK, Enfield D (2013) Atlantic warm pool variability in the CMIP5 simulations. J. Clim. 26: 5315–5336. doi:10.1175/JCLI-D-12-00556.1

Lockwood M (2012) Solar influence on global and regional climates. Surveys in Geophysics 33:503-534

Lockwood M Recent changes in solar outputs and the global mean surface temperature. III. Analysis of contributions to global mean air surface temperature rise. In. Proc Proceedings of the Royal Society of London A: Mathematical, Physical and Engineering Sciences. The Royal Society

Lockwood M, Fröhlich C Recent oppositely directed trends in solar climate forcings and the global mean surface air temperature. II. Different reconstructions of the total solar irradiance variation and dependence on response time scale. In. Proc Proceedings of the Royal Society of London A: Mathematical, Physical and Engineering Sciences. The Royal Society

Loder JW, Wang Z (2015) Trends and variability of sea surface temperature in the Northwest Atlantic from three historical gridded datasets. Atmosphere-Ocean 53: 510-28. Available at: http://dx.doi.org/10.1080/07055900.2015.1071237

Logemann K, Harms I (2006) High resolution modelling of the North Icelandic Irminger Current (NIIC). Ocean Sci. 2: 291–304. doi:10.5194/os-2-291-2006

Lohmann G, Rimbu N, Dima M (2005) Where can the Arctic Oscillation be reconstructed? Towards a reconstruction of climate modes based on stable teleconnections. Climate of the Past Discussions 1:17-56

Lohmann K, Mignot J, Langehaug HR, et al. (2015) Using simulations of the last millennium to understand climate variability seen in palaeo-observations: Similar variation of Iceland-Scotland overflow strength and Atlantic Multidecadal Oscillation. Clim. Past 11: 203–216. doi:10.5194/cp-11-203-2015

Luterbacher J, Dietrich D, Xoplaki E, Grosjean M, Wanner H (2004) European seasonal and annual temperature variability, trends, and extremes since 1500. Science 303:1499-1503

Madec G, NEMO team (2008) NEMO ocean engine. Note du Pole de modelisation, Institut Pierre-Simon Laplace (IPSL), France

Mann ME, Bradley RS, Hughes MK (1998) Global-scale temperature patterns and climate forcing over the past six centuries. Nature 392:779-787

Mann ME, Jones PD (2003) Global surface temperatures over the past two millennia. Geophysical Research Letters 30

Mann ME, Rutherford S (2002) Climate reconstruction using 'Pseudoproxies'. Geophysical Research Letters 29

Mann ME, Rutherford S, Wahl E, Ammann C (2007) Robustness of proxy-based climate field reconstruction methods. Journal of Geophysical Research: Atmospheres 112: 1–18. doi:10.1029/2006JD008272

Mann ME, Zhang Z, Rutherford S, Bradley RS, Hughes MK, Shindell D, Ammann C, Faluvegi G, Ni F (2009) Global signatures and dynamical origins of the Little Ice Age and Medieval Climate Anomaly. Science 326:1256-1260

Marchal O, Cacho I, Stocker TF, Grimalt JO, Calvo E, Martrat B, Shackleton N, Vautravers M, Cortijo E, van Kreveld S (2002) Apparent long-term cooling of the sea surface in the northeast Atlantic and Mediterranean during the Holocene. Quaternary Science Reviews 21:455-483

Marchal O, Waelbroeck C, Colin de Verdière A (2016) On the Movements of the North Atlantic Subpolar Front in the Preinstrumental Past*. Journal of Climate 29:1545-1571

Marcott SA, Shakun JD, Clark PU, Mix AC (2013) A reconstruction of regional and global temperature for the past 11,300 years. science 339:1198-1201

Marshall J et al. (2001) North Atlantic Climate Variability: Phenomena, Impacts and Mechanisms. International Journal of Climatology 21: 1863-98. doi:10.1002/joc.693

Marsland SJ, Haak H, Jungclaus JH, Latif M, Röske F (2003) The Max-Planck-Institute global ocean/sea ice model with orthogonal curvilinear coordinates. Ocean modelling 5:91-127

McGregor HV, Evans MN, Goosse H, Leduc G, Martrat B, Addison JA, Mortyn PG, Oppo DW, Seidenkrantz MS, Sicre MA, Phipps SJ (2015) Robust global ocean cooling trend for the pre-industrial Common Era. Nature Geoscience 8: 671–677. doi:10.1038/ngeo2510

Meehl GA, Arblaster JM, Matthes K, Sassi F, van Loon H (2009) Amplifying the Pacific climate system response to a small 11-year solar cycle forcing. Science 325:1114-1118

Meehl GA, Boer GJ, Covey C, Latif M, Stouffer RJ (2000) The coupled model intercomparison project (CMIP). Bulletin of the American Meteorological Society 81:313-318

Meehl GA, Covey C, McAvaney B, Latif M, Stouffer RJ (2005) Overview of the coupled model intercomparison project. Bulletin of the American Meteorological Society 86:89

Meehl GA, Washington WM, Wigley T, Arblaster JM, Dai A (2003) Solar and greenhouse gas forcing and climate response in the twentieth century. Journal of Climate 16:426-444

Mette MJ, Wanamaker AD, Carroll ML, Ambrose WG, Retelle MJ (2016) Linking large-scale climate variability with Arctica islandica shell growth and geochemistry in northern Norway. Limnology and Oceanography 61: 748–764. doi:10.1002/lno.10252

Moberg A, Sonechkin DM, Holmgren K, Datsenko NM, Karlén W (2005) Highly variable Northern Hemisphere temperatures reconstructed from low-and high-resolution proxy data. Nature 433:613-617

Moffa-Sánchez P, Hall IR, Barker S, Thornalley DJ, Yashayaev I (2014) Surface changes in the eastern Labrador Sea around the onset of the Little Ice Age. Paleoceanography 29:160-175

Moreno-Chamarro E, Zanchettin D, Lohmann K, Jungclaus JH (2016) An abrupt weakening of the subpolar gyre as trigger of Little Ice Age-type episodes. Climate Dynamics:1-18

Müller W, Roeckner E (2008) ENSO teleconnections in projections of future climate in ECHAM5/MPI-OM. Climate dynamics 31:533-549

Muscheler R, Adolphi F, Herbst K, Nilsson A (2016) The revised sunspot record in comparison to cosmogenic radionuclide-based solar activity reconstructions. Solar Physics 291:3025-3043

Neale RB, Richter J, Park S, Lauritzen PH, Vavrus SJ, Rasch PJ, Zhang M (2013) The mean climate of the Community Atmosphere Model (CAM4) in forced SST and fully coupled experiments. Journal of Climate 26:5150-5168

Nicol D (1951) Recent species of the veneroid pelecypod Arctica. J Wash Acad Sci 41: 102–106
Osborn TJ, Briffa KR (2006) The spatial extent of 20th-century warmth in the context of the past 1200 years. Science 311:841-844

Otterå OH, Bentsen M, Drange H, Suo L (2010) External forcing as a metronome for Atlantic multidecadal variability. Nat. Geosci. 3: 688–694. Available at: http://dx.doi.org/10.1038/ngeo955. doi:10.1038/ngeo955

Palmer M, Gray L, Allen M, Norton W (2004) Solar forcing of climate: model results. Advances in space research 34:343-348

Perez J, Menendez M, Mendez FJ, Losada IJ (2014) Evaluating the performance of CMIP3 and CMIP5 global climate models over the north-east Atlantic region. Clim. Dyn. 43: 1–18. doi:10.1007/s00382-014-2078-8

Pongratz J, Reick C, Raddatz T, Claussen M (2008) A reconstruction of global agricultural areas and land cover for the last millennium. Global Biogeochemical Cycles 22

Pope VD, Gallani ML, Rowntree PR, Stratton RA (2000) The impact of new physical parametrizations in the Hadley Centre climate model: HadAM3. Clim. Dyn. 16: 123–146. doi:10.1007/s003820050009

Pyrina M, Wagner S, Zorita E (2017) Evaluation of CMIP5 models over the northern North Atlantic in the context of forthcoming paleoclimatic reconstructions. Climate Dynamics:1-19

Qu X, Huang G. (2015) The decadal variability of the tropical Indian Ocean SST–the South Asian High relation: CMIP5 model study. Climate Dynamics 45:273-89.

Rahmstorf S (2002) Ocean circulation and climate during the past 120,000 years. Nature 419:207-214

Rahmstorf S (2003) Thermohaline circulation: The current climate. Nature 421:699-699

Raible C, Luksch U, Fraedrich K, Voss R (2001) North Atlantic decadal regimes in a coupled GCM simulation. Climate Dynamics 18:321-330

Rayner NA, Brohan P, Parker DE, et al. (2006) Improved analyses of changes and uncertainties in sea surface temperature measured in situ since the mid-nineteenth century: the HadSST2 dataset. J. Clim. 19: 446–469. Available at: http://dx.doi.org/10.1175/JCLI3637.1

Rayner NA, Parker DE, Horton EB, Folland CK, Alexander LV, Rowell DP, Kent EC, Kaplan A (2003) Global analyses of sea surface temperature, sea ice, and night marine air temperature since the late nineteenth century. Journal of Geophysical Research: Atmospheres 108: 4407. doi:10.1029/2002JD002670

Reick CH, Raddatz T, Brovkin V, Gayler V (2013) Representation of natural and anthropogenic land cover change in MPI-ESM. J. Adv. Model. Earth Syst. 5: 459–482. Available at: http://doi.wiley.com/10.1002/jame.20022. doi:10.1002/jame.20022

Reynolds DJ, Butler P, Williams S, Scourse J, Richardson C, Wanamaker A, Austin W, Cage A, Sayer M (2013) A multiproxy reconstruction of Hebridean (NW Scotland) spring sea surface temperatures between AD 1805 and 2010. Palaeogeography, Palaeoclimatology, Palaeoecology 386:275-285

Reynolds DJ, Richardson C, Scourse J, Butler P, Hollyman P, Roman-Gonzalez A, Hall IR (2017) Reconstructing North Atlantic marine climate variability using an absolutely-dated sclerochronological network. Palaeogeography, Palaeoclimatology, Palaeoecology 465:333-346

Reynolds DJ, Scourse J, Halloran P, Nederbragt A, Wanamaker A, Butler P, Richardson C, Heinemeier J, Eiríksson J, Knudsen K (2016) Annually resolved North Atlantic marine climate over the last millennium. Nature Communications 7:13502

Reynolds RW, Rayner NA, Smith TM, Stokes DC, Wang W (2002) An Improved In Situ and Satellite SST Analysis for Climate. Journal of climate 15: 1609–1625. Available at: http://dx.doi.org/10.1175/1520-0442(2002)015<1609:AIISAS>2.0.CO;2

Riedwyl N, Küttel M, Luterbacher J, Wanner H (2009) Comparison of climate field reconstruction techniques: application to Europe. Climate Dynamics 32:381-395

Riedwyl N, Luterbacher J, Wanner H (2008) An ensemble of European summer and winter temperature reconstructions back to 1500. Geophysical Research Letters 35

Rossby T (1996) The North Atlantic Current and surrounding waters: At the crossroads. Reviews of Geophysics 34:463-481

Rotstayn LD, Collier MA, Dix MR, Feng Y, Gordon HB, O'Farrell SP, Smith IN, Syktus J (2010) Improved simulation of Australian climate and ENSO-related rainfall variability in a global climate model with an interactive aerosol treatment. International Journal of Climatology 30:1067-1088

Rowell TW, Chaisson DR, McLane JT (1990) Size and age of sexual maturity and annual gametogenic cycle in the ocean quahog, Arctica islandica (Linnaeus, 1767), from coastal waters in Nova Scotia, Canada. J. Shellfish Res 9: 195–203.

Ruiz-Barradas A, Nigam S, Kavvada A (2013) The Atlantic Multidecadal Oscillation in twentieth century climate simulations: Uneven progress from CMIP3 to CMIP5. Clim. Dyn. 41: 3301–3315. doi:10.1007/s00382-013-1810-0

Rutherford S, Mann M, Delworth T, Stouffer R (2003) Climate field reconstruction under stationary and nonstationary forcing. Journal of Climate 16:462-479

Rutherford S, Mann M, Osborn T, Briffa K, Jones PD, Bradley R, Hughes M (2005) Proxy-based Northern Hemisphere surface temperature reconstructions: sensitivity to method, predictor network, target season, and target domain. Journal of Climate 18:2308-2329

Santer BD, Hansen J, Wigley T, Doutriaux C, Boyle J, Jones P, Meehl G (2001) Accounting for the effects of volcanoes and ENSO in comparisons of modeled and observed temperature trends. Journal of Geophysical Research D Atmospheres 106:28

Scafetta N, West B (2007) Phenomenological reconstructions of the solar signature in the Northern Hemisphere surface temperature records since 1600. Journal of Geophysical Research: Atmospheres 112

Schleussner CF, Runge J, Lehmann J, Levermann A (2014) The role of the North Atlantic overturning and deep ocean for multi-decadal global-mean-temperature variability. Earth Syst. Dyn. 5: 103–115. doi:10.5194/esd-5-103-2014

Schmidt et al. (2006) Present-Day Atmospheric Simulations Using GISS ModelE: Comparison to In Situ, Satellite, and Reanalysis Data. Journal of Climate 19: 153-92. Available at: http://dx.doi.org/10.1175/JCLI3612.1

Schmidt G, Jungclaus J, Ammann C, Bard E, Braconnot P, Crowley T, Delaygue G, Joos F, Krivova N, Muscheler R (2012) Climate forcing reconstructions for use in PMIP simulations of the Last Millennium (v1. 1). Geoscientific Model Development 5:185-191

Schöne BR (2013) Arctica islandica (Bivalvia): A unique paleoenvironmental archive of the northern North Atlantic Ocean. Glob. Planet. Change. 111: 199–225. doi:10.1016/j.gloplacha.2013.09.013

Schöne BR, Castro AD, Fiebig J, Houk SD, Oschmann W, Kröncke I (2004) Sea surface water temperatures over the period 1884–1983 reconstructed from oxygen isotope ratios of a bivalve mollusk shell (Arctica islandica, southern North Sea). Palaeogeography, Palaeoclimatology, Palaeoecology 212: 215-32. doi:10.1016/j.palaeo.2004.05.024

Schöne BR, Fiebig J, Pfeiffer M, et al. (2005) Climate records from a bivalved Methuselah. Palaeogeography, Palaeoclimatology, Palaeoecology 228: 130–148. doi:10.1016/j.palaeo.2005.03.049

Schöne BR, Houk SD, Castro ADF, et al. (2005) Daily growth rates in shells of Arctica islandica: assessing sub-seasonal environmental controls on a long-lived bivalve mollusk. Palaios 20: 78–92. doi:10.2110/palo.2003.p03-101

Schöne BR, Oschmann W, Rössler J, et al. (2003) North Atlantic Oscillation dynamics recorded in shells of a long-lived bivalve mollusk. Geology 31: 1037–1040. doi:10.1130/G20013.1

Schöne BR, Zhang Z, Radermacher P, et al. (2011) Sr/Ca and Mg/Ca ratios of ontogenetically old, long-lived bivalve shells (Arctica islandica) and their function as paleotemperature proxies. Palaeogeogr. Palaeoclimatol. Palaeoecol. 302: 52–64. Available at: http://dx.doi.org/10.1016/j.palaeo.2010.03.016

Schulzweida U., Kornblueh L., and Quast R. CDO User’s Guide, Climate Data Operators, Version 1.5.9, December 2012

Schurer AP, Tett SF, Hegerl GC (2014) Small influence of solar variability on climate over the past millennium. Nature Geoscience 7:104-108

Scourse J, Richardson C, Forsythe G, Harris I, Heinemeier J, Fraser N, Briffa K, Jones P (2006) First cross-matched floating chronology from the marine fossil record: data from growth lines of the long-lived bivalve mollusc Arctica islandica. The Holocene 16:967-974

Seager R, Battisti DS, Yin J, Gordon N, Naik N, Clement AC, Cane MA (2002) Is the Gulf Stream responsible for Europe's mild winters? Quarterly Journal of the Royal Meteorological Society 128:2563-2586

Shapiro A, Schmutz W, Rozanov E, Schoell M, Haberreiter M, Shapiro A, Nyeki S (2011) A new approach to the long-term reconstruction of the solar irradiance leads to large historical solar forcing. Astronomy & Astrophysics 529:A67

Shindell D, Rind D, Balachandran N, Lean J, Lonergan P (1999) Solar cycle variability, ozone, and climate. Science 284:305-308

Shindell DT, Schmidt GA, Mann ME, Rind D, Waple A (2001) Solar forcing of regional climate change during the Maunder Minimum. Science 294:2149-2152

Shindell DT, Schmidt GA, Miller RL, Mann ME (2003) Volcanic and solar forcing of climate change during the preindustrial era. Journal of Climate 16:4094-4107

Shupe MD, Intrieri JM (2004) Cloud radiative forcing of the Arctic surface: The influence of cloud properties, surface albedo, and solar zenith angle. J. Clim. 17: 616–628. doi:10.1175/1520-0442(2004)017<0616:CRFOTA>2.0.CO;2

Smerdon JE (2012) Climate models as a test bed for climate reconstruction methods: pseudoproxy experiments. Wiley Interdisciplinary Reviews: Climate Change 3:63-77

Smerdon JE, Coats S, Ault TR (2016) Model-dependent spatial skill in pseudoproxy experiments testing climate field reconstruction methods for the Common Era. Climate Dynamics 46:1921-1942

Smerdon JE, Kaplan A, Chang D (2008) On the Origin of the Standardization Sensitivity in RegEM Climate Field Reconstructions*. Journal of Climate 21:6710-6723

Smerdon JE, Kaplan A, Zorita E, González-Rouco JF, Evans MN (2011) Spatial performance of four climate field reconstruction methods targeting the Common Era. Geophysical research letters 38. doi:10.1029/2011GL047372

Smith R, Jones P, Briegleb B, Bryan F, Danabasoglu G, Dennis J, Dukowicz J, Eden C, Fox-Kemper B, Gent P (2010) The Parallel Ocean Program (POP) Reference Manual Ocean Component of the Community Climate System Model (CCSM) and Community Earth System Model (CESM). Rep LAUR-01853 141

Smith RD, Maltrud ME, Bryan FO, Hecht MW, Alamos L (2000) Numerical simulation of the North Atlantic Ocean at 1/10 degrees. J. Phys. Oceanogr. 30: 1532–1561. doi:10.1175/1520-0485(2000)030<1532:nsotna>2.0.co;2

Smith TM, Reynolds RW (2004) Improved extended reconstruction of SST (1854-1997). Journal of climate 17: 2466-77. Available at: http://dx.doi.org/10.1175/1520-0442(2004)017<2466:IEROS>2.0.CO;2

Smith TM, Reynolds RW, Livezey RE, Stokes DC (1996) Reconstruction of Historical Sea Surface Temperatures Using Empirical Orthogonal Functions. J. Clim. 9: 1403–1420. doi:10.1175/1520-0442(1996)009<1403:ROHSST>2.0.CO;2

Snyder CW (2010) The value of paleoclimate research in our changing climate. Climatic change 100:407-418

Solanki SK, Usoskin IG, Kromer B, Schüssler M, Beer J (2004) Unusual activity of the Sun during recent decades compared to the previous 11,000 years. Nature 431:1084-1087

Steinhilber F, Abreu JA, Beer J, Brunner I, Christl M, Fischer H, Heikkilä U, Kubik PW, Mann M, McCracken KG (2012) 9,400 years of cosmic radiation and solar activity from ice cores and tree rings. Proceedings of the National Academy of Sciences 109:5967-5971

Stevens B, Giorgetta M, Esch M, Mauritsen T, Crueger T, Rast S, Salzmann M, Schmidt H, Bader J, Block K (2013) Atmospheric component of the MPI-M Earth System Model: ECHAM6. Journal of Advances in Modeling Earth Systems 5:146-172

Stocker T (2014) Climate change 2013: the physical science basis: Working Group I contribution to the Fifth assessment report of the Intergovernmental Panel on Climate Change, Vol. Cambridge University Press

Stott PA, Jones GS (2009) Variability of high latitude amplification of anthropogenic warming. Geophysical Research Letters 36

Stott PA, Tett SFB, Jones GS, Allen MR (2000) External Control of 20th Century Temperature by Natural and Anthropogenic Forcings. Science 290: 2133–2137. doi:10.1126/science.290.5499.2133

Sun S, Bleck R (2006) Multi-century simulations with the coupled GISS-HYCOM climate model: control experiments. Clim. Dyn. 26: 407–428. doi:10.1007/s00382-005-0091-7

Swift JH, Aagaard K (1981) Seasonal transitions and water mass formation in the Iceland and Greenland seas. Deep Sea Research Part A. Oceanographic Research Papers 28: 1107-29. doi:10.1016/0198-0149(81)90050-9

Swingedouw D, Terray L, Cassou C, Voldoire A, Salas-Mélia D, Servonnat J (2011) Natural forcing of climate during the last millennium: fingerprint of solar variability. Climate Dynamics 36:1349-1364

Taboada FG, Anadón R (2012) Patterns of change in sea surface temperature in the North Atlantic during the last three decades: Beyond mean trends. Clim. Change 115: 419–431. doi:10.1007/s10584-012-0485-6

Taylor K, Alley R, Fiacco J, Grootes P, Lamorey G, Mayewski P, Spencer MJ (1992) Ice-core dating and chemistry by direct-current electrical conductivity. Journal of Glaciology 38:325-332

Taylor KE, Stouffer RJ, A. MG (2012) An overview of CMIP5 and the experiment design. Bulletin of the American Meteorological Society 3: 485–498. doi:10.1175/BAMS-D-11-00094.1

Tierney JE, Abram NJ, Anchukaitis KJ, Evans MN, Giry C, Kilbourne KH, Saenger CP, Wu HC, Zinke J (2015) Tropical sea surface temperatures for the past four centuries reconstructed from coral archives. Paleoceanography 30:226-252

Timmreck C, Lorenz SJ, Crowley TJ, Kinne S, Raddatz TJ, Thomas MA, Jungclaus JH (2009) Limited temperature response to the very large AD 1258 volcanic eruption. Geophysical Research Letters 36

Ting M, Kushnir Y, Li C (2014) North Atlantic multidecadal SST oscillation: External forcing versus internal variability. J. Mar. Syst. 133: 27–38. Available at: http://dx.doi.org/10.1016/j.jmarsys.2013.07.006

Ting M, Kushnir Y, Seager R, Li C (2009) Forced and internal twentieth-century SST trends in the North Atlantic*. J. Clim. 22: 1469–1481. Available at: http://dx.doi.org/10.1175/2008JCLI2561.1

Ting M, Kushnir Y, Seager R, Li C (2011) Robust features of Atlantic multidecadal variability and its climate impacts. Geophysical Research Letters 38: 1–6. doi:10.1029/2011GL048712

Tingley MP, Huybers P (2010) A Bayesian algorithm for reconstructing climate anomalies in space and time. Part I: Development and applications to paleoclimate reconstruction problems. Journal of Climate 23:2759-2781

Tréguier A-M, Theetten S, Chassignet EP, Penduff T, Smith R, Talley L, Beismann J, Böning C (2005) The North Atlantic subpolar gyre in four high-resolution models. Journal of Physical Oceanography 35:757-774

Valcke S, Craig T, Coquart L (2006) OASIS3-MCT User Guide OASIS3-MCT 3.0. CERFACS/CNRS SUC URA No1875.
Van Loon H, Meehl GA, Shea DJ (2007) Coupled air-sea response to solar forcing in the Pacific region during northern winter. Journal of Geophysical Research: Atmospheres 112

Vieira LEA, Solanki SK, Krivova NA, Usoskin I (2011) Evolution of the solar irradiance during the Holocene. Astronomy & Astrophysics 531:A6

Volodin EM, Galin VY, Gusev AV, Diansky NA, Smyshlyaev SP, Yakovlev NG (2010) Earth system model of INM RAS. Russ. J. Numer. Anal. Math. Model. 25: 531–545.

Von Salzen K, Scinocca JF, McFarlane NA, Li J, Cole JN, Plummer D, Verseghy D, Reader MC, Ma X, Lazare M, Solheim L (2013) The Canadian fourth generation atmospheric global climate model (CanAM4). Part I: representation of physical processes. Atmosphere-Ocean 51: 104-25.

von Storch H, Zorita E, González-Rouco F (2009) Assessment of three temperature reconstruction methods in the virtual reality of a climate simulation. International Journal of Earth Sciences 98:67-82

Von Storch H, Zorita E, Jones JM, Dimitriev Y, González-Rouco F, Tett SF (2004) Reconstructing past climate from noisy data. Science 306:679-682

Von Storch H, Zwiers FW (1999) Statistical Analysis in Climate Research. Cambridge University Press.

Wahl ER, Ammann CM (2007) Robustness of the Mann, Bradley, Hughes reconstruction of Northern Hemisphere surface temperatures: Examination of criticisms based on the nature and processing of proxy climate evidence. Climatic Change 85:33-69

Walker GT, Bliss EW (1932) World weather. V. Mem. Roy. Meteor. Soc. 4: 53–84.

Wallace JM, Gutzler DS (1981) Teleconnections in the geopotential height field during the Northern Hemisphere winter. Mon. Weather Rev. 109: 784–812.

Wanamaker AD, Butler PG, Scourse JD, et al. (2012) Surface changes in the North Atlantic meridional overturning circulation during the last millennium. Nature Communications 3: 899.

Wanamaker AD, Kreutz KJ, Schöne BR, Introne DS (2011) Gulf of Maine shells reveal changes in seawater temperature seasonality during the Medieval Climate Anomaly and the Little Ice Age. Palaeogeogr. Palaeoclimatol. Palaeoecol. 302: 43–51.

Wanamaker AD, Mette MJ, Whitney NM (2016) CLIVAR Newsletter: The potential for the long-lived bivalve Arctica islandica to contribute to our understanding of past AMOC dynamics. US CLIVAR Var. 14: 13–19.

Wanamaker Jr AD, Heinemeier J, Scourse JD, et al. (2008) Very long-lived mollusks confirm 17th century ad tephra-based radiocarbon reservoir ages for North Icelandic shelf waters. Radiocarbon 50: 399-412. Available at: http://dx.doi.org/10.2458/azu_js_rc.50.3222

Wanamaker Jr AD, Kreutz KJ, Schöne BR, et al. (2009) A late Holocene paleo-productivity record in the western Gulf of Maine, USA, inferred from growth histories of the long-lived ocean quahog (Arctica islandica). Int. J. Earth Sci. 98: 19–29. doi:10.1007/s00531-008-0318-z

Wanamaker Jr AD, Scourse JD, Richardson CA, Butler PG, Reynolds DJ, Ridgeway I (2008) Absolute chronologies from the ocean: Records from the longest-lived, non-colonial animals on earth. PAGES News 16: 4–6

Wang C, Zhang L, Lee S (2014a) A global perspective on CMIP5 climate model biases. Nat. Clim. Chang. 4: 201–205. doi:10.1038/NCLIMATE2118

Wang G, Dommenget D, Frauen C (2014b) An evaluation of the CMIP3 and CMIP5 simulations in their skill of simulating the spatial structure of SST variability. Clim. Dyn. 44: 95–114. doi:10.1007/s00382-014-2154-0

Wang J, Emile-Geay J, Guillot D, Smerdon J, Rajaratnam B (2014) Evaluating climate field reconstruction techniques using improved emulations of real-world conditions. Climate of the Past 10:1-19

Wang Y-M, Lean J, Sheeley Jr N (2005) Modeling the Sun’s magnetic field and irradiance since 1713. The Astrophysical Journal 625:522

Wanner H, Brönnimann S, Casty C, Gyalistras D, Luterbacher J, Schmutz C, Stephenson DB, Xoplaki E (2001) North Atlantic Oscillation–concepts and studies. Surveys in geophysics 22: 321-81. doi:10.1023/A:1014217317898

White WB, Lean J, Cayan DR, Dettinger MD (1997) Response of global upper ocean temperature to changing solar irradiance. Journal of Geophysical Research: Oceans 102:3255-3266

Willebrand J, Barnier B, Böning C, et al. (2001) Circulation characteristics in three eddy-permitting models of the North Atlantic. Prog. Oceanogr. 48: 123–161. doi:10.1016/S0079-6611(01)00003-9

Wilson R, Anchukaitis K, Briffa KR, Büntgen U, Cook E, D'Arrigo R, Davi N, Esper J, Frank D, Gunnarson B (2016) Last millennium northern hemisphere summer temperatures from tree rings: Part I: The long term context. Quaternary Science Reviews 134:1-18

Wilson R, Tudhope A, Brohan P, Briffa K, Osborn T, Tett S (2006) Two-hundred-fifty years of reconstructed and modeled tropical temperatures. Journal of Geophysical Research: Oceans 111

Winton M (2000) A Reformulated Three-Layer Sea Ice Model. Journal of Atmospheric and Oceanic Technology 17: 525-31.

Witbaard R (1996) Growth variations in Arctica islandica L. (Mollusca): a reflection of hydrography-related food supply. ICES Journal of Marine Science: Journal du Conseil 53: 981-7. doi:10.1006/jmsc.1996.0122

Witbaard R, Duineveld G, De Wilde P (1997) A long-term growth record derived from Arctica islandica (Mollusca, Bivalvia) from the Fladen Ground (northern North Sea). Journal of the Marine Biological Association of the United Kingdom 77:801-816

Witbaard R, Jansma E, Klaassen US (2003) Copepods link quahog growth to climate. J. Sea Res. 50: 77–83. Available at: http://dx.doi.org/10.1016/S1385-1101(03)00040-6

Witbaard R, Klein R (1994) Long-term trends on the effects of the southern North Sea beamtrawl fishery on the bivalve mollusc Arctica islandica L. (Mollusca, bivalvia). ICES Journal of Marine Science: Journal du Conseil 51: 99–105. doi: 10.1006/jmsc.1994.1009

Worley SJ, Woodruff SD, Reynolds RW, Lubker SJ, Lott N (2005) ICOADS release 2.1 data and products. International Journal of Climatology 25:823-842

Xoplaki E, Luterbacher J, Paeth H, Dietrich D, Steiner N, Grosjean M, Wanner H (2005) European spring and autumn temperature variability and change of extremes over the last half millennium. Geophysical Research Letters 32

Yang D, Saenko O a. (2012) Ocean Heat Transport and Its Projected Change in CanESM2. J. Clim. 25: 8148–8163. doi:10.1175/JCLI-D-11-00715.1

YASUNAKA S, Hanawa K. (2002) Regime shifts found in the Northern Hemisphere SST field. Journal of the Meteorological Society of Japan 80:119-35.

Yasunaka S, Hanawa K (2011) Intercomparison of historical sea surface temperature datasets. International Journal of Climatology 31: 1056–1073. doi:10.1002/joc.2104

Yoshimura H, Yukimoto S (2008) Development of a Simple Coupler (Scup) for Earth System Modeling. Pap. Meteor. Geophys 59: 19–29. doi:10.2467/mripapers.59.19

Zanchettin D, Rubino A, Jungclaus JH (2010) Intermittent multidecadal-to-centennial fluctuations dominate global temperature evolution over the last millennium. Geophysical Research Letters 37

Zanchettin D, Rubino A, Matei D, Bothe O, Jungclaus J (2013) Multidecadal-to-centennial SST variability in the MPI-ESM simulation ensemble for the last millennium. Climate dynamics 40:1301-1318

Zhang L, Wang C (2013) Multidecadal North Atlantic sea surface temperature and Atlantic meridional overturning circulation variability in CMIP5 historical simulations. J. Geophys. Res. Ocean 118: 5772-5791. doi:10.1002/jgrc.20390

Zhang X, Vincent LA, Hogg WD, Niitsoo A (2000) Temperature and precipitation trends in Canada during the 20th century. Atmosphere-Ocean 38: 395–429. doi:10.1080/07055900.2000.9649654

Zorita E, González-Rouco F (2002) Are temperature-sensitive proxies adequate for North Atlantic Oscillation reconstructions? Geophysical research letters 29

Zorita E, Von Storch H, Gonzalez-Rouco FJ, Cubasch U, Luterbacher J, Legutke S, Fischer-Bruns I, Schlese U (2004) Climate evolution in the last five centuries simulated by an atmosphere-ocean model: global temperatures, the North Atlantic Oscillation and the Late Maunder Minimum. Meteorologische Zeitschrift 13:271-289

List of Figures

List of Tables

Appendix C2

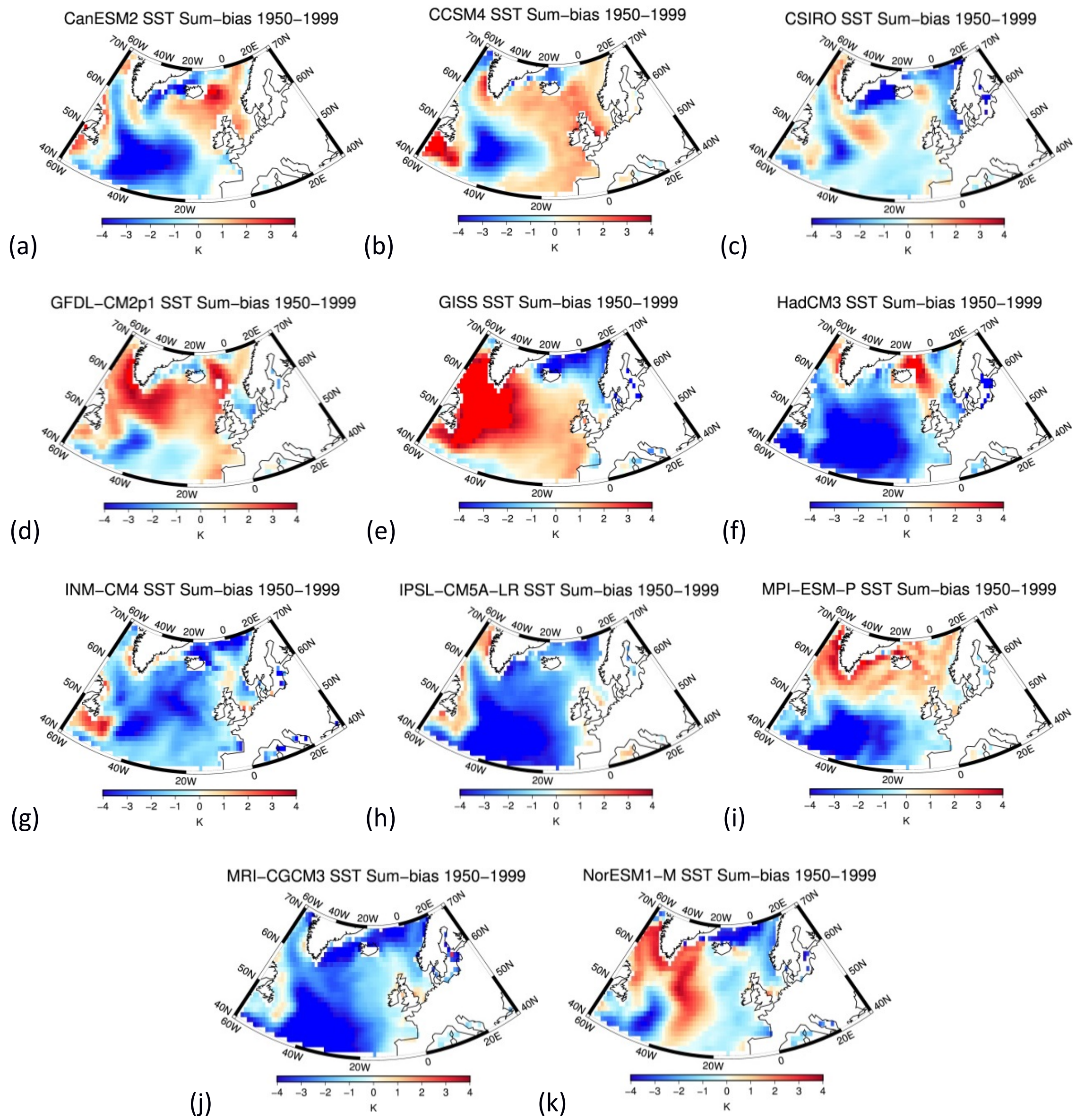

Figure 1A Mean summer SST bias between the 11 CMIP5 Models and COBE2 data, for the period 1950-1999.

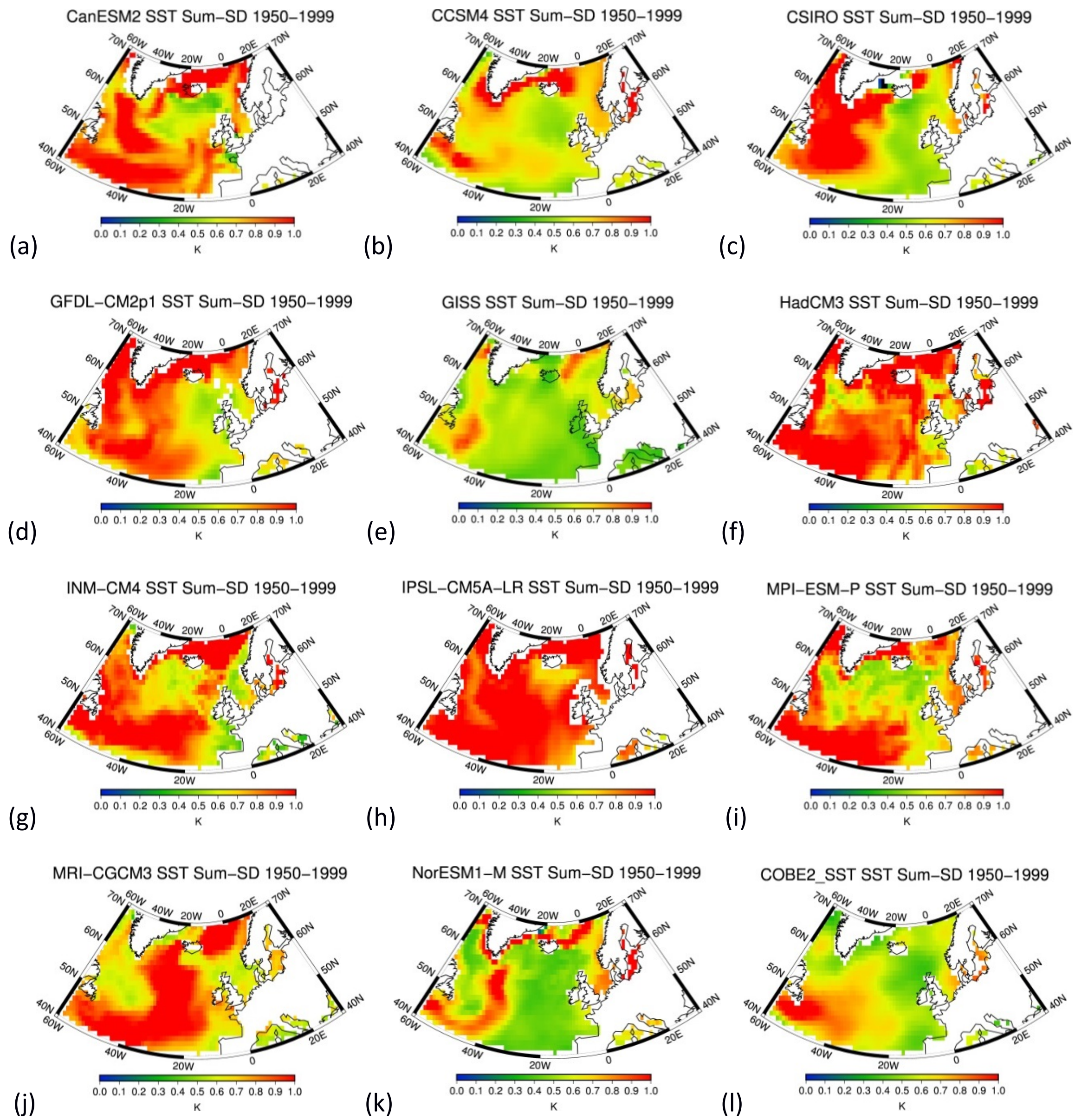

Figure 2A Standard deviation of summer SSTs for 11 CMIP5 Models and COBE2 data, for the period 1950-1999.

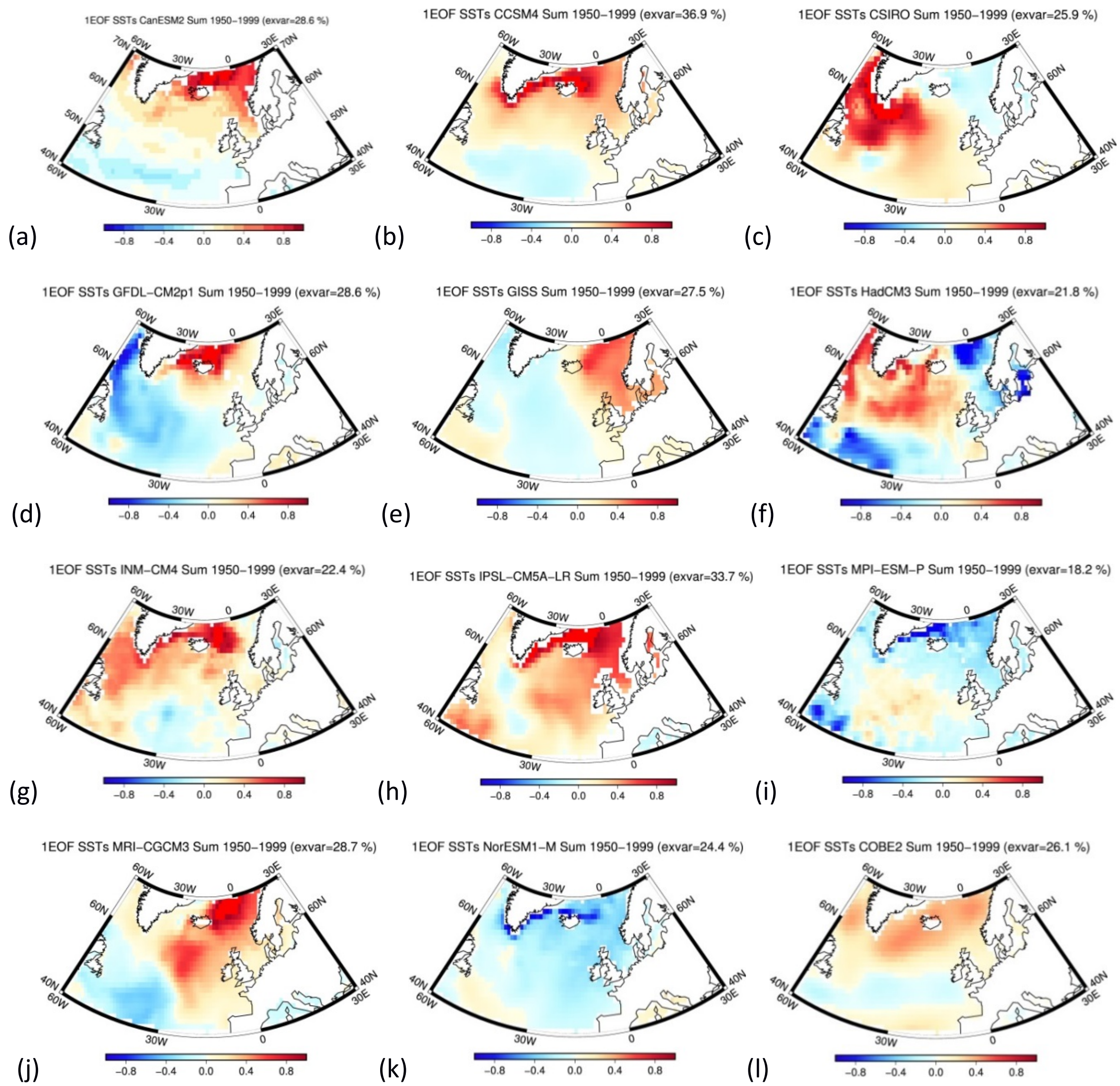

Figure 3A 1st EOF of the detrended summer SSTs of the period 1950-1999, for the 11 CMIP5 Models and COBE2 data.

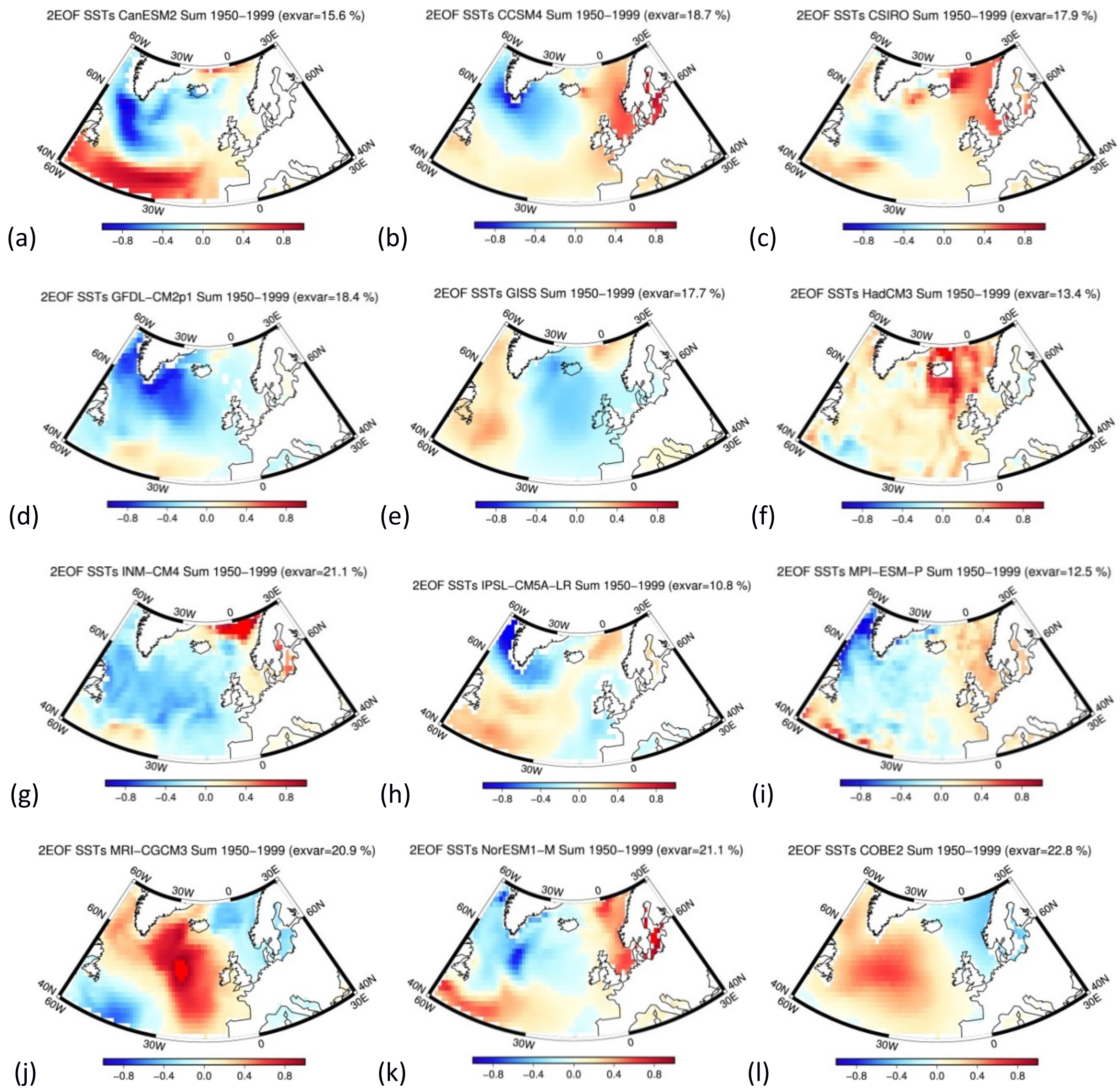

Figure 4A 2nd EOF of the detrended summer SSTs of the period 1950-1999, for the 11 CMIP5 Models and COBE2 data.

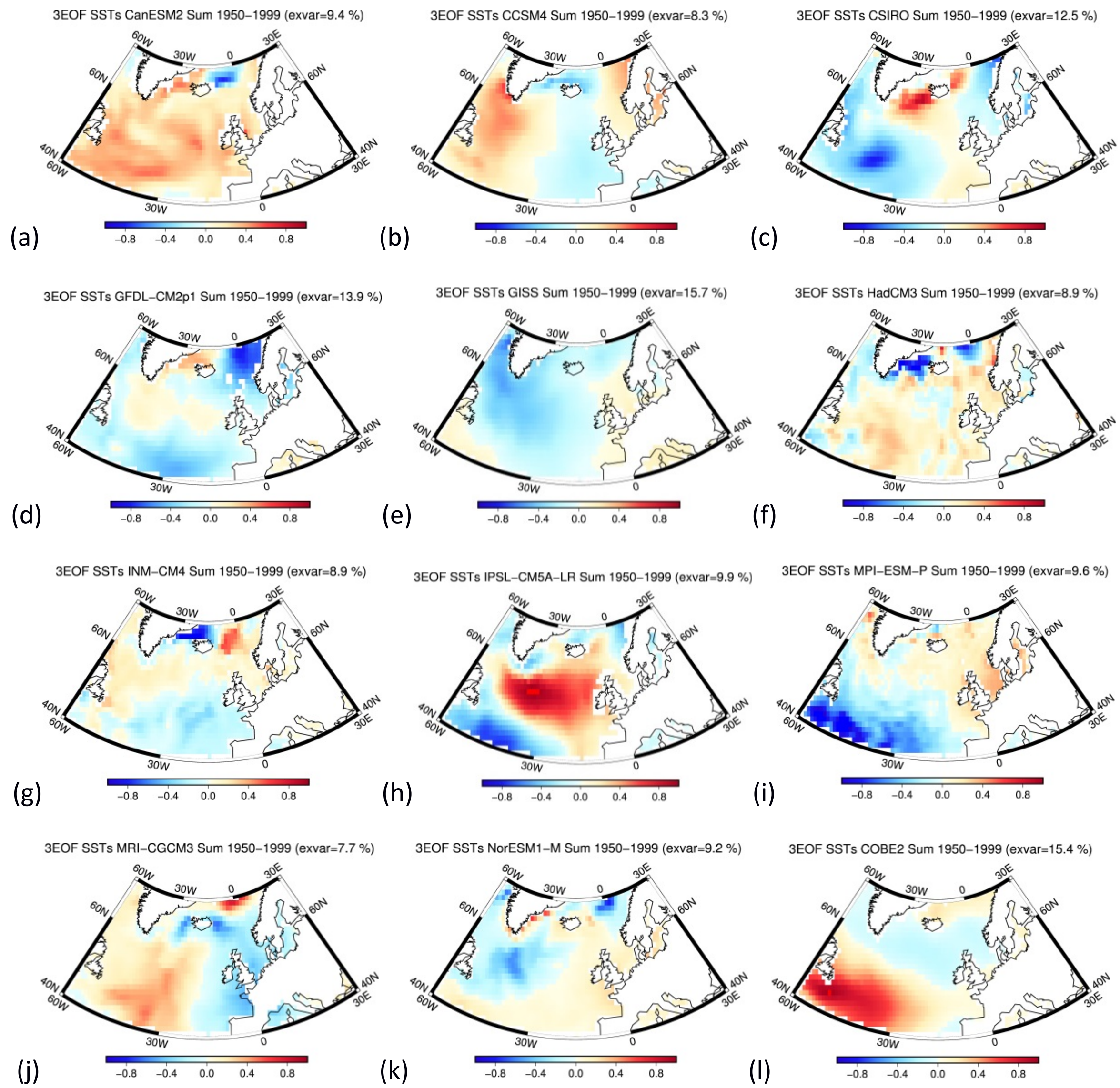

Figure 5A 3rd EOF of the detrended summer SSTs of the period 1950-1999, for the 11 CMIP5 Models and COBE2 data.

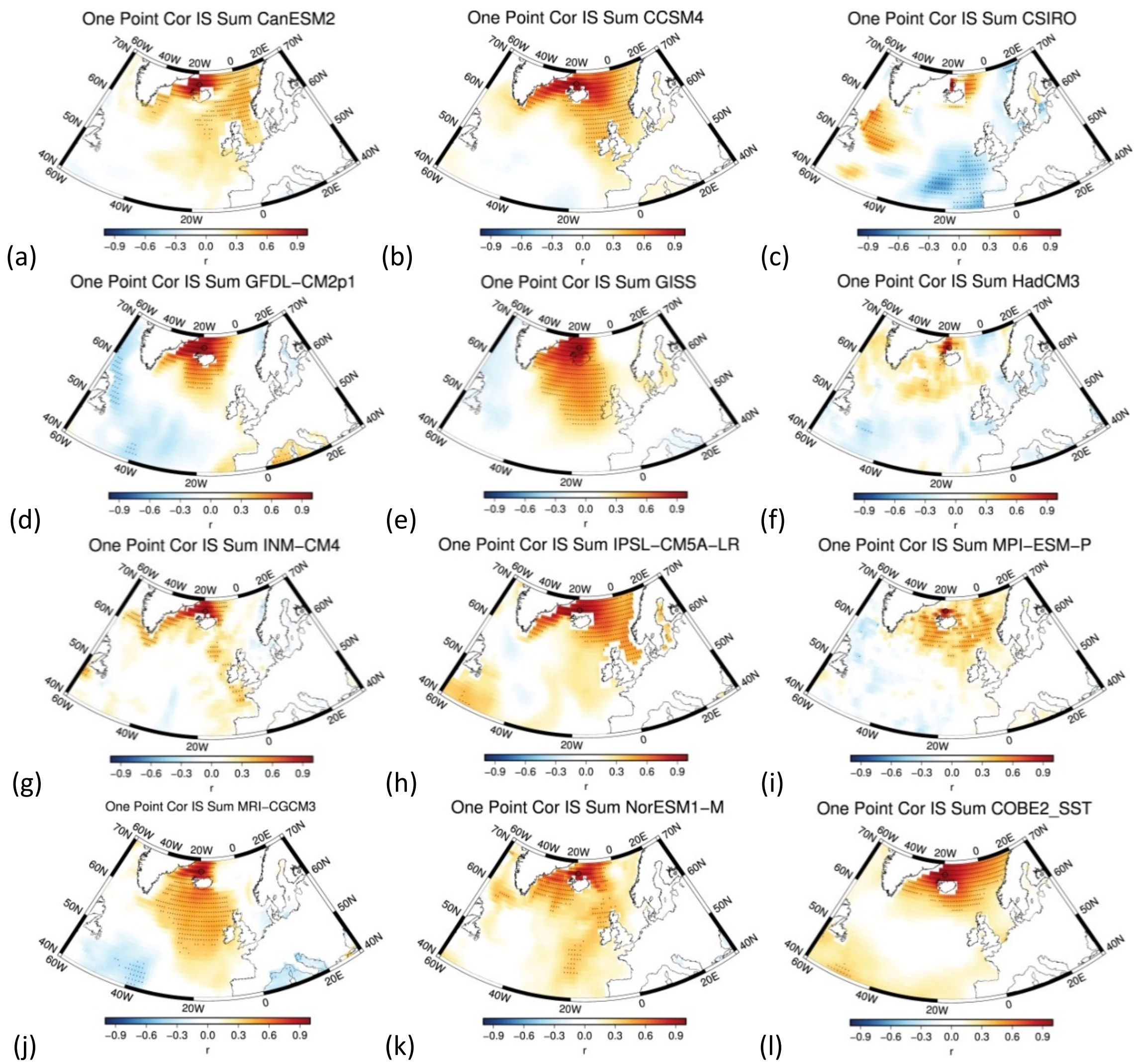

Figure 6A Correlation patterns (one-point correlation maps) for the Icelandic Shelf (IS) summer SSTs, for the period 1950-1999, for the 11 CMIP5 Models and COBE2 data. Hatched areas indicate values statistically significant at the 1% level according to a statistical test taking into account the effect of serial correlated data.

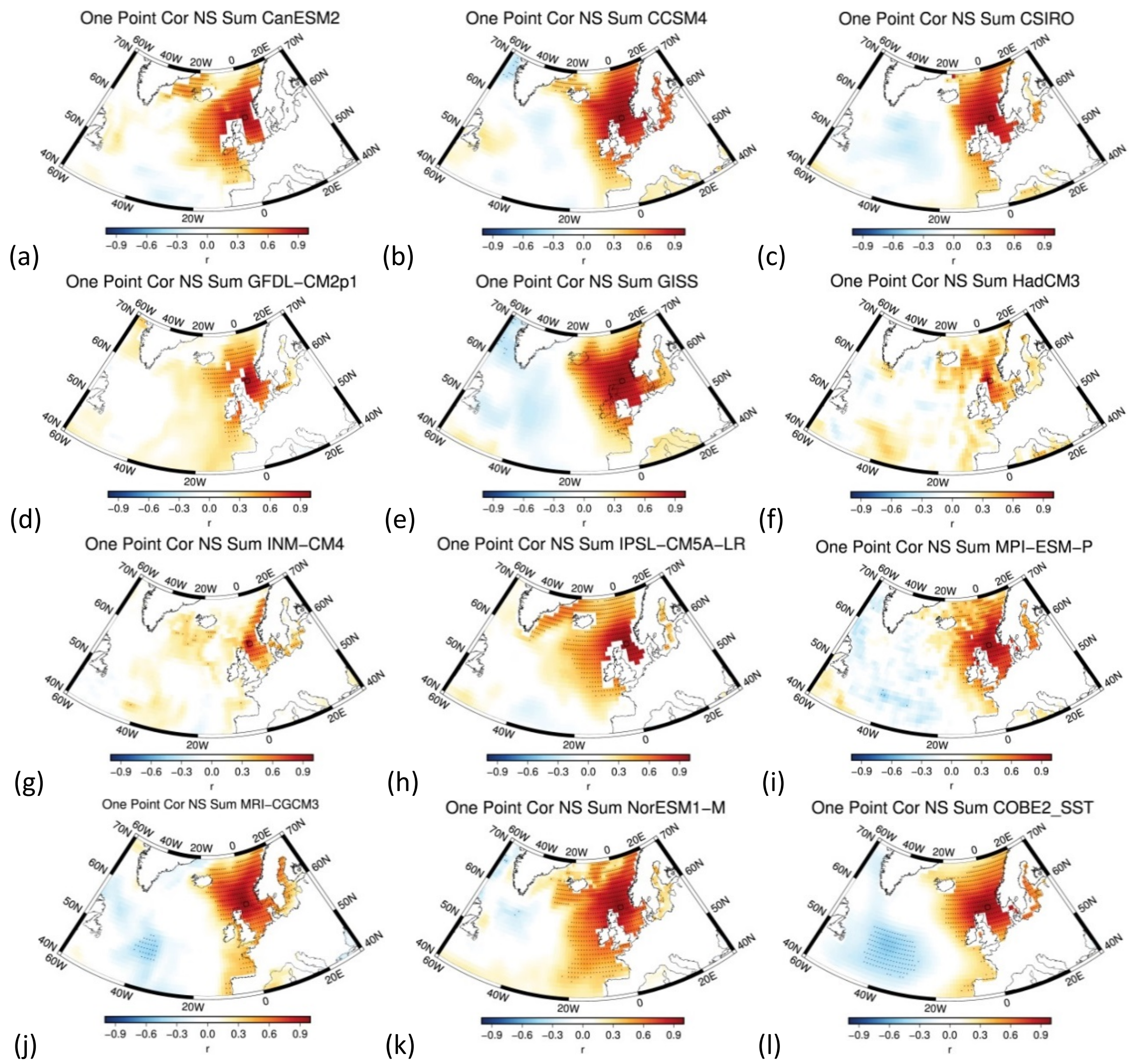

Figure 7A Correlation patterns (one-point correlation maps) for the North Sea (NS) summer SSTs, for the period 1950-1999, for the 11 CMIP5 Models and COBE2 data. Hatched areas indicate values statistically significant at the 1% level according to a statistical test taking into account the effect of serial correlated data.

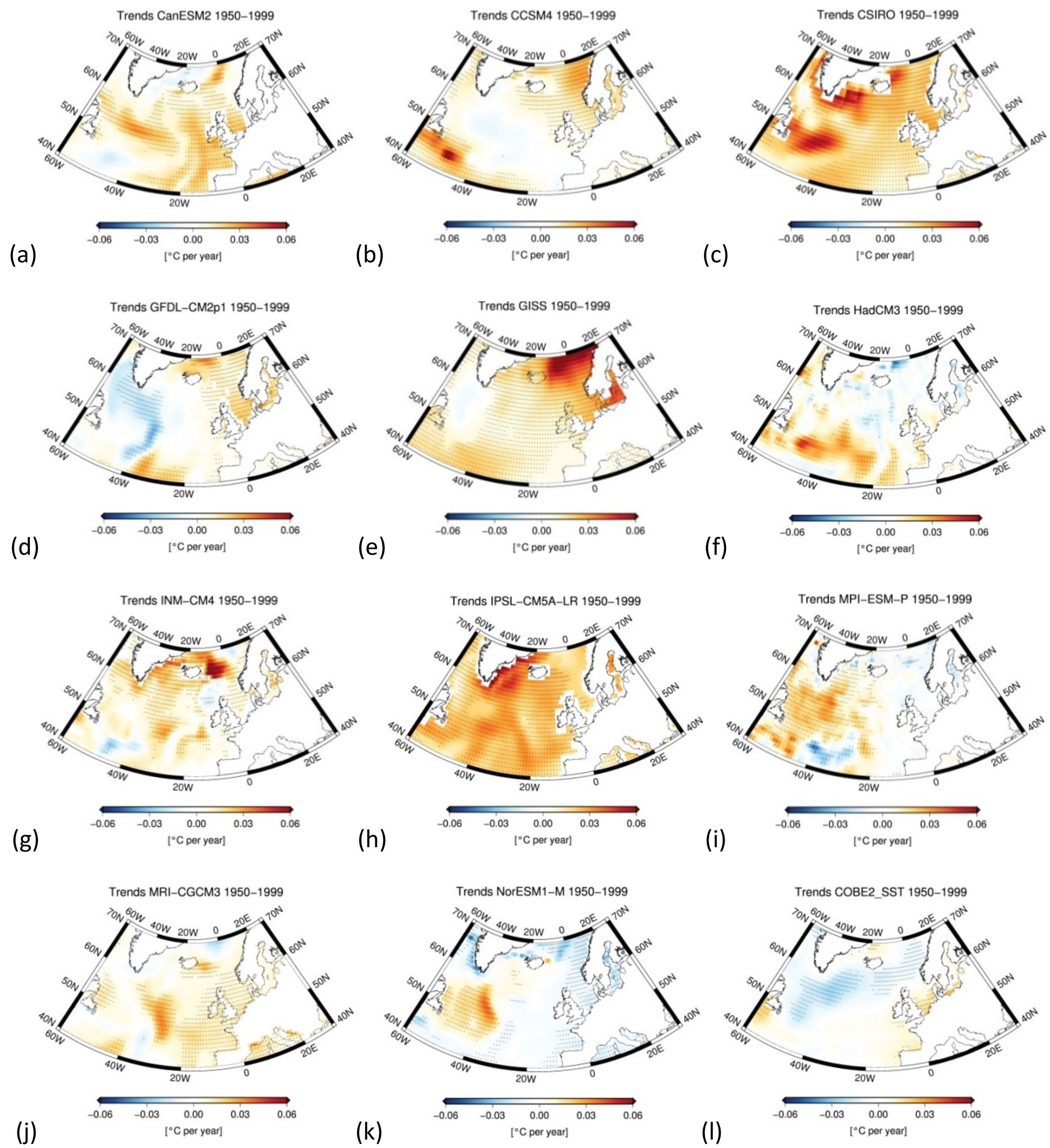

Figure 8A Summer SST trends of the period 1950-1999 as calculated with COBE2 data and the 11 CMIP5 models used in this study. Hatched areas indicate values statistically significant at the 1% level according to a statistical test taking into account the effect of serial correlated data.

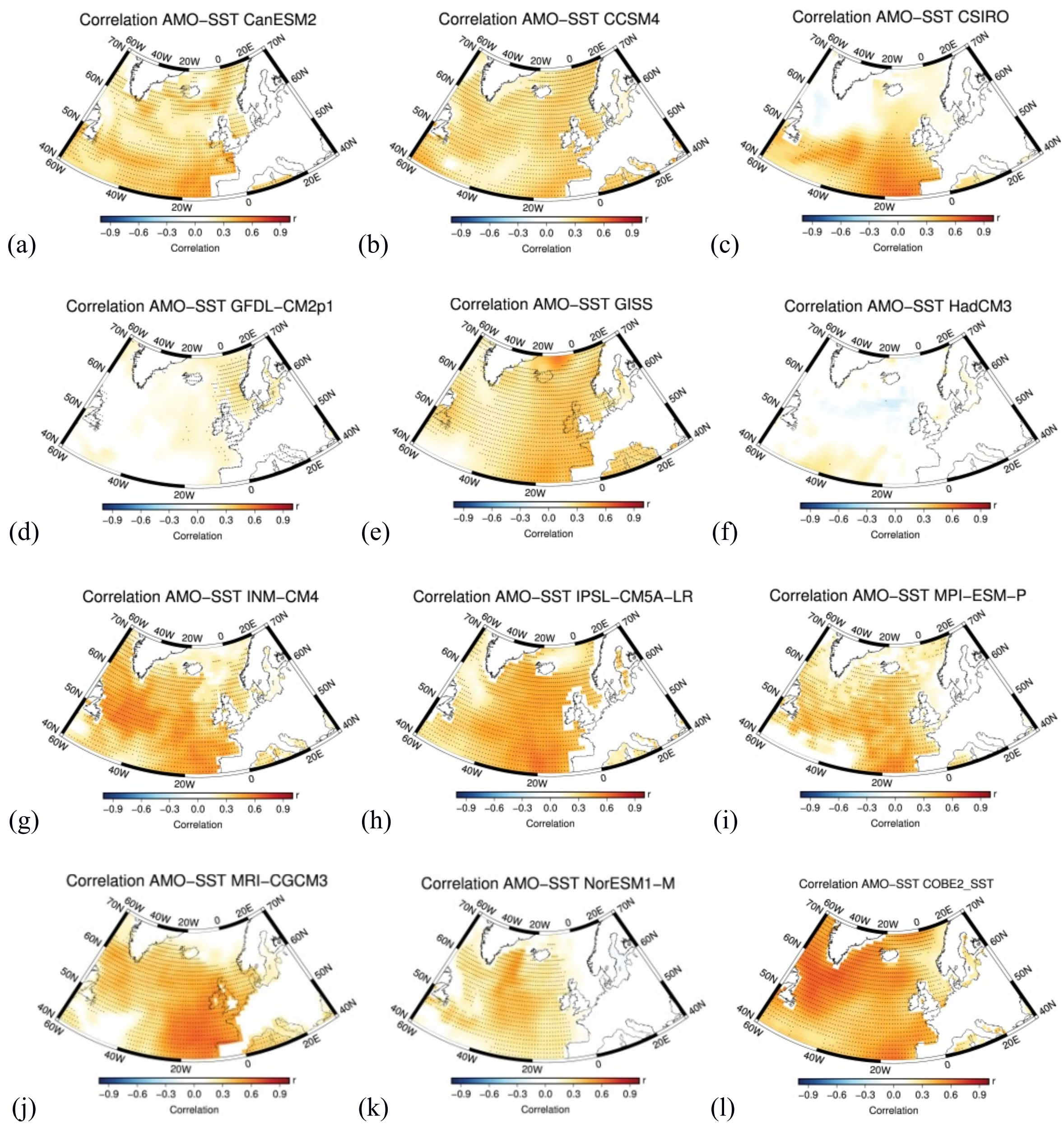

Figure 9A Spatial structure of AMO for the 11 CMIP5 models and COBE2 data, for the period 1850-2005. *The AMO spatial structure for the models GFDL and HadCM3 was calculated for the years 1861-2005 and 1859-2005, respectively

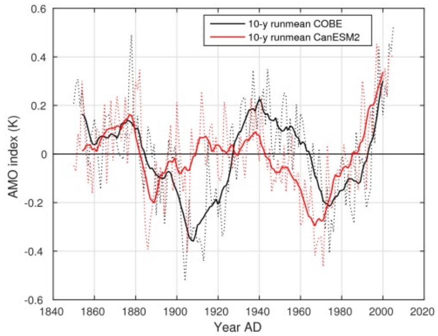
10-y runmean COBE
10-y runmean CanESM2
AMO index (K)
Year AD

(a)

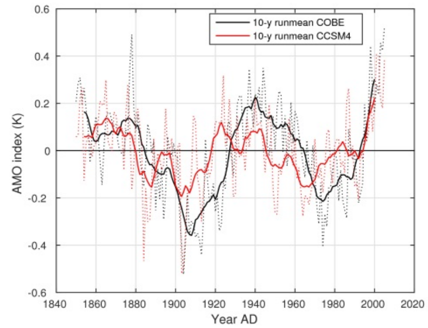
10-y runmean COBE
10-y runmean CCSM4
AMO index (K)
Year AD

(b)

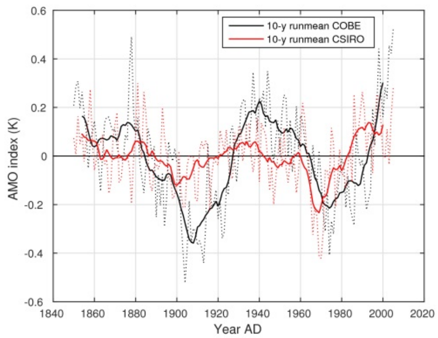
10-y runmean COBE
10-y runmean CSIRO
AMO index (K)
Year AD

(c)

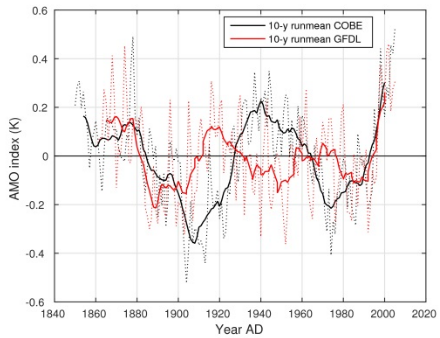
10-y runmean COBE
10-y runmean GFDL
AMO index (K)
Year AD

(d)

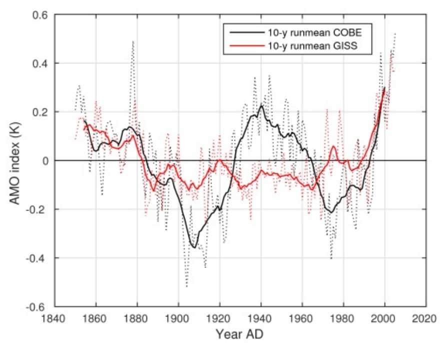
10-y runmean COBE
10-y runmean GISS
AMO index (K)
Year AD

(e)

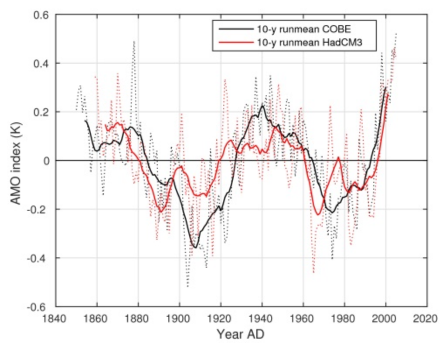
10-y runmean COBE
10-y runmean HadCM3
AMO index (K)
Year AD

(f)

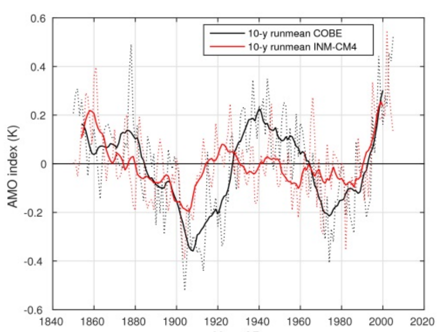
10-y runmean COBE
10-y runmean INM-CM4
AMO index (K)
Year AD

(g)

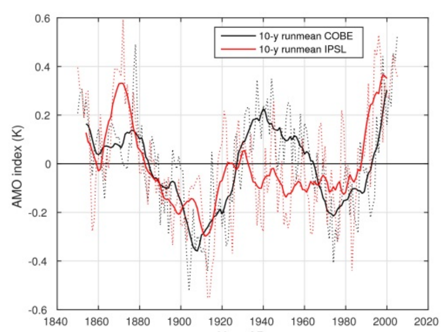
10-y runmean COBE
10-y runmean IPSL
AMO index (K)
Year AD

(h)

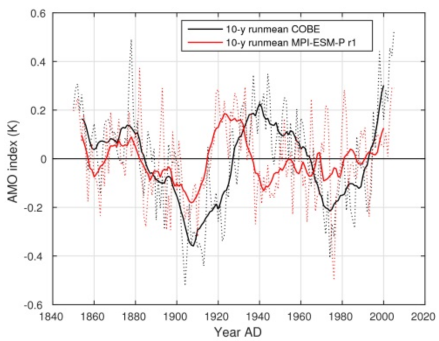

(i)

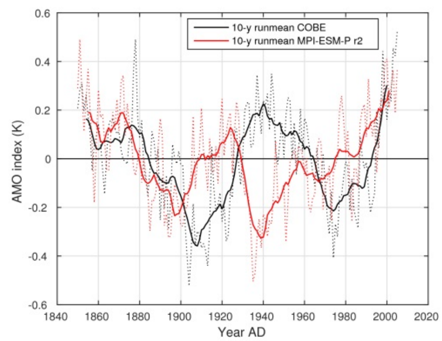

(j)

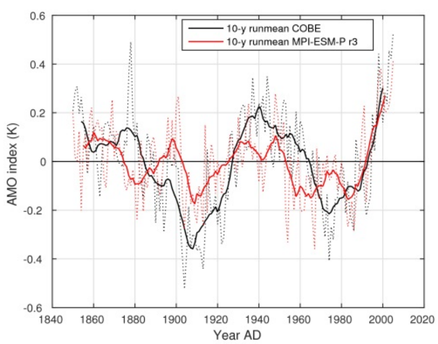

(k)

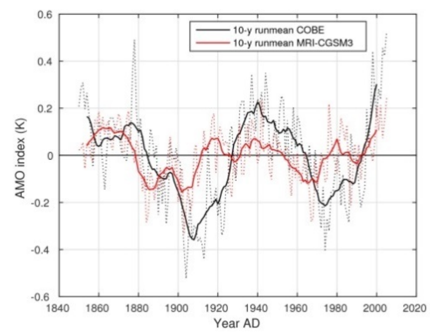

(l)

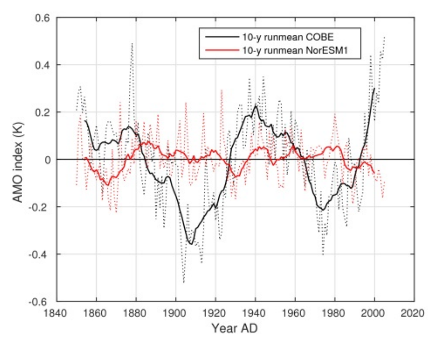

(m)

Figure 10A AMO index as calculated from COBE2_SSTs (black dotted line) and from CMIP5 model SSTs (red dotted line). Black and red solid lines are the ten year running mean for the COBE2 and models, respectively. The order in which the models are shown are: a) CanESM2, b) CCSM4, c) CSIRO, d) GFDL, e) GISS, f) HadCM3, g) INM-CM4, h) IPSL, i) MPI-ESM-P r1, j) MPI-ESM-P r2, k) MPI-ESM-P r3, l) MRI-CGCM3 and m) NorESM1.

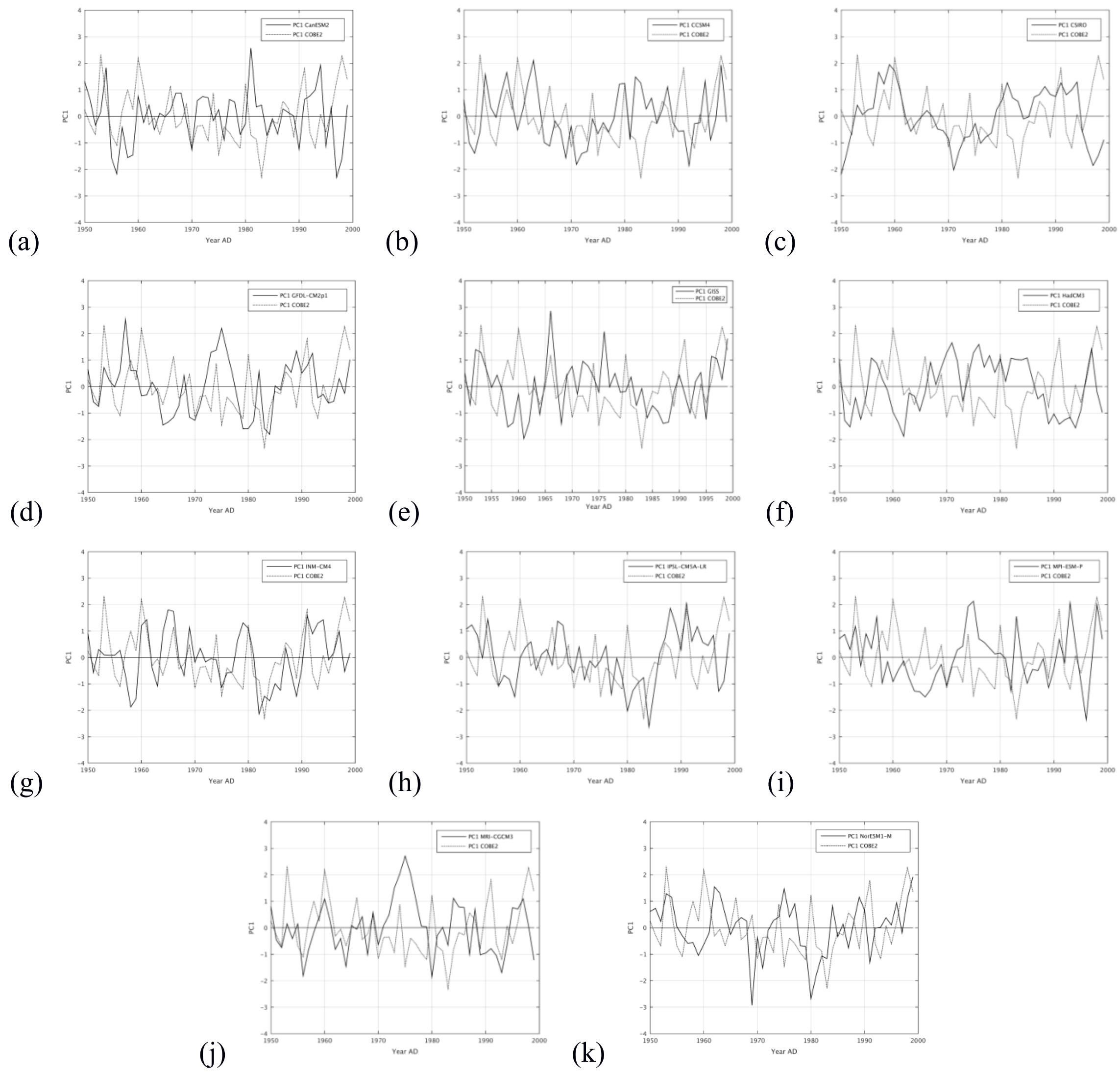
(a) (b) (c) (d) (e) (f) (g) (h) (i) (j) (k)

Figure 11A Temporal evolution of the 1st EOF pattern for the period 1950-1999, for the 11 CMIP5 models (solid line) and the COBE2 data (dotted line), in the order mentioned in Figure 1A.

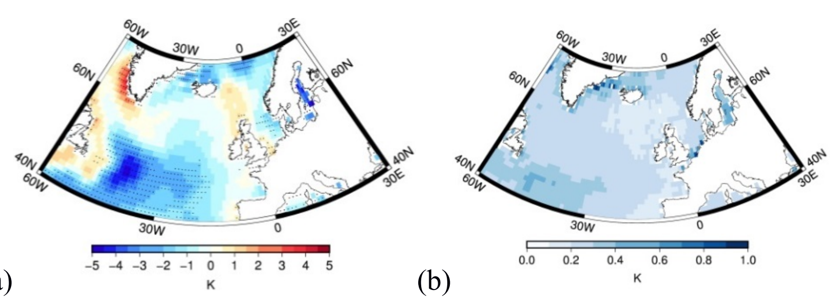

(a) (b)

Figure 12A CMIP5 a) mean model bias and b) mean model variance, for the period 1950-1999. Hatched areas indicate agreement of at least 7 models, on the sign of their individual bias to COBE2 data.

Appendix C3

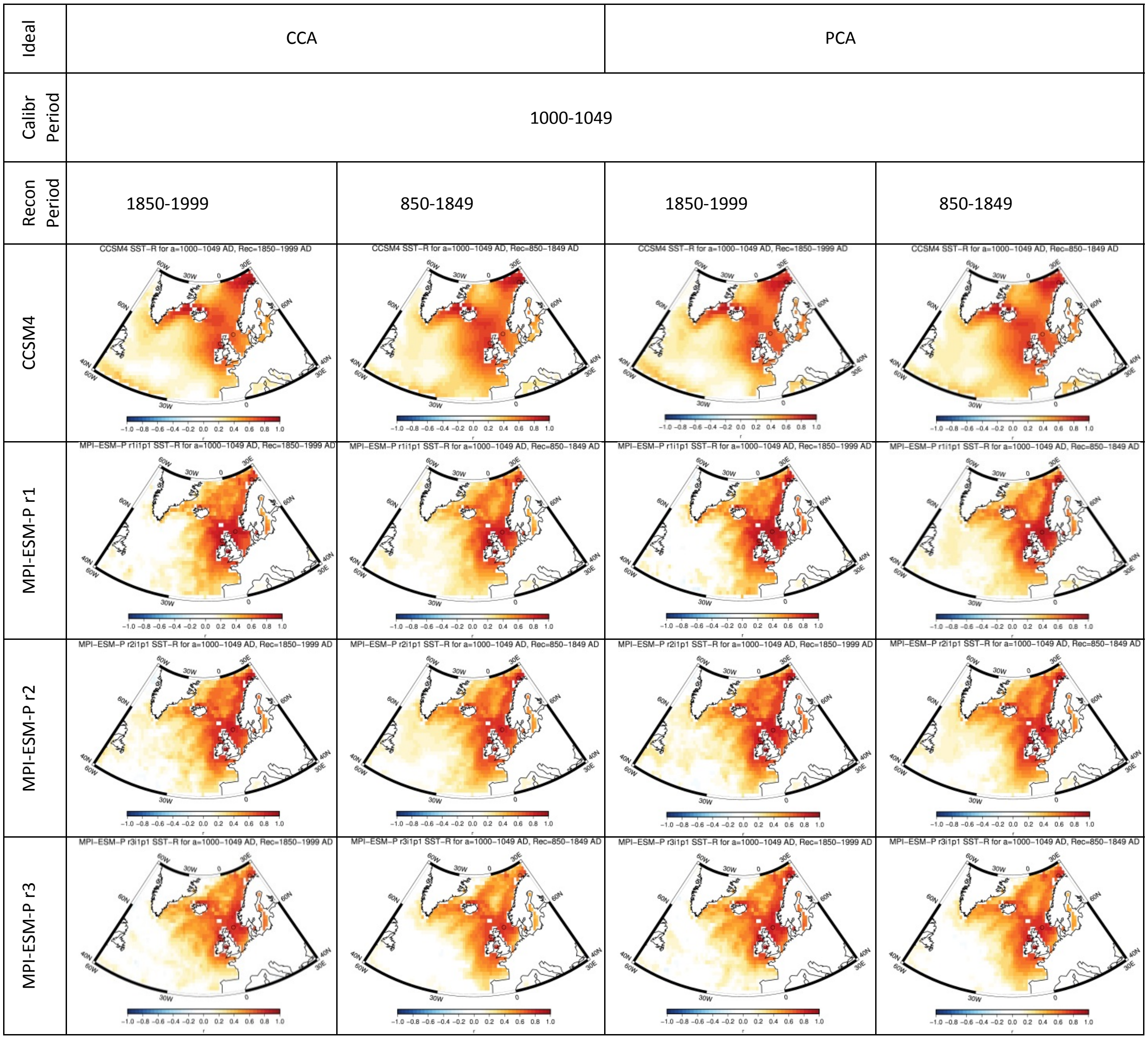

Figure 1S: Correlation coefficient between the reconstructed and the original SST-anomaly evolution of the NA field during the preindustrial (column 2 and 4) and industrial era (column 1 and 3). The results are given for the MCA calibration period (1000—1049 AD) and for the two different reconstruction methods (1st and 2nd column CCA, 3rd and 4th column PCA) for the models CCSM4 (1st row) and three realizations of the MPI-ESM-P model (2nd, 3rd and 4th row).

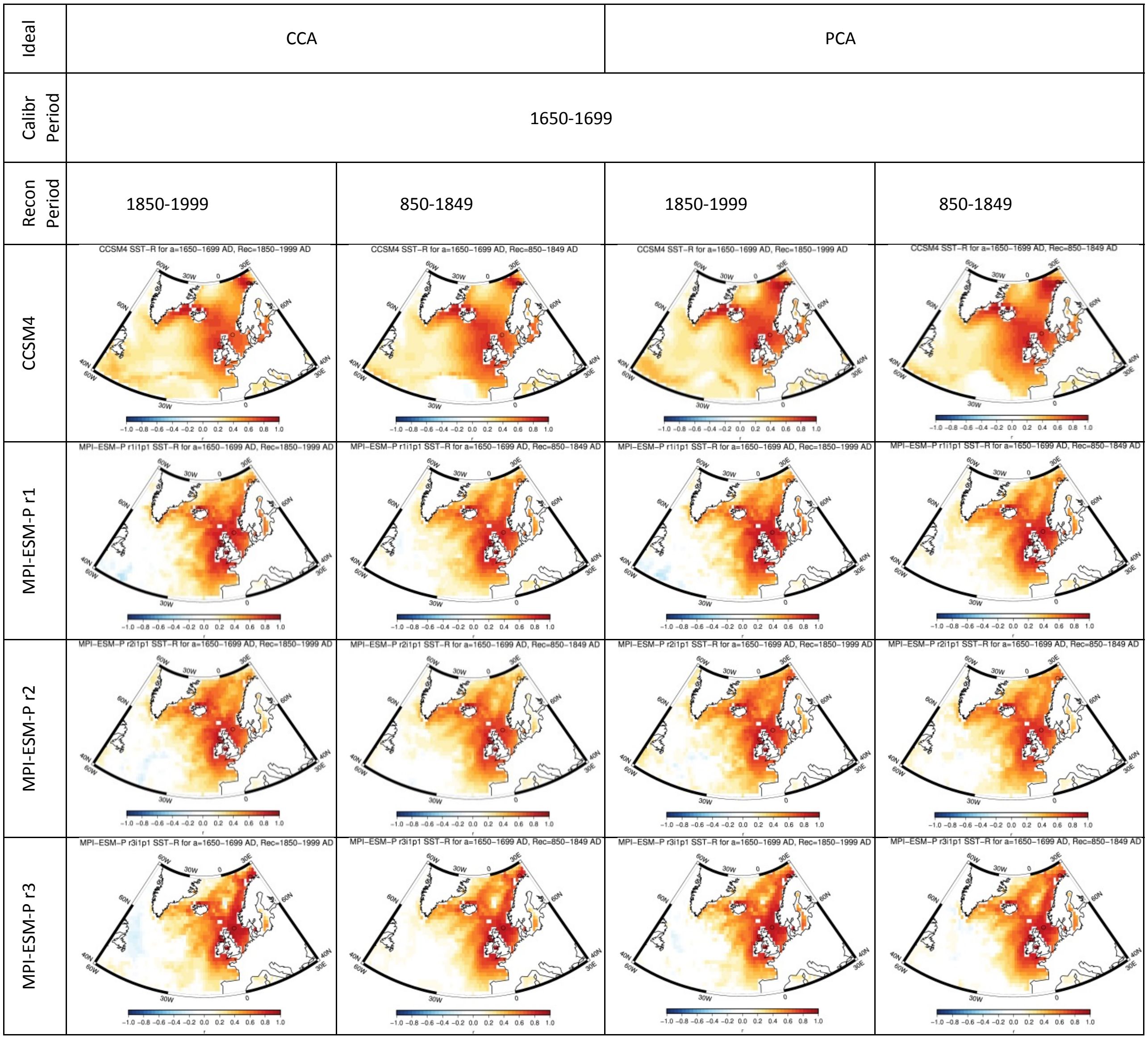

Figure 2S: As in Fig. 1S, but the results are given for the LIA calibration period (1650—1699 AD).

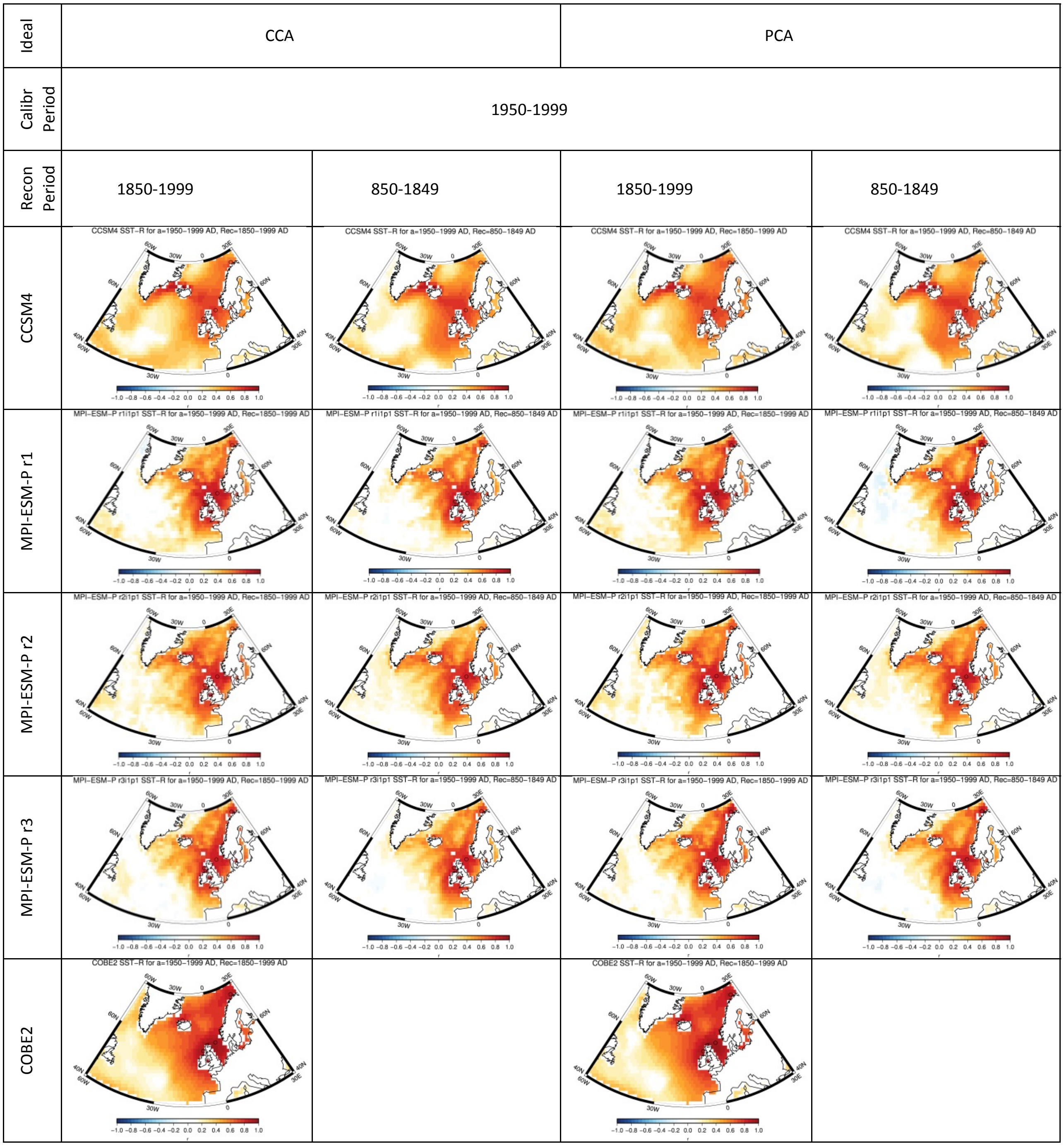

Figure 3S: As in Fig. 1S, but the results are given for the recent calibration period (1950—1999 AD). The last row contains the pseudo-proxy results of the COBE2 reanalysis data.

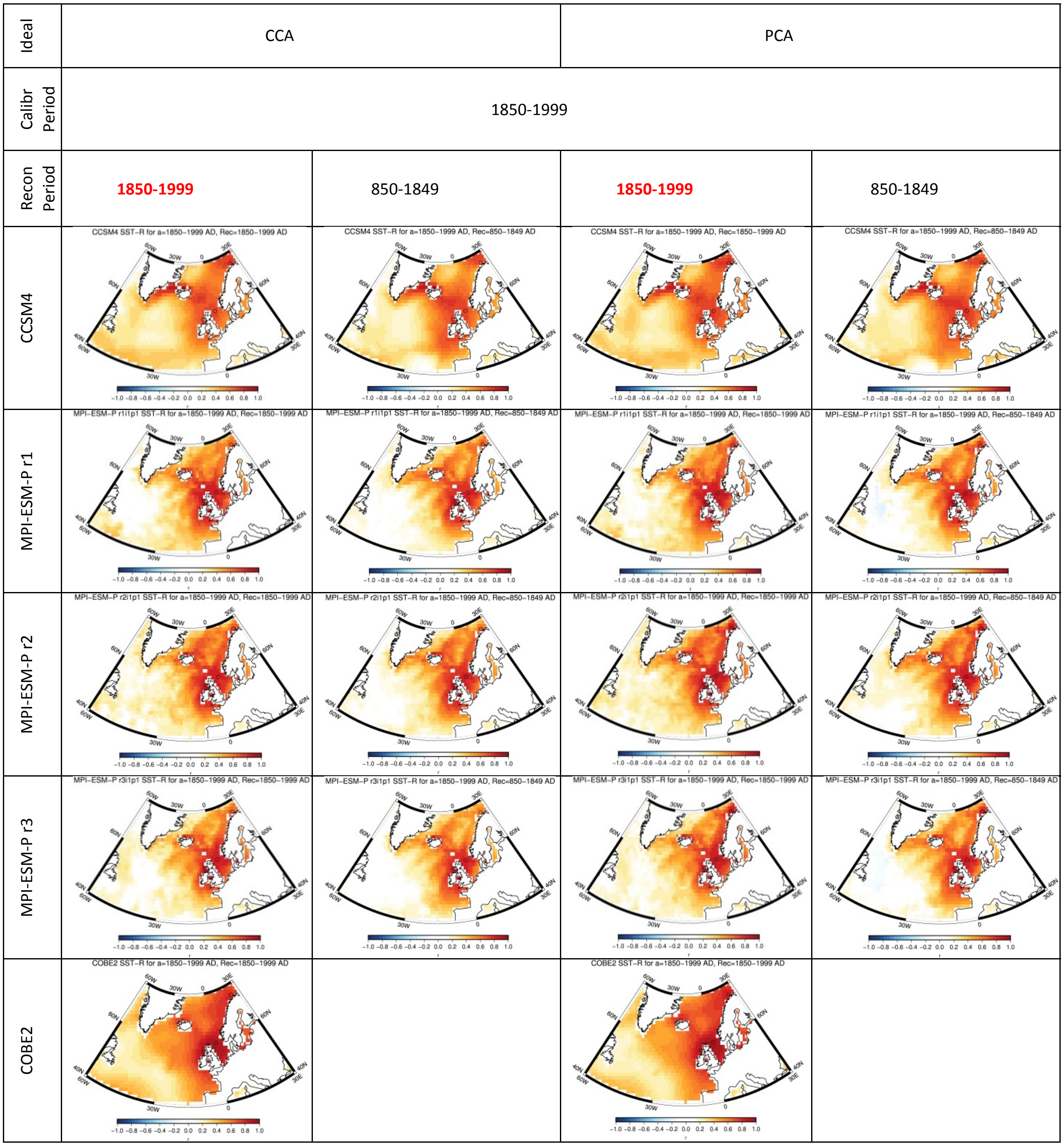

Figure 4S: As in Fig. 3S, but the results are given for the industrial calibration period (1850—1999 AD).

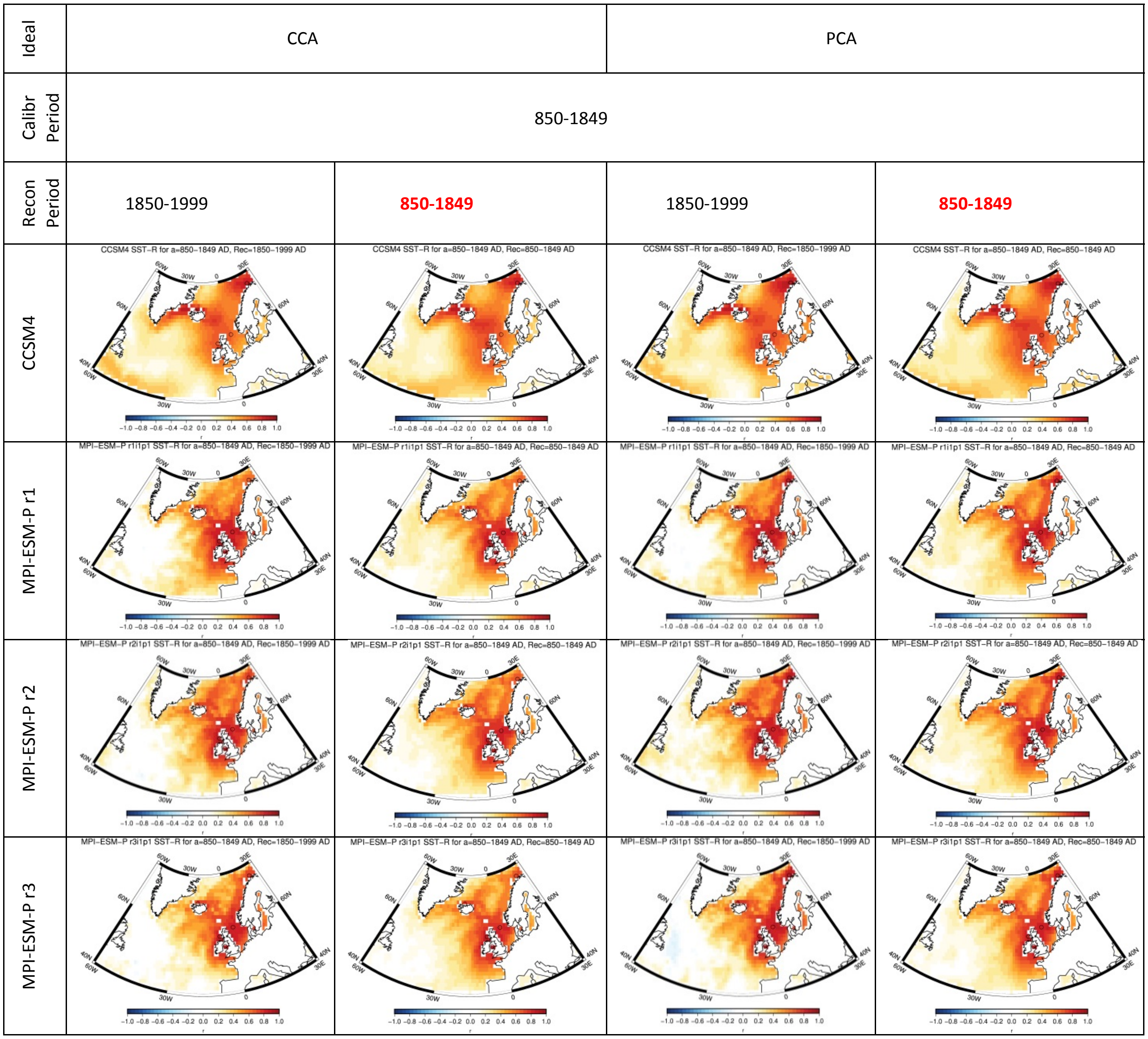

Figure 5S: As in Fig. 1S, but the results are given for the pre-industrial calibration period (850—1849 AD).

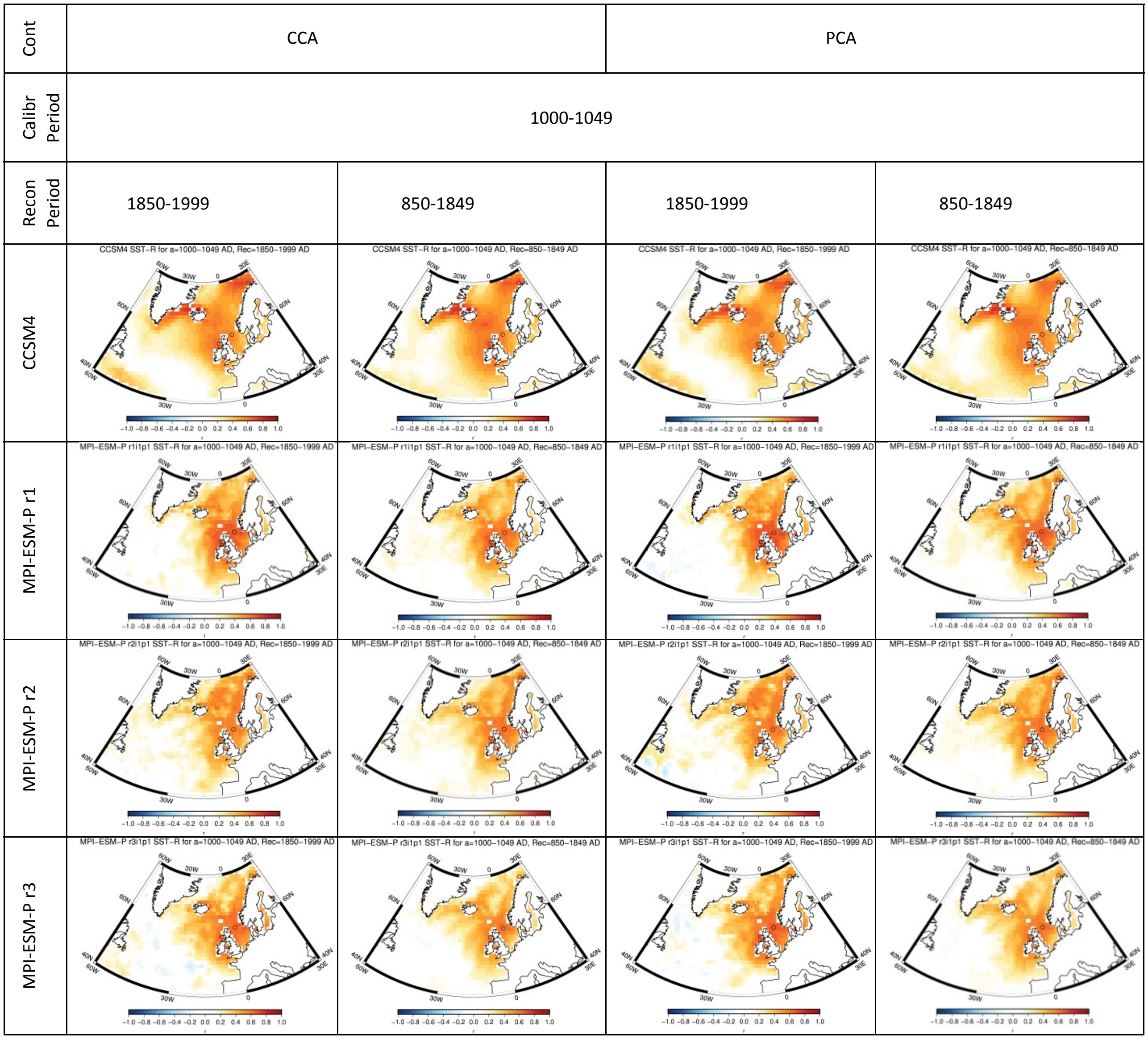

Figure 6S: As in Fig. 1S, but the results are given for the noise contaminated pseudo-proxy experiment.

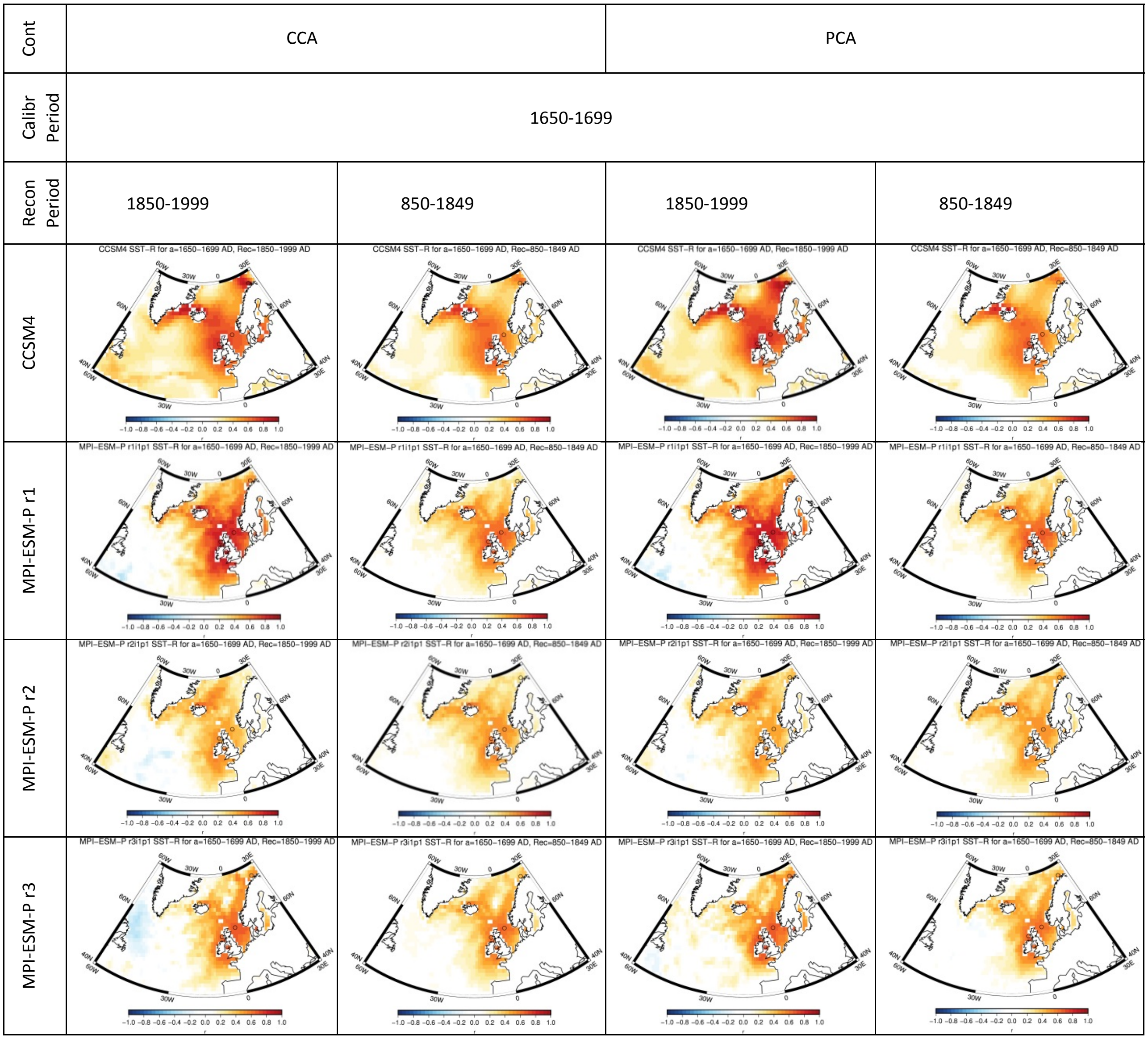

Figure 7S: As in Fig. 2S, but the results are given for the noise contaminated pseudo-proxy experiment.

Cont	CCA		PCA	
Calibr Period	1950-1999			
Recon Period	1850-1999	850-1849	1850-1999	850-1849
CCSM4	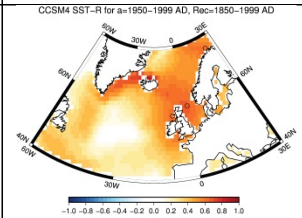	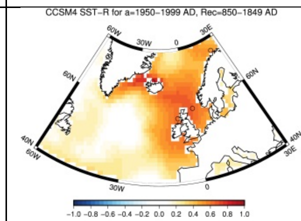	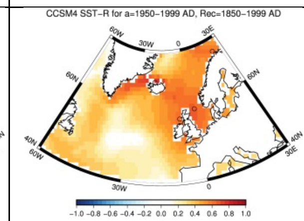	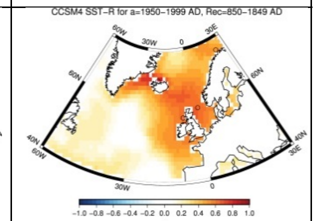
MPI-ESM-P r1	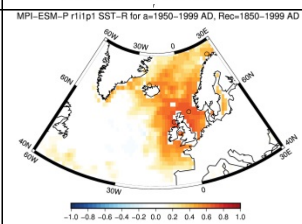	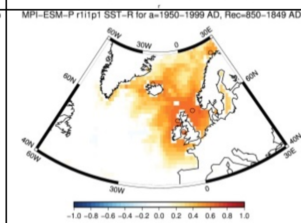	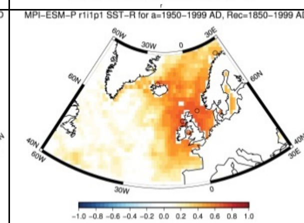	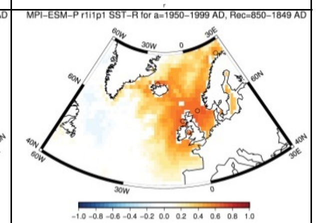
MPI-ESM-P r2	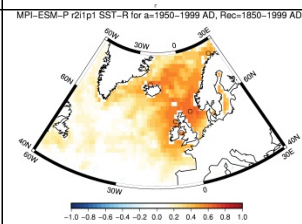	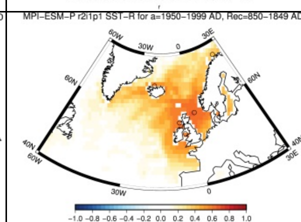	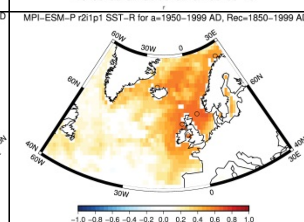	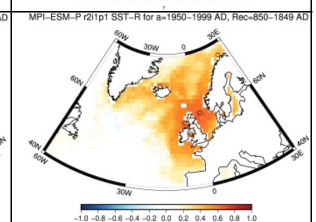
MPI-ESM-P r3	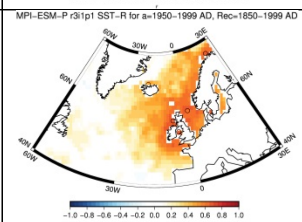	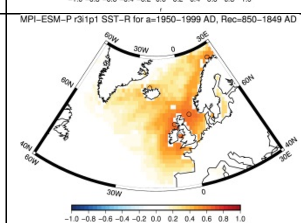	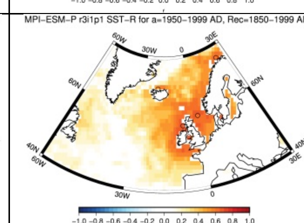	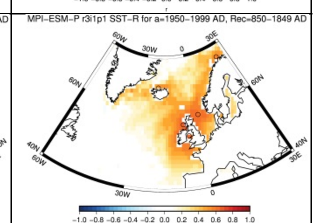
COBE2	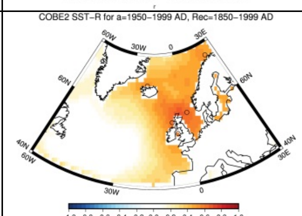		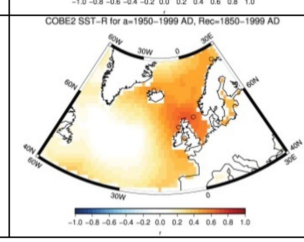	

Figure 8S: As in Fig. 3S, but the results are given for the noise contaminated pseudo-proxy experiment.

Cont	CCA		PCA	
Calibr Period	1850-1999			
Recon Period	**1850-1999**	850-1849	**1850-1999**	850-1849
CCSM4	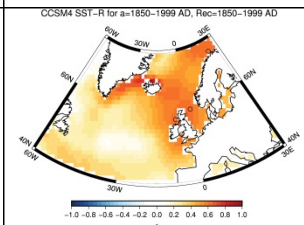	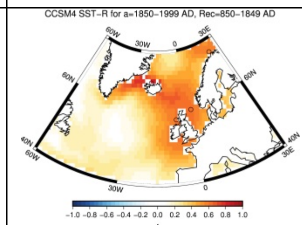	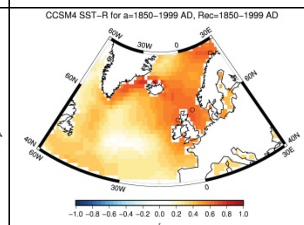	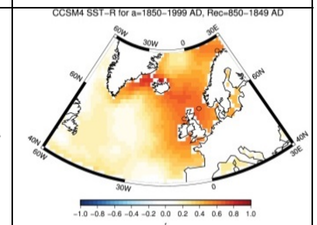
MPI-ESM-P r1	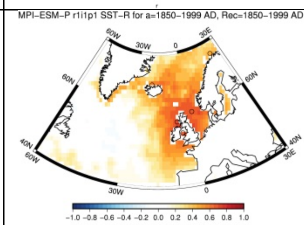	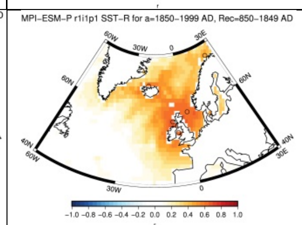	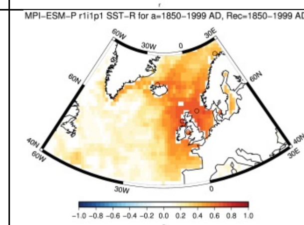	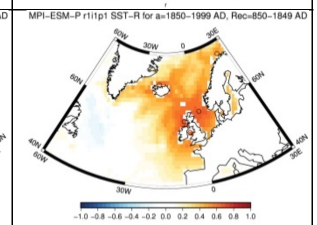
MPI-ESM-P r2	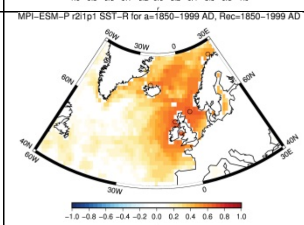	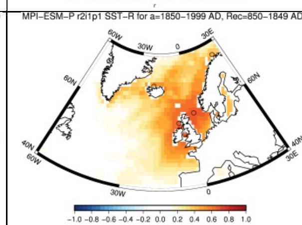	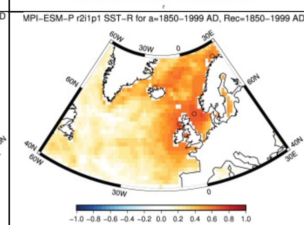	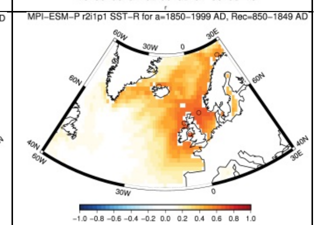
MPI-ESM-P r3	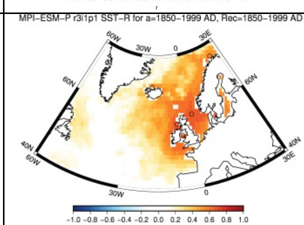	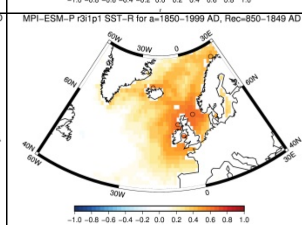	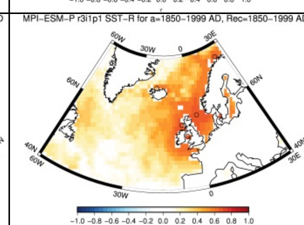	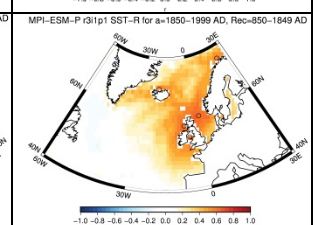
COBE2	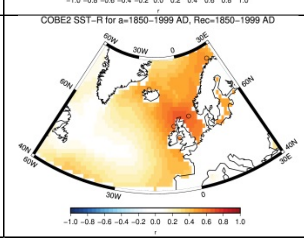		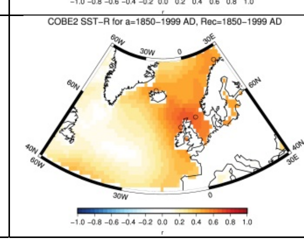	

Figure 9S: As in Fig. 4S, but the results are given for the noise contaminated pseudo-proxy experiment.

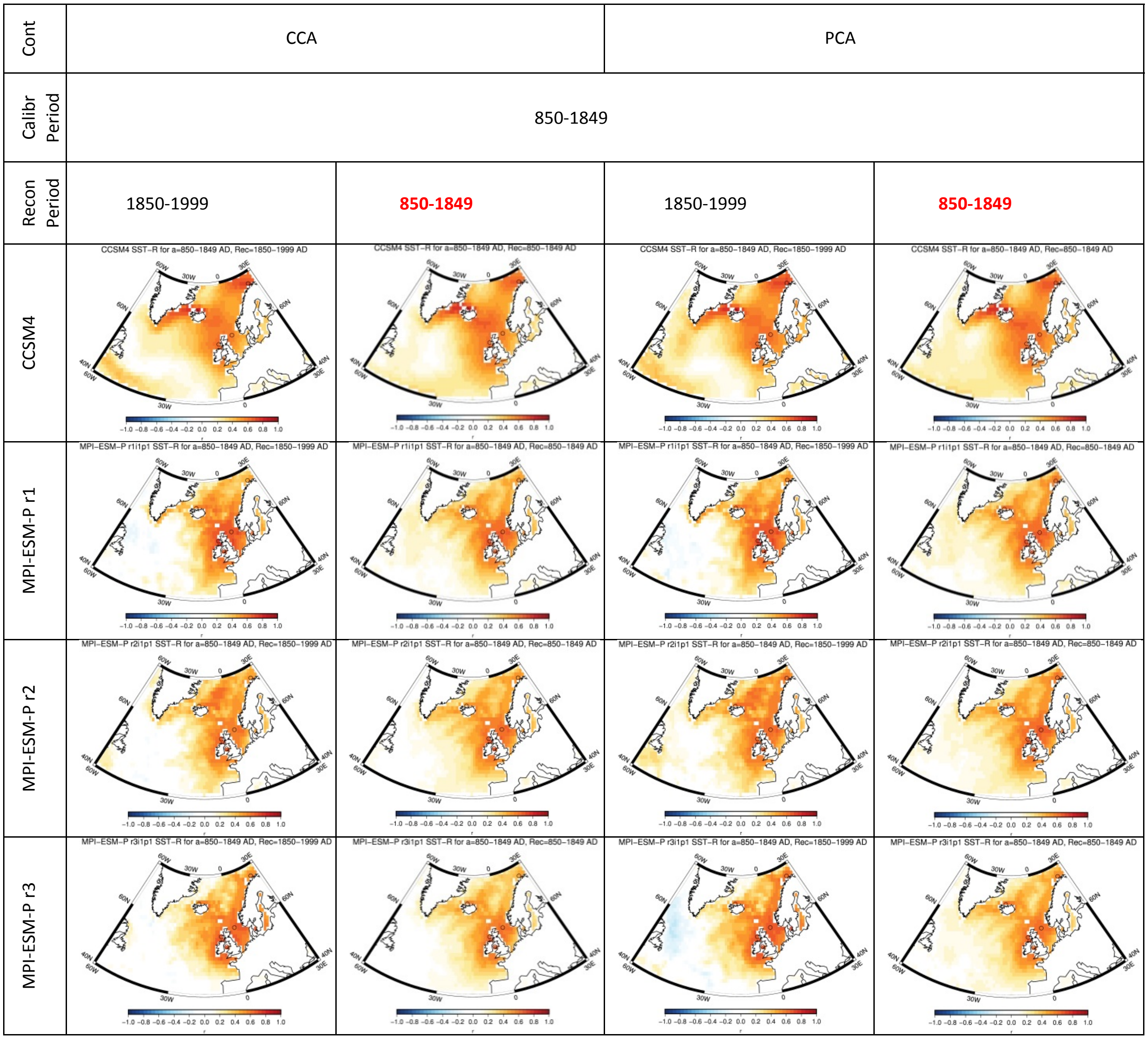

Figure 10S: As in Fig. 5S, but the results are given for the noise contaminated pseudo-proxy experiment.

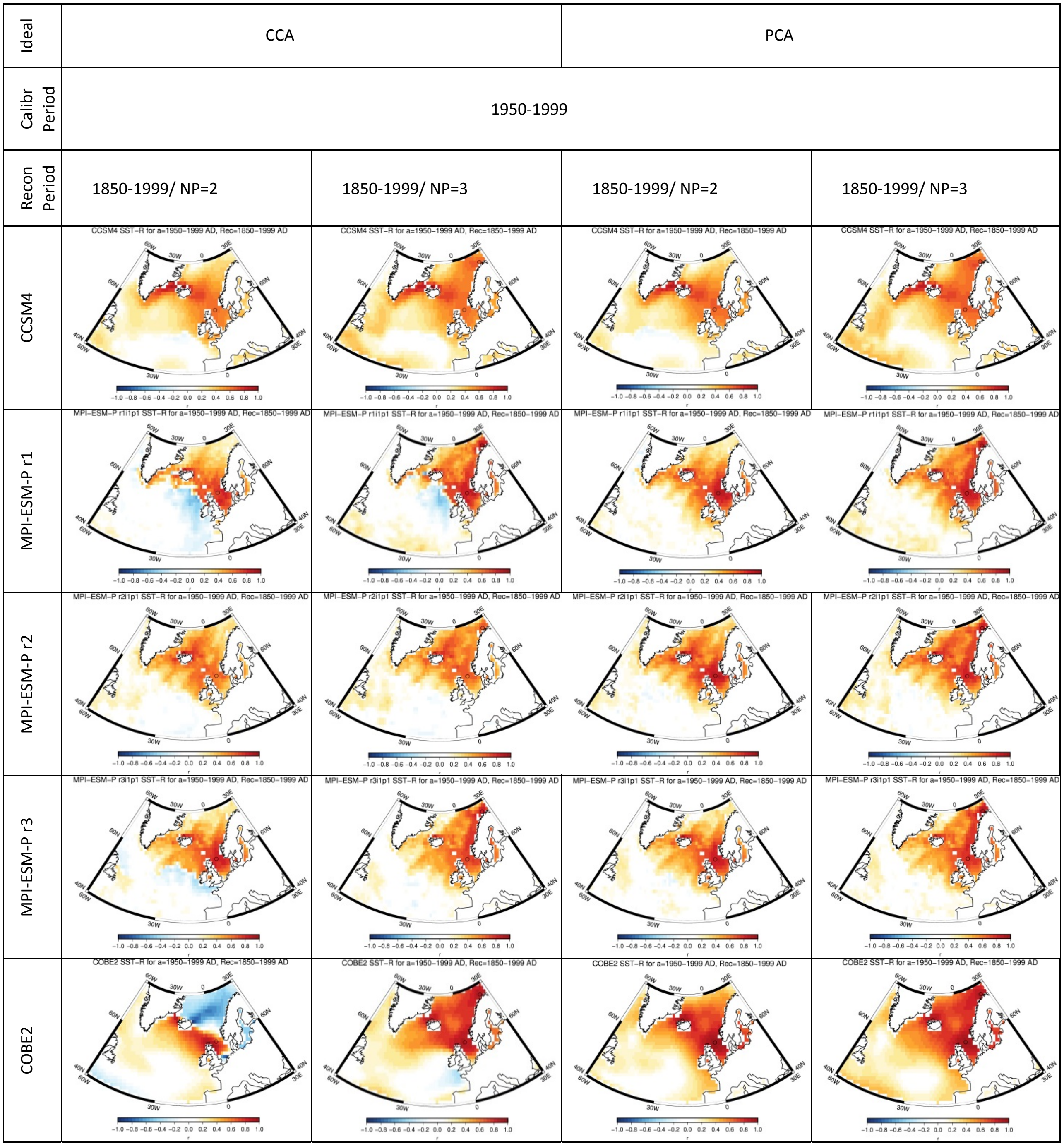

Figure 11S: Correlation coefficient between the reconstructed and the original SST-anomaly evolution of the NA field during the preindustrial era, when the number of proxy locations used is NP=2 (1st and 3rd column) and NP=3 (2nd and 4th column). The results are given for the recent calibration period (1950—1999 AD) and for the two different reconstruction methods (1st and 2nd column CCA, 3rd and 4th column PCA) for the model CCSM4 (1st row), three realizations of the MPI-ESM-P model (2nd, 3rd and 4th row) and COBE2 reanalysis data (5th row).

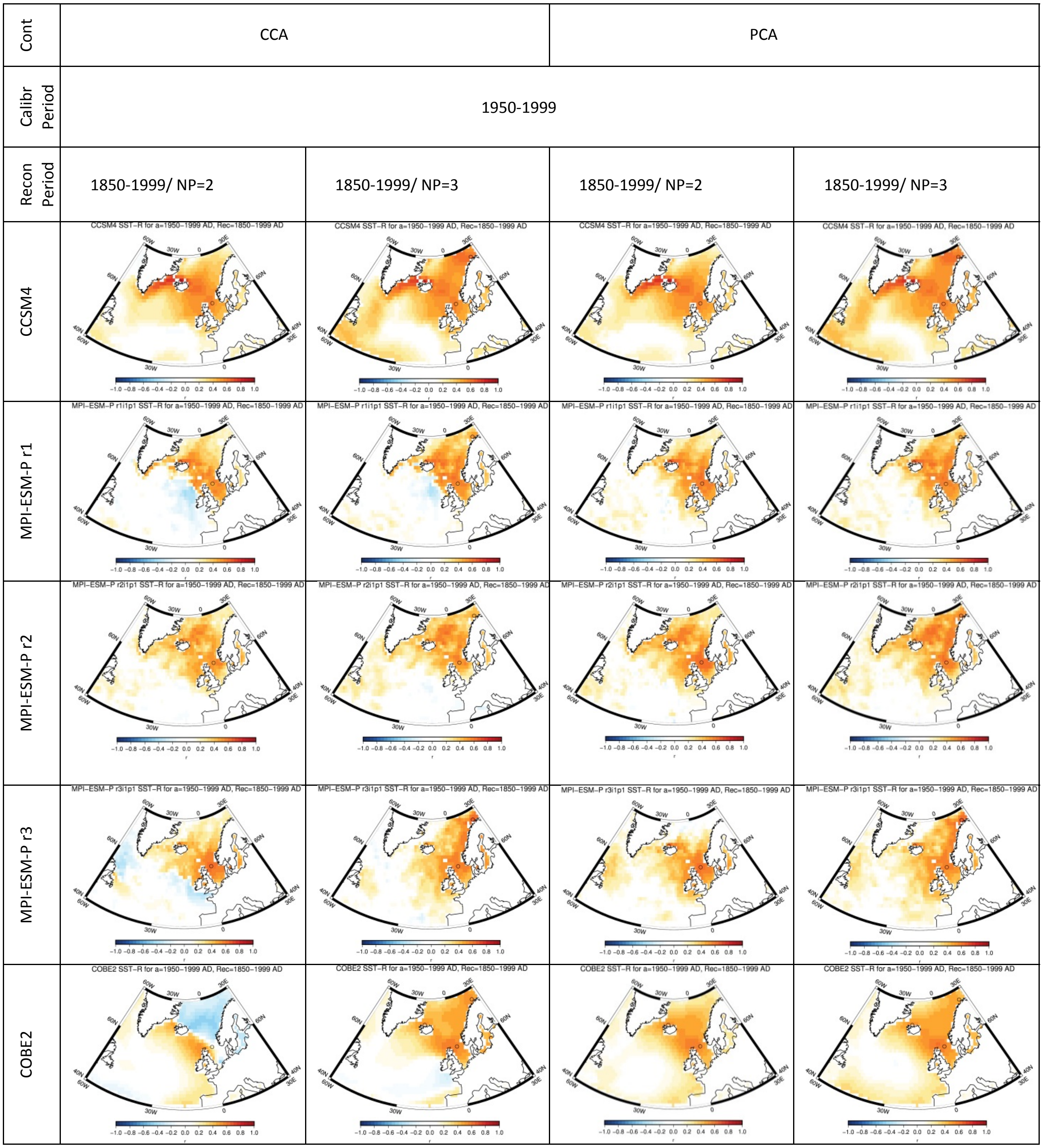

Figure 12S: As in Fig. 11S, but the results are given for the noise contaminated pseudo-proxy experiment.

Appendix C4

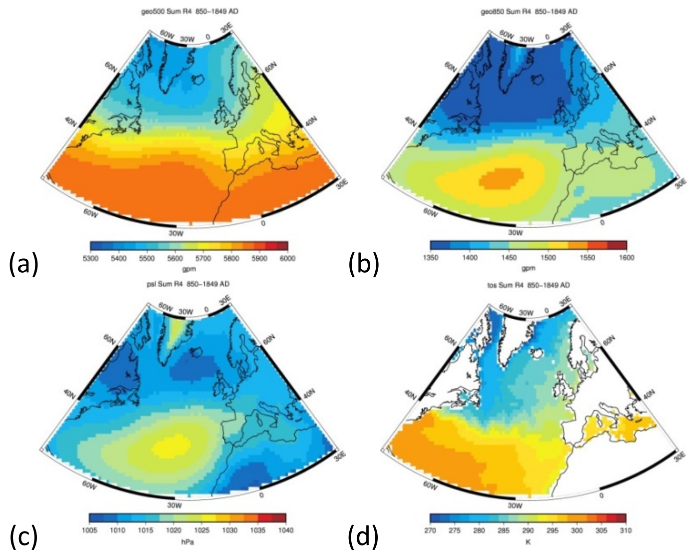

Figure 1K Mean summer values for a) geo500 hPa, b) geo850 hPa, c) psl and d) SST for the period 850—1849 AD and the realization R4.

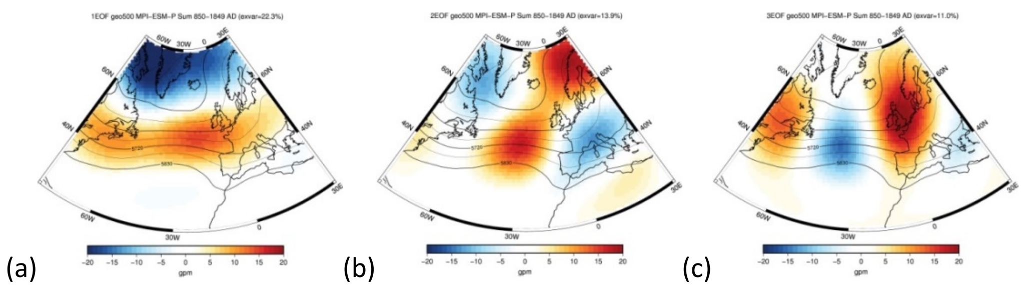

Figure 2K Summer EOFs of geo500 for the realization R4, for the period 850—1849 AD. a)EOF1, b)EOF2 and c)EOF3.

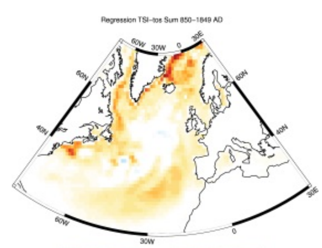

Figure 3K Regression of the TSI anomalies to the SST of the NA basin for the period 850—1849 AD and the realization R1.

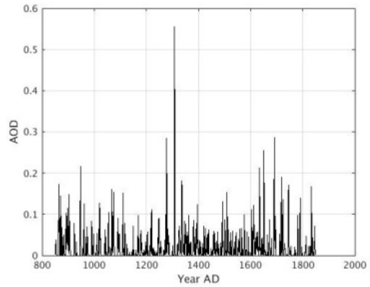

Figure 4K Aerosol Optical Depth due to volcanic aerosols, for the area 30°N—90°N and the period 850—1849 AD.

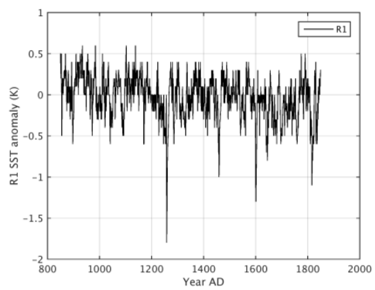

(a)

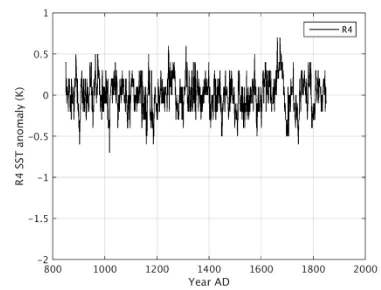

(b)

Figure 5K Detrended SST anomalies, averaged over the NA basin for the period 850—1849 AD and the realization a) R1 and b) R4 of the MPI-ESM-P model.

Acknowledgements

First of all I would like to thank Dr. Sebastian Wagner and Dr. Eduardo Zorita for advising me and helping me whenever necessary. Their support, knowledge and patience were essential for the accomplishment of my PhD.

I would also like to thank Prof. Dr. Johanna Baehr for being the chair of my Advisory Panel and her guidance throughout.

Furthermore, I am thankful for the chance to be a PhD student at the School of Integrated Climate System Science (SICSS) of the Cluster of Excellence on Integrated Climate System Analysis and Prediction (CliSAP) in Hamburg. Moreover, this work was supported by the project ARAMACC, an EU-funded Marie Curie Initial Training Network.

Last but not least I would like to thank my family for their love and support not only during this PhD, but throughout my life.

Eidesstattliche Versicherung

Hiermit erkläre ich an Eides Statt, dass ich die vorliegende Arbeit selbstständig und ohne fremde Hilfe angefertigt, keine anderen als die angegebenen Quellen und Hilfsmittel benutzt und die den benutzten Quellen wörtlich oder inhaltlich entnommenen Stellen als solche kenntlich gemacht habe. Diese Arbeit hat in gleicher oder ähnlicher Form noch keiner Prüfungsbehörde vorgelegen.

Unterschrift:

Datum:
Juni 16, 2017